INFORMATION TO USERS

This manuscript has been reproduced from the microfilm master. UMI films the text directly from the original or copy submitted. Thus, some thesis and dissertation copies are in typewriter face, while others may be from any type of computer printer.

The quality of this reproduction is dependent upon the quality of the copy submitted. Broken or indistinct print, colored or poor quality illustrations and photographs, print bleedthrough, substandard margins, and improper alignment can adversely affect reproduction.

In the unlikely event that the author did not send UMI a complete manuscript and there are missing pages, these will be noted. Also, if unauthorized copyright material had to be removed, a note will indicate the deletion.

Oversize materials (e.g., maps, drawings, charts) are reproduced by sectioning the original, beginning at the upper left-hand corner and continuing from left to right in equal sections with small overlaps.

Photographs included in the original manuscript have been reproduced xerographically in this copy. Higher quality 6" x 9" black and white photographic prints are available for any photographs or illustrations appearing in this copy for an additional charge. Contact UMI directly to order.

Bell & Howell Information and Learning
300 North Zeeb Road, Ann Arbor, MI 48106-1346 USA
800-521-0600

Single Bubble Sonoluminescence

Manas Dan

A Thesis

in

The Department

of

Physics

Presented in Partial Fulfillment of the Requirements

for the Degree of Doctorate of Philosophy at

Concordia University

Montreal, Quebec, Canada

April 2000

ABSTRACT

Single Bubble Sonoluminescence

Manas Dan, Ph. D.

Concordia University, 2000

In recent years considerable attention has been directed to the phenomenon of *single bubble sonoluminescence, SBSL* in which a single, stable, acoustically levitated bubble is made to oscillate with sufficiently large amplitude so as to emit picosecond light pulses in each cycle of the acoustic drive pressure. Remarkably, the phenomenon represents about twelve orders of magnitude of energy focusing.

SBSL has been carefully and thoroughly studied in part of parameter space by previous authors. In the present work, the experimental observation of the influence of another important parameter namely the ambient pressure will be presented. It is the first complete and controlled study of the modifications of the bubble dynamics and SL emission due to the variation of the ambient pressure. It has been observed that the equilibrium radius as well as the maximum radius increase as the ambient pressure is decreased at constant driving pressure. Furthermore the expansion ratio (R_{max}/R_{min}) increases as the ambient pressure is decreased, resulting in a change in the SL radiation. The intensity of SL emission increases about seven times for only a fifteen percent decrease of ambient pressure

at constant driving pressure. However, it is not possible to push SL radiation beyond a certain limit by continuously decreasing the ambient pressure. On the other hand increasing the ambient pressure decreases the equilibrium radius, as well as the expansion ratio leading to a decrease of SL intensity.

Amongst the SBSL emissions the light emission has been investigated rather elaborately. The other single bubble emission is the *acoustic emission, AE.* Here a detailed study of AE will be presented. The AE has been measured by a calibrated needle hydrophone in different regimes of bubble motion. The hydrophone response shows a large amplitude AE pulse which corresponds to the principal collapse, along with smaller amplitude pulses which can be associated with the after bounces of the bubble just after the initial collapse. The pressure amplitudes of the main AE spike are much weaker below the sonoluminescing regime. The amplitude of the principal AE spike in the sonoluminescing regime is about 1.2 atm at 7.2 mm from the bubble. The rise time as well as the FWHM of the principal spikes and after bounces in three different regimes of bubble motion has been reported. A light scattering experiment has been carried out to study the bubble dynamics. An extremely strong correlation between the results of light scattering and those of AE has been found.

ACKNOWLEDGEMENTS

It is indeed a pleasure to express my gratitude and appreciation to Professor David Cheeke for his personal and professional advice, critical comments, and patience in directing this dissertation.

I would like to acknowledge my appreciation to Dr. Lou Kondic for major contributions to many of the theoretical results presented in this dissertation. I would also like to thank him for many enlightening discussions and much help with my project.

I am especially grateful to Professor Ron Roy for his scientific expertise and valuable suggestions during the course of this work.

I wish to express my appreciation to the members of my dissertation committee, Dr. David Cheeke, Dr. Ron Roy, Dr. Mariana Frank, Dr. Panagiotis Vasilopoulos, Dr. John Capobianco, and Dr. S. Twareque Ali for their useful scientific and editorial comments and valuable time.

My sincere thanks go to my colleagues Steve Beaudin, Xing Li, Yuxing Zhang, Julien Banchet, Kevin Shannon, Gino Rinaldi, Mario Venditti, Zhongxi Zhang, Gurnam Manku, Derek Nelligan, Sebastien Guillon, and Abdulwahab Sallabi and the other faculty and non faculty members particularly Ms. Gloria Thompson and Ms. Lynn Chapmann of the Physics Department of Concordia University for their

help and cooperation during my graduate study.

I wish to offer special thanks to Professor Z. Q. Wang for many exciting discussions during the course of this project. I would like to thank Mr. Mostafa Showleh for allowing me to use instruments in the undergraduate laboratory and for technical helps.

I am thankful for the financial support I enjoyed from the Concordia University Graduate Fellowship.

I am indebted and grateful to Professors Joya Sen, S. Twareque Ali and Mrs. Fauzia Ali for encouraging me in graduate studies and making my stay in Montreal so wonderful and memorable. I enjoyed many stimulating non-academic discussions with them.

I would like to take this opportunity to thank and express my appreciation to my very special friends Sabina and Nilu for their continuing encouragement, help and cooperation during my graduate studies especially during my thesis writing. I am thankful for the wonderful friendship Sabina, and Nilu shared with me.

Finally, I express my deepest gratitude to my wonderful parents and family for their love, affection, and moral support. Without their inspiration I would not be where I am now.

Contents

List of Figures

List of Tables

Chapter 1

Introduction

Sonoluminescence - Sound to Light

Single Bubble Sonoluminescence, SBSL - is the weak emission of light associated with the violent collapse of a single bubble trapped in a liquid supporting an acoustic standing wave field. The phenomenon can lead to a remarkable degree of energy concentration (as high as 12 orders of magnitude). In other words, sonoluminescence is a means of making energy run uphill. Within our present day understanding the hallmarks of this phenomenon are: (i) the conversion of kHz frequency sound energy into the production of very sharp light pulses about 50 - 300 ps in width, (ii) an amazingly precise synchronicity (few parts in 10^{11}) between SBSL pulses and the driving acoustic field, and (iii) a continuous emission

spectrum extending from the visible to the ultraviolet regime, with no identifiable spectroscopic lines within nanometer resolution. Experimental studies have indicated that the intensity and the spectral distribution of the emitted radiation are very sensitive to the experimental parameters i.e. temperature of the host liquid, amount of dissolved gas concentration in the liquid, acoustic drive amplitude, doping of noble gases etc.

1.1 The Motivation Behind the Work

In the present work, two phenomena associated with SBSL have been investigated. Firstly, the details of the SBSL radiation have been explored in different liquids at various liquid temperatures with several gas concentrations. However, there has been no detailed study of the changes of SL emission as well as the bubble dynamics with the variation of ambient pressure, P_0. Furthermore, of particular interest in the present work is the dissociation hypothesis, DH of Lohse *et al.* for natural air bubbles in water. Simply stated, DH proposes that the air and water vapor molecules are ionized due to the high temperature and pressure generated at the moment of collapse and recombine into water soluble compounds with the exception of the inert gas component (1% argon for air), so that the gas inside the bubble then progressively transforms into pure argon. One of the goals of the

present work was to test the DH.

Secondly, during the catastrophic collapse of the bubble under the influence of the external acoustic field, the bubble not only emits a burst of light but also it launches a very sharp spike of acoustic signal followed by a few after bounces into the liquid surrounding the bubble. These are known as Acoustic Emissions (AE). The objective of the work is to compare the AE with light scattering and with the recent theories on AE. Additionally, a detailed study of the after bounces in different regimes of bubble motion has also been carried out.

1.2 The Organization of the Work

This work is organized as follows:

- Chapter I: *Introduction*: An historical background of the subject of cavitation and SL will be presented in this chapter. An account of the existing models of SL will be given here. Lastly, the importance of studying SL will be explained.

- Chapter II: *Theory of Bubble Dynamics*: The equation of motion of a spherical bubble in a liquid driven by an acoustic field will be derived. The radius versus time, $R(t)$ curves of the bubble will be plotted. The pressure and tem-

perature inside the bubble will also be computed from the bubble dynamics.

- Chapter III: *Experimental Setups and Details*: The details of the experimental setup and the technique to achieve single bubble sonoluminescence will be reported here. The detection systems of SBSL emissions will be outlined as well. A general description of the light scattering technique to get the $R(t)$ of the bubble will be detailed next. Finally experimental setups for modification of ambient pressure and for measurement of acoustic emissions will be reported.

- Chapter IV: *Effect of Ambient Pressure on SBSL*: The goal of the research of the modification of ambient pressure will be sketched at first. The theory of ambient pressure on SBSL will be described next along with the experimental results of the ambient pressure effect. The results will be compared and discussed with the theory of ambient pressure.

- Chapter V: *Study of Acoustic Emission*: After defining the goal of the research on acoustic emissions a brief theoretical overview will be presented. The experimental results on acoustic emissions will be reported as well. A qualitative comparison of the experimental results will be done in the light of available theories.

- Chapter VI: *Summary and Conclusion*: A summary and conclusions of the present work will be presented. Some future experiments which are needed to be done to better understand the mechanism of SBSL will be suggested.

1.3 Historical Background of Cavitation and Sonoluminescence

To know the history of SL we have to learn the historical development of the subject of cavitation. From the hydrodynamics point of view, Daniel Bernoulli [1] in 1738, showed how a rapid flow could produce a drop in pressure in a liquid. Euler argued that the consequence of a drop in pressure could create a tension in a liquid. If this tension exceeds the tensile strength of a liquid. the liquid might eventually rupture creating cavitation. So *cavitation* refers to the formation of a new surface or cavity within the body of a liquid and subsequent stimulated bubble activity due to flow, acoustic waves, decompression or electromagnetic irradiation etc. In the middle of the nineteenth century the subject of cavitation attracted the attention of scientific community with the development of high-speed and high-powered steam turbine. In this work only acoustic cavitation will be discussed. Acoustic cavitation may be defined as the cavitation under acoustic stress.

In 1894, trials of the new destroyer *H. M. S. Daring* failed to meet the expected specifications, revealing that insufficient thrust was developed and consequently reducing the speed and efficiency. Sir John Thornycroft and Sedney Barnaby [2] observed creation of voids and bubbles surrounding the moving propellers. Rapid erosion of the propeller blades was also noticed. To overcome the problem associated with the propellers, Lord Rayleigh was invited to join the committee to investigate the problem in 1917. The prolific Lord Rayleigh, as has happened so often, set out to solve the problem. He calculated the pressure generated in an incompressible fluid after a *spherical portion of the fluid is suddenly annihilated.* His ingenious work [3] laid the founding stone of the theory of cavitation dynamics. The erosion of the propeller and its poor efficiency were associated with the phenomenon of cavitation. The problem was solved simply by increasing the surface area and decreasing the speed of the propeller. Sonoluminescence was not predicted by Rayleigh, but as will be seen later, the theoretical basis of it had already been laid.

Sonoluminescence has a long history of itself. In 1927, Richards and Loomis [4] studied the effects of ultrasonic waves on liquids and demonstrated that ultrasonic waves enhance certain chemical reactions in liquids. Schmitt *et al.* [5] in 1929, observed that hydrogen peroxide, H_2O_2 or something analogous to it was formed when an aqueous solution containing dissolved oxygen was irradiated with intense

ultrasonic wave. The formation of peroxide was associated with the cavitation produced in the liquid by the high frequency sound field. Later in 1932, it was noted by Beuthe [6] that the amount of energy required to produce peroxide was much larger than that of the applied acoustic field. In fact Beuthe concluded that collapses of cavitating bubbles created the proper chemical conditions resulting in the dissociation of either water or dissolved molecular oxygen into oxygen ions which ultimately recombined to produce peroxide. It was mentioned in the article by Frenzel and Schultes [7] that a professor named Mecke had calculated the amount of energy needed to produce peroxide from water to be approximately 2 eV which is about the energy of the visible photons. Professor Mecke predicted light from the process of irradiation of liquids with high intensity ultrasound and it was Frenzel and Schultes in 1934 first reported the luminescence from water under intense insonification. They recorded tiny light spots on a photographic plate placed over the liquid chamber. According to them the friction between the moving bubble and the viscous liquid resulted in the separation of charges, similar to that what is found in our everyday experience when shoes are rubbed on carpets. The accumulated charge finally discharged to create the spark. It should be worth mentioning that Marinesco and Trillat [8] (1933) observed fogging (stripes of pattern) of photographic plates immersed in water bath under ultrasonic field. However, whether that pattern was a primary effect of ultrasound on silver halides

of the plate or a secondary one was not clear at all. Zimakov [9] also noticed a luminescence of the vapor on top of the ultrasonic bath but again there was no valid and conclusive evidence that it was due to ultrasound. It is now appropriate to mention why the history of the cavitation process has been presented at the beginning. It is simply because SL requires the cavitation process for its existence although not all processes of cavitation can lead to SL.

Historically, SL was produced by immersing a high power ultrasonic horn into a liquid and insonating globally the whole volume of the liquid in an uncontrolled way. Therefore, as expected the resulting cavitation field is a *bubble cloud* with multiple bubbles emitting light in a chaotic and uncontrolled fashion. Multiple bubble cavitation regimes are generally classified into two types i.e. (i) transient and (ii) stable. In case of transient cavitation each bubble lives only a fraction of a second (few acoustic cycles only) and dies in a violent collapse. On the other hand, stable cavitation is a more disciplined and controlled phenomenon lasting longer, although the movement of each bubble is unsynchronized with that of its neighbor. The light emission from multiple bubbles has been termed as multi-bubble sonoluminescence, MBSL.

The characteristics of MBSL such as the intensity and the spectrum of the emitted radiation were measured by several researchers. The dependence of the SL intensity on the amplitude and the frequency of the driving field and other

parameters such as liquid temperatures, dissolved gases and host liquids have also been investigated thoroughly. The properties of cavitation bubbles as secondary source of sound emitting spherical waves (i.e. acoustic emission) were studied as well. However, the uncontrolled and random motions of bubbles and non-reproducibility of exact experimental conditions hampered the progress and interest of the subject for several decades. Furthermore, theoretical models always assume a single spherical bubble and its dynamics under an ultrasonic field have been modeled whereas in real experimental situations it has never been possible to trap a single individual bubble by an acoustic field until fairly recently. We will come back to this later. Nonetheless, there are certain experimental observations which seemed to be quite reliable and worth mentioning. In 1937, Chambers [10] studied the effect of physical parameters of several (about 36) aqueous and non aqueous liquids on the SL intensity. He concluded, amongst other things, that the intensity of the SL radiation increases with the decrease of bulk liquid temperature. Prudhomme *et al.* [11] (1957) noticed that SL intensity increased with the atomic number of the dissolved noble gases. Jarman [12] (1959) studied several liquids and reported that the intensity of sonoluminescence scales up with σ^2/p_v where σ is the surface tension and p_v is the vapor pressure of the liquid. Following Jarman's σ^2/p_v parameter Kuttruff [13] (1962) reported extremely bright SL from mercury. Although Frenzel *et al.* [7] observed no light emission from degassed

water, Rosenberg [14] (1962) mentioned light emission at a larger driving pressure. Several researchers [15, 16, 17, 18] measured the spectrum of the emitted light reporting contradictory results of line emission as well as broad band radiation. Speaking of the optical spectrum, another spectrum i.e. the acoustic emission spectrum had been studied by Esche [19] in 1952. He found that harmonics of the driving frequency were generated at low drive amplitude. However, as the drive amplitude was increased well beyond the threshold of cavitation, sub-harmonics as well as ultra-harmonics started appearing in the spectra. It is to be noted that Negishi [20] (1961) observed SL and acoustic emission simultaneously. Kuttruff [13] captured shock waves using the method of Schlieren imaging. He also heard cavitation noise with the emission of the SL light.

In this context, it is to be noted that the case of MBSL, called sonochemistry, has been studied for several years, particularly by Suslick *et al.* [21, 22]. The authors and others invetigators have shown directly that MBSL is characterized by asymmetric bubble collapse near walls or other bubbles. Later Flint and Suslick [23] estimated the temperature and pressure at the center of the collapsing bubble to be approximately 5000 K and 500 atmospheres respectively. The authors also noticed that most metals melt at the impact of high-velocity interparticle collision produecd by shock waves from cavitation in liquid-solid slurries. Recently, McNamara *et al.* [24] used multi-bubble sonoluminescence as a spectroscopic probe of

temperatures inside cavitaing bubbles. The authors changed the properties of the gas-vapor mixture within the bubble, thus varying the effective emission temperature for MBSL from 2300 to 5100 K.

Although uncontrolled and chaotic features of multiple bubble cavitation made meaningful and reliable measurements quite a challenging task, scientists had been trying to control certain aspects ascribed to cavitation. Towards this end it was Saksena and Nyborg [25] in 1970, who showed that under certain experimental conditions sonoluminescence results from water/glycerine mixture without cavitation noise. They also found out that the light emission occurs with the same periodicity or the frequency of the applied sound field. Later, in 1985, Crum and Reynolds [26] reported large amounts of light emissions from the pressure antinodal points in moderate pressure amplitude of approximately (0.17 ± 0.03) MPa. And the cavitation was described to be a stable cavitation and not transient in nature. Finally, a major breakthrough was achieved by Filepe Gaitan, a graduate student working towards his doctoral degree under the supervision of Professor Larry Crum in the National Center for Physical Acoustics in the University of Mississippi, when they [27] reported, in an article published in the *Journal of the Acoustical Society of America* the trapping of a single sonoluminescing bubble in a water/glycerine mixture supporting a standing wave field. In this context, the attention of the readers must be drawn to a recent letter in the August issue of

Physics World by Seth Putterman [28] of UCLA. He reported the discovery of single bubble sonoluminescence back in 1970 by Paul R. Temple, a Master's student in the University of Vermont, Burlington, USA. According to Putterman, Temple *et al.* [29] observed the light emission at each acoustic cycle from a single bubble trapped in a resonant sound field. The measured width of the light pulse was approximately 20 ns and instrument limited. Temple *et al.* presented their results at the 81st meeting of the *Acoustical Society of America* in 1971. However, it is reported that the degassing of the liquid was not as extensive as Gaitan's. Their effort to increase the light intensity was hindered in practice by the issue of stability of the bubble and hence Putterman concluded that in spite of the discovery of this remarkable phenomenon no further work had been done at that time.

1.4 Models of MBSL

As the experimental results on multi-bubble sonoluminescence continued to appear so did the different models and theories trying to explain the phenomenon. Below we will describe the existing models:

- **The Triboluminescent Model (1936):** Chambers [10] observed light emission from 14 out of 36 pure liquids insonated by audible sound waves. He

related the sonic-luminescence to the tribo-luminescence - the luminescence that occurs when the quasi-crystalline structure of liquid breaks suddenly as the cavity forms and grows in the liquid. (It should be noted that back then liquids were supposed to be quasi-crystalline in structure).

- **The Balloelectric Model (1939):** The balloelectric model for sonoluminescence was proposed by Harvey [30] in 1939. In his model Harvey argued that cavitating gas bubbles develop considerable amount of electrical charge during the expansion phase. But when it collapses the size of the bubble decreases leading to an increase in electric field until a discharge takes place in the gas inside the bubble which causes the luminescence. (Electric potentials produced by increase in the surface of a fluid are called balloelectric or Lenard potential).

- **The Electrical Microdischarge Model (1940):** This model is based on the idea [31] of the statistical variation of charge distribution in non spherical gas cavities created during cavitation process and thus leading to microdischarges within the bubble producing weak luminescence.

- **The Mechanochemical Model (1949):** Weyl and Marboe [32] put forward that as the bubble expands in the cavitation field it destroys the quasi-crystalline structure at the newly created surface. This process produces ions

which recombine radiatively to create luminescence.

- **The Hot-Spot Model (1950):** In 1950, Noltingk and Neppiras [33] introduced the hot-spot model. This model proposed that during the dramatic collapse, the contents inside the bubble become adiabatically heated to a few thousands of kelvin. Accordingly, SL was described as an incandescence from a very hot gas inside the bubble. In this context, we should mention that Jarman [34] proposed a variant of the hot-spot model incorporating the formation of shock waves inside the collapsing bubble that gives rise to black-body radiation. Hickling [35] was able to explain sonoluminescence from different gases just by including the thermal conductivity of the gas in the hot-spot theory.

- **The Chemiluminescent Model (1950):** Griffing [36] predicted a very high temperature rise during the catastrophic collapse of the bubble creating a favorable condition for the production of oxidizing agent such as H_2O_2. The H_2O_2 then dissolves into the liquid initiating a host of chemical reactions some of which could be chemiluminescent in nature. In the beginning of the eighties Seghal *et al.* [37, 38, 39, 40, 41] and Chendke *et al.* [42] carried out extensive research based on the idea of chemiluminescence.

- **The Anion Discharge Model (1974):** This model is electrical in nature. According to this hypothesis [43] the adsorption and induced polarization of gas molecules at the gas-liquid interface neutralize the anions on the bubble surface giving rise to charge. When the bubble undergoes rapid compression charge density crosses the disruption gradient at the interface resulting in light emission.

As of now, none of the models mentioned above could explain all the experimental results. Most of these early theories were qualitative and speculative in nature, mainly due to the fact that there was no experiment done in controlled conditions. Most of them were rejected in course of time and as more experiments were carried out. Recent experimental studies prove conclusively that the light pulse is emitted at or near the minimum of the collapse ruling out the triboluminescent, microdischarge and mechanochemical hypotheses. That the SL pulse is emitted during the expansion phase of the cavitation process was the very basis of these hypotheses. Following the balloelectric model it is naturally expected that the SL intensity should be sensitive to the changes of electrical conductivities of the liquids. But the experiments carried out with liquids of different electrical conductivities showed no change of SL intensity. Furthermore no relatively stronger emission from homonuclear gases makes it easy to reject the anaion discharge model

as well. Although most of the earlier models are of historical interest right now, yet it is to be noted here that these theories clearly guided the course of further experimental and theoretical studies. At this point it is worth mentioning that one of the earliest theories namely the *shock wave model of Jarman* [34], which was rejected by the opinion of the day, presently is being revisited and gaining its solid ground to be the basis of some present day models. So it won't be an exaggeration to mention that some of these models sowed the seeds for further experimental and theoretical works particularly the hot-spot and the chemiluminescent models. The serious interest to measure the spectrum of the SL [37, 38, 39, 40, 41] and an attempt to fit it with a black body radiation gained momentum from the hot-spot theory. Other workers [25, 22, 44, 24] observed molecular and/or atomic bands in the SL spectrum indicating that some sort of chemical process must be going on inside the very hot bubble interior. In most of the cases the spectra were explained on the basis of complex chemical transitions. Naturally, the hot-spot and the chemiluminescent models are the two relevant ones which lend some support in explaining the light emission.

It is clearly understandable that multi-bubble situation makes meaningful measurements extremely difficult. In MBSL it has never been possible to study a single, isolated bubble as the cavitation field always contains a large number of bubbles of different sizes (usually in the order of microns) with extremely short time scales

(usually in nanoseconds). So studies of MBSL inherently involve some kind of averaging both temporal and spatial. As it is highly improbable to get an exactly identical ensemble of bubbles or even bubble clouds, and in any case many of the experimental parameters were unspecified, it has never been possible to recreate the same experimental conditions. As a consequence, models trying to explain the phenomenon have always had some serious drawbacks. Furthermore, theoretically it has never been easy to take into account all the interactions amongst the bubbles in an ensemble. Hence, the discovery of single bubble sonoluminescence by Gaitan [27, 45] was a major breakthrough in advancing both the experimental and theoretical investigations. It thus became possible for the first time to study cavitation under highly controlled conditions.

1.5 Studies on Single Bubble Sonoluminescence

The primary interest of Gaitan and his colleagues was to study the radius versus time, $R(t)$ of a sonoluminescing bubble and compare it with the several existing hydrodynamic models. Their original work clearly showed that SBSL appears in a train of light flashes whose phase is highly synchronized with the driving acoustic field. Additionally, they found that the light emission occurs at the end of the main collapse of the bubble. Proposing *chemiluminescence* as the origin of light

emission, a temperature of 2000 - 3000 degree Kelvin was estimated. These findings are indeed very exciting but a more startling revelation about the amazing features of SBSL came out from the studies of Putterman's group in UCLA. They started making precisely quantitative measurements of the characteristics of SBSL. According to their measurements the most striking aspects of SBSL are (1) the very sharp light pulses(less that 50 ps) [46, 47] [later it was found that the pulse width varies from 60 - 250 ps [48] or 40 - 350 ps [49]], (2) the amazingly precise synchronicity of the light pulses with the driving sound field [46], (3) the continuous emission spectrum extending from the infrared to the ultra violet regime [50] and (4) high emitted peak power (more than 30 mW) [50]. Barber estimated the pulse width (an upper bound of 50 ps) of the light by the relative response of a SBSL pulse in comparison to a 34 ps Hamamatsu PLP-01 light pulser using a micro channel plate-photomultiplier tube (MCP-PMT). The idea to use a streak camera to measure the pulse width of SBSL failed due to insufficient light intensity of SBSL [51]. From the integrated charge response of the PMT. they estimated that each SL flash contains somewhere between 10^5 - 10^6 photons.

We all know that a measurement of the emission spectrum is a key issue to understand the physical and chemical processes involved in the production of light. Hiller *et al.* [50] in August 1992 first reported the spectrum of SBSL. They showed that the spectrum of the bright sonoluminescence is continuously extending from

the visible down to the ultraviolet cut off of water ($\sim$ 200 nm). Imaging the SL onto the input slit of a spectrometer by a F/0.85 51 mm biconvex quartz lens and reducing the slit width down to 25 μm, no spectral line of 1 nm resolution is found. Following the idea [38] of measuring the spectrum at lower temperatures, they found that the intensity of SL increases by a factor of ten when the water is cooled from 22 degree to 10 degree Celsius and the spectrum becomes heavily skewed to the UV. The spectrum at room temperature can be fitted to blackbody spectrum at 25,000 K and similarly the spectrum at 10 degree Celsius can be matched to the one of temperature is more that 50,000 K. They concluded that "if a spectral peak exists, it lies at photon energies above 6eV" [50].

In December 1992, Barber *et al.* [52] reported light scattering results to determine the dynamics of the sonoluminescing bubble. Following this approach they inferred the equilibrium radius, R_0 and maximum radius, R_{max} of the bubble indirectly by matching the experimental $R(t)$ with the theoretical Rayleigh-Plesset (RP) equation. From their work they suggested that an imploding shock wave could initiate the light emission.

With the exciting revelations of new data on the characteristics of SBSL - the research on the subject progressed basically along two avenues - on one avenue the very basic question "what is the mechanism of light emission" has been asked and on the other one experimental studies and verifications of the phenomenon in

parameter space have been carried out.

With the growing speculation of temperatures of thousands and millions of Kelvin at the center of the collapsing bubbles, there has been a steady increase in the number of models to explain such high temperatures and observed spectra [see [53, 54] for recent reviews]. In fact, such exciting observed properties have led to an abundance of theories trying to explain the basic mechanism of light emission. It is very important to note that there has been no independent and direct measurement of temperature at the center or even inside the bubble. Hence each model has been fitted with the experimental data (particularly the pulse width and spectral radiance) to estimate the temperature at the center. We will describe the models in chronological order along with the major experimental and theoretical developments of the subject.

There was no specific model of SBSL based on **black-body radiation**. However, while presenting their very first measurement of SBSL spectrum, Hiller *et al.* [50] fitted the experimental curve with the black-body spectrum. Surprisingly enough, the data were well fitted for source temperatures of 25,000 K and more than 50,000 K with SBSL spectra at water temperatures of 22 and 10 degree Celsius respectively. However, this model has some inherent shortcomings. For a blackbody spectrum to be observed the gas must be opaque to radiation. Since Barber *et al.* [52] estimated that the size of the light emitting region is nearly

comparable to the wavelength of the emitted light it would be hard to imagine how the photons achieve thermal equilibrium with the matter as they require several oscillations before emitting [55]. Again, Eberlein [56, 57] pointed out that the energy associated with the spectrum below the cut off region of water would produce macroscopic effects in the surrounding liquid such as dissociation. She also mentioned that the process involving the production of black-body radiation must be orders of magnitude too slow to produce the picosecond light pulses. Later the experimental evidence which completely discards the black-body model will be discussed.

Considering the bubble as a "spherical hole in a dielectric medium" the late noble prize winner Julian Schwinger [58, 59, 60, 61, 62, 63] proposed sonoluminescence to be the dynamical counterpart of the static **Casimir effect**. According to Schwinger the static Casimir effect is "an observable non-classical electromagnetic force of attraction between two parallel (perfectly) conducting plates". According to him during the extremely rapid collapse, the two diametrically opposite dielectric walls of the bubble reproduce the condition to create dynamical Casimir light which is seen as sonoluminescence. However, recent experiments on acoustic emissions (where due to the high compression in the bubble an outgoing acoustic pulse is launched in the liquid) [64, 65, 66] show that the velocity of the bubble wall remains much smaller than what is needed to create the proper conditions for the

dynamical Casimir effect. Furthermore, this model has been criticized by Milton et al. [68, 69] pointing out that the static Casimir energy which is quite relevant in this case is too small to result in a large burst of photons as seen in sonoluminescence. In a very recent article Brevik *et al.* [70] argued that Casimir energy might be identified with van der Wall's interactions and hence the volume effect to calculate the energy cannot be present and is irrelevant. On the other hand, Visser *et al.* [71] modified Schwinger's original idea and proposed that SL occurs due to a sudden change of the refractive index as a function of space and time. According to them, this abrupt change in refractive index will result in real photons from zero point fluctuations. It was also pointed out that the details of bubble collapse particularly the ratio, R_{max}/R_0, are not very important. Finally, they suggested experimental investigations of femtosecond changes in the refractive index of the gas and of the liquid surrounding the bubble.

Following the original idea of Jarman [34] in 1993, Greenspan *et al.* [72] and Wu and Roberts [73, 74] presented the shock wave model in which they considered the dynamics of the gas (basically air) inside the bubble coupled with the motion of the bubble wall. They took into account the generation and propagation of shocks inside the gas. Following this model they proposed that the air inside the collapsing bubble becomes completely ionized by the compression of the imploding shock wave and ultimately gives rise to **Bremsstrahlung**. They calculated millions of

degrees of temperature and extremely high density at the center of the bubble. Consistent with the experimental observation they also got a peak power of 30 mW. The calculated optical pulse width is extremely sharp of the order of 1.2 ps. However, this model is not free from criticism. The temperatures reported here are orders of magnitude higher than those deduced from experimental data [50]. Furthermore, the experimental spectrum which resembles the black-body one is not easy to match with the Bremsstrahlung one. Again Eberlein [56, 57] mentioned that temperatures, as high as those predicted by the model of Wu and Roberts must produce observable effects in the surrounding liquid. However, no such effects have ever been observed, raising doubts about the validity of high temperatures and as a whole about the shock wave model itself.

As mentioned earlier, while the theorists were busy trying to explain the origin of SL, experimentalists kept on exploring the parameter space of SBSL. In October 1994, Hiller *et al.* [75] first reported that sonoluminescence is extremely sensitive to the doping of noble gases. They observed that the intensity of SL radiation from a nitrogen filled bubble increases by a factor of 30 if the bubble is doped by only 1% of argon. Amongst other things, they discovered that the spectral density of emitted light depends strongly on the amount and type of noble gas used for doping. For example, the spectrum of a helium doped bubble shifts towards into the UV compared to that of an argon or xenon doped one. These experimental data

proved the inability of the shock wave model just because the doping of noble gases has not been accounted for by this model. It was concluded that though the light emission is very sensitive to the experimental parameters, yet the characteristics of the emitted radiation more or less remains robust throughout the parameter space.

Lother Frommhold and Anthony A. Atchley [76] [1994] estimated the intensity and the profile of the emitted light in the visible and near UV region of the spectrum of N_2 - N_2, N_2 - Ar etc. pairs of interacting molecules based on the idea of **collision-induced emission (CIE)**. According to them, pairs of interacting molecules produce collision-induced dipoles. When the temperature of a gas is inadequate for electronic excitation, molecules like N_2, Ar with inversion symmetry do not absorb or emit radiation in the visible or infrared whereas collision-induced dipoles do. At high temperatures, energy re-emission occurs to vibrational bands and high overtone bands in the visible region. For sonoluminescence the authors proposed the overlap-induced dipoles are mostly responsible for the emission and the temperatures involved are of the orders of many thousands of kelvin. Following this model, they could explain the amount of light emitted with an assumption of only 10,000 - 20,000 K. It was also concluded that spectral emission profile is not related to Planck's law. However, this model has been criticized for adopting adjustable parameters and indeterminate points [57]. Furthermore it is difficult to

imagine getting photons of energy > 6eV from the collisions of molecules at such lower temperatures.

At the same time Hickling [77] advanced the idea that sonoluminescence could be the result of cracking of an ice shell formed near the gas liquid interface at the maximum compression phase when the pressure of the order of > 1 GPa could be reached. However, this model did not gain any experimental support.

In 1995, Löfstedt *et al.* [78] attempted to explain the experimental results of Hiller *et al.* [75] and Barber *et al.* [79] based on the idea of standard theory of rectified diffusion [80]. Experimentally, it was observed that stable SBSL in pure argon requires strong degassing $c_i/c_0 = 0.004$ whereas SBSL in air only requires degassing of $c_i/c_0 = 0.4$. Based on the hydrodynamic calculations Löfstedt *et al.* found the steady-state-balance of mass flow between the bubble and gas dissolved in the surrounding fluid for argon bubble but not for air bubbles. To explain this discrepancy between the degree of degassing required to achieve stable SBSL in air bubbles for experiments and hydrodynamical calculations they concluded that there is a "yet unidentified mass ejection mechanism" involved in air bubbles to understand SL.

In the mean time, another approach trying to explain the light emission was advanced by Bernstein *et al.* [81] [1995]. This approach is known as **Confined Electron Model**. According to this model, high density and high temperature

are produced in fluid during the final phase of the bubble collapse and voids of different size (broad distribution) are formed. They derived the bubble temperature and reduced density based on an adiabatic collapse process. The gas inside the bubble becomes ionized by the high temperature resulting in the production of electrons which get trapped in the voids. Finally discrete transitions of these confined electrons give rise to SBSL. These electrons have been treated in a standard quantum mechanical calculation as electrons in a box. Following this model they obtained the spectra of rare gases (Xe, Ar, and He) and found good correlation with experiments. The visible and ultraviolet spectrum of the emitted light is due to the closely spaced electron energy levels in the voids. The continuous emission spectra results from the blurring of discrete energy levels, due to spatial broad distribution of voids sizes. They proposed that the very short emission time scale is highly correlated with the emitted power which is a function of reduced density. They predicted emission temperatures of 20,000 - 60,000 K based on their spectra of rare gases. The model that ionization potential will be a driving factor for SBSL. The basic model predicts a high emitted optical power of 300 mW which is about 100 times greater than that observed in experiments. Hence only a very small degree of ionization of the order of 0.1 % is needed for agreement with experiment. While this model is simple and soundly based physically, there has not as yet been any detailed experimental support fot it.

In an effort to expand the parameter space of SBSL, Weninger *et al.* [82] in 1995, first reported SBSL from non-aqueous fluids. They observed SBSL from a host of non-aqueous fluids such as n-dedocane, 1-pentanol, 1-butanol, 1-propanol, Si oil, ethanol, 2-propanol etc. They also discovered that the SL intensity is a very sensitive function of the fluid temperature, the partial pressure of the dissolved gases and the type of fluid involved as a host. The absence of molecular transitions in the spectrum of the emitted light showed clearly that the chemical nature of the fluid plays no role in the process. This work, and more particularly the observations in [83, 84] of the absence of Swan lines due to transitions among excited states of C_2 in SBSL, prove beyond reasonable doubt that the conditions achieved in SBSL are totally different than those of MBSL. Furthermore, the temperature and densities associated with SBSL are completely different from those of MBSL [85].

To account for both MBSL and SBSL Berstein *et al.* [86] published a very interesting synthesis of the molecular and electronic emission model. The basic idea is that molecular and electronic emission are two different chemical processes - the molecular one governs at lower temperatures, where as the electronic emission dominates at higher temperatures. In other words, in MBSL where there is a broad distribution of bubble sizes and the neighboring bubbles interact with each other, molecular emission becomes the dominant process leading to temperatures ranging from 5,000 - 15,000 K. On the other hand, in SBSL the collapse of the single bubble

is very well controlled so that electronic (continuous) emission regime is achieved resulting in temperatures in the range of 20,000 - 100,000 K.

Motivated by the original idea of Schwinger that sonoluminescence might be similar to dynamic Casimir effect, Eberlein [57, 56] advanced the theory of **quantum vacuum radiation** for sonoluminescence. Generalizing the theory of the Unruh effect [87] which states that a uniformly accelerated mirror emits photons of similar spectral distribution as that of a blackbody, she proposed that this type of photon could be generated by two moving dielectric interfaces or a dielectric and the vacuum. According to her, sonoluminescence is the first real world example of this kind of phenomenon. However, several investigators such as Unnikrishnan *et al.* [88] pointed out that this model could not account for the sensitivity of radiation to doping of noble gases and also to the dependence on liquid temperatures. Others [89, 90] challenged this model saying that the velocity of the bubble wall is not large enough to get the predicted number of photons. Completely unrealistic parameters such as the velocity of the bubble wall of the order of or even higher than the velocity of light has been taken to explain the observed experimental results.

In the mean time, a group of investigators [96] concentrated mainly on the question of *what determines the parameter regime of SBSL*? Towards this end Brenner *et al.* [91] studied the point of stability of a sonoluminescing bubble. With

the help of the phase diagrams they showed that in low viscous liquids parametric instability sets in before the Rayleigh-Taylor (RT) instability. However, since the parametric instability acts over time scales longer than the diffusion time scale the bubble readjusts itself by diffusion processes and slowly re-enters into the stable SL regime. In contrast, in the case of highly viscous liquids the RT instability, which acts in the time scale of 10^{-9} s, is encountered first. The bubble therefore gets destroyed immediately.

In 1996, Holt and Gaitan [96] were the first to report an elaborate investigation on stability boundaries in the parameter space of SBSL. The authors studied the region of parameter space namely acoustic pressure, P_a and eqilibrium radius, R_0 in which stable SBSL occurs in air-water system. They observed that for dissolved gas concentration above 50 % of saturation, an oscillating bubble is unstable whereas for below 50 % of sturation the bubble is stable with respect to shape instability. They also identified the role of diffusional stability on SBSL air bubble which later laid the ground work for Lohse *et al.*

The sensitivity of the SL radiation to the doping of noble gases and consequently the failure of the standard hydrodynamic theory to explain the stability of air bubbles, led Lohse *et al.* [92, 93, 94, 95] to suggest an additional mechanism, chemical in nature, to be involved in sonoluminescence. According to them, the temperature inside the collapsing bubble exceeds the dissociation temperature

($\approx$ 9000 K) of oxygen (O) and nitrogen (N), leading to the formation of oxygen and nitrogen radicals. These radicals then react with the hydrogen and oxygen radicals produced from the ionization of water vapor. Ultimately, recombinations of these radicals produce highly water soluble compounds such as hydrogen peroxide (H_2O_2), nitrous acid (HNO_2), and nitric acid (HNO_3) etc. However, the inert gas components (such as 1 % argon etc.) which do not react with water vapor remains inside the strongly driven bubble. This process is called *rectification of an air bubble into an argon bubble* by Lohse et. al. This chemical rectification process seems to resolve the observed discrepancy between the theory and the experimental results. Recent experiments [96, 97, 98, 99, 100, 101] have supported this hypothesis with conclusive evidence. These will be discussed later.

Weninger *et al.* [64] [1997] reported experimental results based on the idea of pulsed Mie-scattering technique which showed that during the very final phase of the bubble collapse the wall velocity exceeds Mach 4 (where Mach = velocity of the particle in medium/velocity of sound in the gas). The authors propose that this leads to the generation of shock waves in the gas entrapped in the bubble.

Furthermore, Prosperetti [102] and Longuet-Higgins [103] criticized the idea of a perfectly spherical bubble collapse in an acoustic field. Prosperetti argued that during the compression phase, a high-speed jet strikes the other side of the bubble wall and as a result of the impact, light is emitted which is termed **fractolumi-**

nescence. He also explained why cooling the host liquid or addition of surface active material change the light emission. However, how the bubble overcomes the impact of the jet and still remains stable over billions of cycle cannot be explained following this model. The computed pulse width is equal to or less than 50 ps.

Lepoint *et al.* [104] advanced an alternative **electrodynamic** hypothesis. According to them several needlelike micro jets are formed due to the non-spherical perturbations or the RT instability during the very final moment of collapse. The tips of these microjets become electrically charged and produce such an enormous field that electrons are emitted and a micro plasma is formed which is the origin of sonoluminescence. They reported the calculated pulse width to be less that 10 ps. However, according to this model the effects of dissolved gases, liquid temperature etc. on SL intensity are still open questions.

In May 1997, Moss *et al.* [105] [see also [106]] at LLNL calculated pulse widths and spectra of a single sonoluminescing bubble using the rigorous numerical codes of inertial confinement fusion to examine the final phase of bubble collapse. They studied the imploding shock with the state-of-the-art equation of state for the gas inside the bubble along with plasma thermal conduction. Following their model Moss *et al.* were able to calculate the measured pulse width and emission intensities considering the opacity and other physical processes associated with plasma. But surprisingly enough, their calculation of spectral flux of a nitrogen (N_2) bubble is

approximately 1/25 that of an air bubble. However, in the case of an argon (Ar) bubble the calculated spectrum is similar to that of an air bubble. This calculation agrees surprisingly well with and theoretically supports the rectification hypothesis of Lohse *et al.* Their computed pulse widths are less than 50 ps (FWHM $\approx$ 15 ps).

Later, Mohanty *et al.* [107] proposed sonoluminescence as a **cooperative many body phenomenon** in a two step process. In the first step the population inversion of excited atoms and molecules is achieved at the high temperature and pressure created at the minimum of the bubble collapse initiated by ultrasound. The second step is the spontaneous emission of the excited atoms to the ground state. However, due to the extremely small distances between the excited atoms, which are of the order of the wavelength of emitted light, they proposed there would be a phase correlation in the electromagnetic field. With this model they proposed less than 10 ps pulse width for the emitted pulse. But as we will see in the following paragraph their model cannot explain the relative large pulse widths found in later measurements by Gompf et al.

Further, Lothar Frommhold [108] computed the spectra of noble gases in the temperature between 5,000 - 40,000 K and observed good agreement at electron temperatures of 20,000 K for heavier inert gases with the measured spectra of sonoluminescence. Hence he proposed **electron - neutral-atom bremsstrahlung** might be at the origin of light emission.

On the other hand, in an exciting development in August 1997, Gompf *et al.* [48] resolved the flash width of sonoluminescing bubble using the *Time-Correlated Single Photon Counting (TC-SPC)* technique. The basic principle behind this technique is that a time-to-amplitude converter (TAC) is started with a first photon from the SL pulse and it is stopped with the arrival of the second photon from the same pulse. Due to the identical statistical distribution of the start and stop pulse, the autocorrelation of the pulse shape can be measured. Finally the SBSL pulse width can be measured by deconvolution if the response of the instrument (for TCSPC) is known. Gompf *et al.* measured the full width at half-maximum (FWHM) following this method. The measured FWHM varies from 60 ps to 250 ps depending on the amount of dissolved gas in the liquid and also on the driving pressure. But the most surprising observation of this experiment is that using optical filters Gompf *et al.* showed that the flash widths are independent of wavelengths of light. This very observation completely rules out the simple adiabatic heating as a mechanism for sonoluminescence. It would result in much longer pulses at long wavelengths than in the short wavelengths if the adiabatic heating process were responsible for the light emission as the bubble would spend much longer time in the low temperature (red wavelength range) as it heats up than the high temperature range (the UV range). Later Hiller it et al. [49] independently confirmed Gompf's results. They measured pulse width from 40

- 350 ps for mixtures of various gases in water. They concluded that the gas inside the bubble becomes plasma under the extreme condition of bubble collapse. Furthermore, a weak dependence of the pulse width with temperature has been reported by Moran *et al.* [109]. They observed that the SBSL FWHM varies with wavelength at 3 degree C but not at 24 degree C. However, with this technique the direction of asymmetry between the leading and trailing edge of the SL pulse could not be resolved. Later, with the help of a streak camera Pecha *et al.* [110] measured both the pulse width and shape of the SL pulse. It was found that that the pulse shape is nearly Gaussian with slightly slower decay for low driving pressure. But at higher driving pressure the decay time in the falling edge of the pulse increased, leading to a larger pulse width. On the other hand the rising time of the pulse remains nearly unchanged. The increasing asymmetry of the light pulses in higher driving pressures seems to denote slower reexpansion as predicted by the bubble dynamics. In a word, Pecha's measurements by a streak camera not only confirmed the pulse widths measured by Gompf *et al.* but also resolved the asymmetry of the pulse.

It should be noted that the absence of line or band emissions would suggest that the possible mechanism for light emission might be thermal Bremsstrahlung. But the predicted temperature of 10,000 K on the basis of observed and computed collapse of a typical sonoluminescing bubble cannot provide adequate temperature

for thermal Bremsstrahlung to take place. However, the inclusion of the concept of formation of shock during the final phase of the bubble collapse providing an additional energy focusing as it converges to the center of the bubble and could create some form of plasma of the gas for a extremely short duration. The **plasma model** of Moss *et al.* [105] seems to predict most of the observed features including the acoustic emission. However, following this model the predicted pulse width is less than 50 ps whereas it is now known that the pulse widths are much larger than those calculated by them. However, recently Moss *et al.* [111] suggested that generation of shock inside the collapsing bubble is not a necessary condition to get SL. Finally, in April 1999 Hilgenfeldt *et al.* [112, 113] [see also [114]] presented the most comprehensive model for the light emission. They were able to deduce this model with the help of few well established and known concepts. Since the simple RP dynamics describes the highly non–linear bubble motion accurately, they used this hydrodynamic equation to capture the complete cycle of motion and the consequent conditions generated by the bubble collapse. For the most part of the bubble motion the temperature inside the bubble which is coupled with R(t) is assumed to be spatially uniform [i.e. isothermal behavior] [105, 115, 116] except for the few nano-second during the final phase of collapse. During this time the heating is assumed to be governed by a time dependent poly-tropic exponent [117, 118] [i.e. adiabatic behavior] which is a function of bubble radius, bubble wall velocity

and temperature of the gas. By taking into account the dissociation of molecular gases under the condition generated by the bubble collapse and thereby ensuring the stability of the bubble they computed temperatures in the range of 20,000 - 30,000 K of the inert gas components of air caught inside the bubble. Thus the hot noble gases become ionized and the thermal energy gets distributed among the ions and neutral atoms. Considering the finite opacity of the gases and following the Kirchoff's law which states absorption and emission are reciprocal mechanisms, Hilgenfeldt *et al.* explained the light emission to be thermal bremsstrahlung and recombination radiation. Following this model they were able to explain the widths, shapes, intensities and spectra of the light correctly and also as functions of experimental parameters such as driving pressure, frequency, gas concentrations, type of gases and temperature of the host liquid etc. So far this model explains all the experimentally observed quantities associated with SBSL. As a test of its validity this model also predicts a wavelength dependence of the pulse width for a strongly forced xenon bubble.

1.6 Importance of the Research

As Putterman aptly mentioned [53] " Among fluid phenomena, sonoluminescence (SL), the transduction of sound into light is unique in that the energy enters the

fluid at low energy and long wavelengths, where the equations of fluid mechanics apply, but the resulting fluid mechanical motion sets up a transformation of the sound energy into degrees of freedom, visible photons, which are not describable by the original equations of fluid mechanics. In sonoluminescence, the sound energy is concentrated by twelve orders of magnitude and emitted as a flash of light". This amazing degree of energy concentration achieved in sonoluminescence clearly draws the attention of researchers from all faculties of science and engineering.

Furthermore, research on this subject has profound effects on the question of using high power ultrasound in medical diagnostics. Is it safe to use high power ultrasound wave on human body or what is the effect of cavitation and associated phenomena on humans? The answers to all these questions are deeply related to the research on SL.

The research on MBSL, which is also closely related to that of SBSL revealed that exotic chemical species [22] could be created with the help of effects accompanied with SL. So better understanding of the phenomenon could lead to surprisingly new discoveries.

Although the mechanism behind SL is much debated, with the very active research in the subject, rather quick progress to uncover the mysteries of SL has been achieved. Does it require any exotic or new physics to answer the question of light emission from collapsing bubble? Hilgenfeldt [112] has answered that **no**

such exotic or new physics behind SL. The temperature inside the collapsing bubble in its present form is also not too exciting. However, the research in the subject won't stop here. Now the research should be directed towards maximizing the effect or in the words of Hilgenfeldt [120] **upscaling sonoluminescence.** As Robert Apfel [114] wonders what would be the temperature inside the bubble if one can make the bubble ten times or more larger in diameter. Would there be then the possibility of having some conditions suitable for nuclear (hot) fusion? As a next step could it be possible to uncover the parameter space such that the bubble - could be driven so hard that neutrons - the signature of fusion reaction would be detected? The answers to these questions are still unclear but as Robert Apfel mentions [114] "a small community of sonoluminescence researchers is quietly going on with this work, trying to avoid the hype that accompanied the **cold fusion** claims ten years ago". So it can be said the excitement of the subject will not die down in years to come.

Chapter 2

Bubble Dynamics

Introduction

In this chapter, a theoretical investigation of the motion of a single bubble in a liquid will be presented. The bubble is driven by a acoustic standing wave field which varies sinusoidally. The dynamics of the bubble is intimately related with the acoustic field and several other parameters of the host liquid. The coupling between the bubble and the liquid via the acoustic field manifests itself in mass and heat flow, optical and acoustical radiation, etc.. At first the equation of motion of the bubble with some specific assumptions will be developed. Furthermore, the equations of temperature and pressure inside the bubble which are closely related to the bubble motion or bubble radius will be derived. Secondly, different coupling

mechanisms between the bubble and the liquid will be presented. Finally, to get the radius vs. time curve $R(t)$, a numerical solution of the bubble equation will be performed. The plots of $R(t)$ and driving pressure vs. time, $P_a(t)$, calculated on the basis of the parameters of the experiments performed in our laboratory will be shown.

The approach presented in the rest of this chapter follows closely those of T. G. Leighton [119] and L. Kondic [137].

2.1 Bubble Equation

2.1.1 Response of a Bubble to a Static Pressure

Let us consider a bubble of radius R_0 in equilibrium in a liquid at a hydrostatic pressure P_0. The internal pressure within the bubble is given by

$$P_i = P_g + P_v, \tag{2.1}$$

where P_g and P_v are the pressures of the gas and the vapor of the liquid inside the bubble. Considering the pressure due to surface tension, the internal pressure is,

$$P_i = P_0 + \frac{2\sigma}{R_0} \tag{2.2}$$

where σ denotes the surface tension of the liquid. Hence the gas pressure inside the bubble,

$$P_g = P_0 + \frac{2\sigma}{R_0} - P_v \tag{2.3}$$

If the pressure in the liquid changes from P_0 to P_∞ in a quasi-static manner, the bubble will change from R_0 to R, in response to the change. The gas pressure within the bubble will be,

$$P = P_g \left(\frac{R_0}{R}\right)^{3\kappa} = \left(P_0 + \frac{2\sigma}{R_0} - P_v\right)\left(\frac{R_0}{R}\right)^{3\kappa} \tag{2.4}$$

Here it is assumed that the gas obeys a polytropic law and κ is the polytropic exponent. Hence the pressure immediately beyond the bubble wall is:

$$P_L = \left(P_0 + \frac{2\sigma}{R_0} - P_v\right)\left(\frac{R_0}{R}\right)^{3\kappa} + P_v - \frac{2\sigma}{R} \tag{2.5}$$

2.1.2 The Rayleigh Equation

In 1917, Lord Rayleigh published a pioneering paper [3] describing the collapse of an empty spherical cavity in an incompressible liquid known as "the Rayleigh cavity collapse". Since the cavity contains no gas and the surface tension of the liquid is ignored, the liquid pressure, P_L, just outside the bubble wall is zero. Therefore, the work done by the hydrostatic pressure P_∞, when the cavity has contracted from its initial radius R_m, to an instantaneous radius R is: $\frac{4}{3}\pi P_\infty (R_m^3 - R^3)$

This work is equal to the kinetic energy of the liquid. Thus

$$\frac{4}{3}\pi P_\infty (R_m^3 - R^3) = \frac{1}{2}\rho \int_R^\infty 4\pi r^2 \dot{r}^2 \, dr \tag{2.6}$$

where ρ is the density of the liquid.

Since the liquid is assumed to be incompressible and considering the rate of mass flow to be constant, we can write

$$\frac{\dot{r}}{\dot{R}} = \frac{R^2}{r^2} \tag{2.7}$$

where a dot represents derivative with respect to time. Substituting, Eq. (2.7) into Eq. (2.6) and by integrating we get,

$$\frac{4}{3}\pi P_\infty (R_m^3 - R^3) = 2\pi\rho R^3 \dot{R}^2 \tag{2.8}$$

and therefore,

$$\dot{R}^2 = \frac{2P_\infty}{3\rho}\left(\frac{R_m^3}{R^3} - 1\right) \tag{2.9}$$

This equation gives the velocity of the cavity wall. It is to be noted that the velocity reaches infinity as the bubble radius approaches zero ($R \to 0$).

2.1.3 The Rayleigh-Plesset (RP) Equation

To derive the RP equation the following assumptions are made:

- The bubble remains spherical at all times. This radial symmetry will be satisfied in the long wavelength limit of the acoustic field, meaning $kR \ll 1$, where k is the wave number of the sound field and R the radius of the bubble.
- The liquid is incompressible.
- Spatially uniform conditions for temperature, pressure, and density etc. exist inside the bubble throughout the bubble oscillation.
- There is no mass or heat flow between the liquid and the bubble.
- No body forces, such as gravity, are present.

It is to be noted that these assumptions put serious limitations on the model particularly when the pulsations are large and the bubble wall velocity becomes comparable to the velocity of sound in the liquid. However, in most situations, we are able to reproduce the bubble motion very accurately, for most of the acoustic period, except for a few nano seconds near the minimum of the collapse.

Let us now assume that a bubble of equilibrium radius R_0 is at rest in an incompressible viscous liquid. A hydrostatic pressure P_0 acts on the bubble at time $t < 0$. If a time varying pressure $P(t)$ acts on the liquid so that the total liquid pressure at some point remote from the bubble can be represented by

$$P_\infty = P_0 + P(t) \tag{2.10}$$

at time $t > 0$, it can be expected that the bubble radius will change from R_0 to R in response to the change of this forcing pressure. Equating the work done by the hydrostatic pressure P_L in the liquid layer adjacent to the bubble minus the work done by P_∞, with the kinetic energy of the liquid surrounding the bubble gives,

$$\int_{R_0}^{R}(P_L - P_\infty)4\pi R^2\, dR = 2\pi\rho R^3\dot{R}^2 \tag{2.11}$$

Following Poritsky [121] an extra term, $\frac{4\mu\dot{R}}{R}$ resulting from the continuity of the normal stress at the liquid-gas interface, has been added to the Eq. (2.5) which yields,

$$P_L = \left(P_0 + \frac{2\sigma}{R_0} - P_v\right)\left(\frac{R_0}{R}\right)^{3k} + \frac{2\sigma}{R} - \frac{4\mu\dot{R}}{R} \tag{2.12}$$

where μ is the coefficient of viscosity of the liquid.

Now substituting Eqs. (2.10) and (2.12) in Eq. (2.11), then differentiating it with respect to R and following a few simple mathematical steps we obtain:

$$R\ddot{R} + \frac{3}{2}\dot{R}^2 = \frac{1}{\rho}\left[\left(P_0 + \frac{2\sigma}{R_0} - P_v\right)\left(\frac{R_0}{R}\right)^{3k} + \frac{2\sigma}{R} - \frac{4\mu\dot{R}}{R} - P_0 - P(t)\right] \tag{2.13}$$

Lauterborn [122] proposed that this equation be known as RPNNP equation after the names of its contributors Rayleigh [3], Plesset [123], Noltingk and Neppiras [33, 124], and Poritsky [121]. However, this equation is well known as the Rayleigh-Plesset equation. In case of SL experiments, the time varying pressure term $P_a(t)$ should be represented by

$$P_a(t) = -P_a\cos(\omega t) \tag{2.14}$$

as the bubble is driven by a sinusoidal acoustic wave. Here, ω denotes the angular frequency and P_a is the sound pressure amplitude. The negative sign represents the initial tension at $t = 0$.

It is to be noted that the Eq. (2.13) can also be written in the form (see [74] and the references therein).

$$R\ddot{R}+\frac{3}{2}\dot{R}^2 = \frac{1}{\rho}\left[P_g(R) - P_0 - P_a(t) - \frac{2\sigma}{R}\right] - \frac{4\mu\dot{R}}{\rho R} + \frac{R}{\rho c}\frac{d}{dt}\left[P_g(R) - P_a(t)\right] \quad (2.15)$$

To close the Rayleigh-Plesset equation (i.e. 2.15), an equation of state for the gas has to be taken into account. For rapid changes in the bubble radius the adiabatic equation of state [125] for the gas will be used. The gas pressure $P_g(R,t)$ inside the bubble is assumed to obey a van der Waals type process equation

$$P_g(R,t) = P_g(R(t)) = \left(P_0 + \frac{2\sigma}{R_0}\right)\left(\frac{R_0^3 - h^3}{R^3(t) - h^3}\right)^{\kappa} \quad (2.16)$$

and temperature $T_g(R)$ is given by

$$T_g(R) = \frac{P_0 R_0^{3(\kappa-1)}}{(R^3 - h^3)^{(\kappa-1)}} \quad (2.17)$$

where h the van der Waals hard-core radius and is given by

$$h = \frac{R_0}{8.86} \quad (2.18)$$

(for argon) [126].

It is to be noted that the Eq. (2.17) assumes homogeneity of the pressure inside the bubble. This however is not satisfied during the final moment of the

bubble collapse. Therefore, a more elaborate investigation of gas dynamics is required. But the phase of the collapse only lasts a few nanoseconds of the several microsecond period of the bubble motion. Hence this approximation does not effect the bubble equation significantly.

In general there is no analytical solution of the Rayleigh-Plesset equation (2.15). For large amplitude oscillations, it can only be solved numerically. The numerical solution of this equation will be presented in the next section. But before going any further we would like to discuss the linear resonance frequency of the bubble. From linearization of Eq. (2.15) i.e. by putting $R = R_0 + r$ and assuming small-amplitude oscillation, i.e. $r/R_0 \ll 1$, we obtain the following equation involving r

$$\ddot{r} + \omega_r^2 r = \frac{P_a}{\rho R_0} \sin(\omega_a t) \tag{2.19}$$

where only the first order terms are retained neglecting the higher order terms. Viscosity and the acoustic radiation terms are not taken into account here as well. Further, ω_r denotes the resonance frequency given by

$$\omega_r^2 = \frac{1}{\rho R_0^2}\left[3\kappa\left(P_0 + \frac{2\sigma}{R_0}\right) - \frac{2\sigma}{R}\right] \tag{2.20}$$

For bigger bubbles the surface tension term can be neglected and Eq. (2.20) can be written as

$$\omega_r^2 = \frac{3\kappa P_0}{\rho R_0^2} \tag{2.21}$$

Eq. 2.21 was first derived by Minnaert [127] assuming $\kappa = 1$.

For large air bubbles in water $f_0 R \sim 3$ where f_0 is the frequency, expressed in Hertz and R, is in meters. Using this approximate formula, it follows that an air bubble of $4\mu m$ would resonate at 1 MHz, while for an applied frequency of 20kHz, the resonant bubble radius would be about 160 μm.

2.2 Different Coupling Mechanisms

2.2.1 Standard Diffusion and Rectified Diffusion

From our every day experience it is noticed that a gas bubble in a liquid dissolves away slowly just because the gas inside diffuses out to the liquid. So the question that naturally comes to mind is, how does a gas bubble remain stable for many hours in a liquid. To understand this problem we have to note that there are two competing effects that take place. One of them is the standard mass diffusion due to the difference of the gas concentrations between the bubble and the liquid. This is a relatively slow process and acts over the time scale of seconds [128]. The second one, known as the rectified diffusion process, depends on the acoustic pressure [80, 129]. Rectified diffusion is a direct consequence of the application of a sound field. There are two mechanisms involved in rectified diffusion.

The first mechanism is the surface area effect. During the compression phase

of the acoustic period, when the bubble contracts below the equilibrium size, the concentration of gas inside the bubble increases, and as a result gas diffuses out of the bubble. In contrast, during the expansion phase, when the bubble expands beyond the equilibrium size, the concentration of gas in the interior of the bubble decreases, resulting in a back flow of gas from the liquid to the bubble. Because the bubble spends more time in these larger radii than at the smaller radii and since the rate of diffusion of gas is directly proportional to the surface area of the bubble, there is a net increase in the amount of gas in the bubble.

The second mechanism is the shell effect. The concentration gradient between the dissolved gas in the liquid and the gas inside the bubble determines the diffusion rate. Considering a spherical shell of liquid surrounding the bubble, when the bubble contracts, the shell of the liquid thickens, leading to a reduction of gas concentration near the bubble wall. Therefore, more gas diffuses out of the bubble than when the bubble is at the equilibrium radius. On the other hand, when the bubble expands, the liquid shell becomes thinner, resulting in an increase in the gas concentration and consequently the rate of gas diffusion is greater than the average. Therefore, there is a net effect of convection enhanced rectified diffusion.

Hence, the two processes, standard diffusion and the rectified diffusion may not compensate each other and the bubble can grow with time. The reason why the net mass flow can be neglected is that when the bubble reaches its steady state

regime meaning the total mass inflow is equal to total mass outflow. It has been observed experimentally [27] that the bubble requires a few seconds to attain this equilibrium radius. For this reason we can neglect this effect in our approximate treatment of bubble dynamics.

2.2.2 Thermal Coupling

The heat conduction between the bubble and the liquid must be considered. Nepiras [128] assumed that there is no heat flow between the bubble and the liquid in the experimental parameter space of SL regime. This means that the bubble interior can be assumed to follow the adiabatic law. However, the heat flow has been considered in greater detail by Crum [130, 131]. Prosperetti [118, 132, 133, 134, 135] and later by Hilgenfeldt [113, 136]. The interplay of changes of gas temperature inside the bubble due to bubble dynamics (expansion and compression of gas) and temperature changes because of thermal conduction are taken care of by the polytropic exponent, κ. The previous authors argued that if the bubble motion is faster during collapse than the time scale of heat conduction through the bubble, then an adiabatic collapse can be assumed, where $\kappa = \gamma$ where γ is the ration of specfic at constant pressure to that of at constant volume ($\gamma = \frac{5}{3}$ for argon). However, during the expansion phase when the bubble motion is slow,

heat conduction occurs faster than the bubble wall velocity, so that the bubble acts isothermally, i.e. $\kappa = 1$. So in general we can assume the value of κ lies between γ and 1. In the formulation of bubble equation, it is assumed that the bubble follows adiabatic law for the whole cycle of its motion. Though this assumption has to be relaxed to get a more precise equation of bubble motion, yet for the present purpose, the assumption of no heat exchange across the bubble is quite accurate in reproducing the experimental data.

2.2.3 Spatial Uniformity of the Gas in the Bubble

Spatial uniformity of the physical and thermodynamic properties of bubble interior has been assumed in deriving the equation of motion of the bubble wall. A uniform bubble interior means the temperature, pressure, and the density of the bubble content are uniform throughout the whole bubble. The light emission must be determined by the uniform temperature inside the bubble. For most of the theoretical models described earlier it is also assumed that oscillations of the bubble about its equilibrium radius are small. Hence spatial uniformity in the interior of the bubble can be assumed without much of an error [137]. This assumption considerably simplifies the problem. But there is no clear experimental evidence whether this is true or not. However, when the bubble is driven strongly, meaning

when the bubble wall velocity becomes comparable to or even greater than the local speed of sound in the gas, this assumption has to be relaxed in order to understand this problem in more detail. Clearly, for strong enough forcing when the bubble wall velocity attains approximately four times the velocity of sound in the gas [138, 64], shock waves can be generated inside the gas which will bounce back and forth inside the bubble and the spatial temperature distribution in the bubble will be highly inhomogeneous [73, 115, 139, 140, 141]. But following Hilgenfeldt *et al.* [112, 113] it can be seen that even by assuming spatial uniformity we can reproduce most of the experimental observations quite accurately.

2.3 Solution of the Rayleigh-Plesset Equation

The numerical solution of the Rayleigh-Plesset equation (2.15) yields the radius of the bubble as a function of time. In the case of SBSL, the acoustic driving pressure is slightly above 1 atm. and the size of the bubble is much smaller than the resonant bubble size. The bubble radius, (R) vs. time. (t) curve takes on a characteristic form as shown in Fig. 2.1(a). Values of the parameters used in the numerical solution of the R-P equation are measured in our laboratory. Adaptive time steps were chosen to solve nemerically the R-P equation. The time step was $5 * 10^{-}14$ sec from 17.5 μs to 22.5 μs. For the rest of the acoustic cycle the time

step was $5 * 10^{-}12$ sec. Values of these parameters are listed in the Table 2.1. The acoustic driving pressure is shown in Fig. 2.1(b).

The solution of the R-P equation represents the typical nonlinear response of the bubble where the bubble grows many times larger than its equilibrium radius, R_0. In this particular example, the bubble grows from an R_0 of 6.0 μm to a R_{max} of 49.0 μm. As shown in Fig. 2.1 in one acoustic period, during the negative part of the driving field when the net pressure goes negative, the bubble grows slowly. Interestingly enough, when the bubble attains its maximum size, the driving field turns into compression phase simultaneously, leading to a positive net pressure. The liquid surrounding the bubble then acts like a piston and the bubble undergoes a catastrophic collapse which is then followed by a few after bounces as shown in the Fig 2.1(a). The period of oscillation of the after bounces is determined approximately by the reciprocal of the pulsating resonance frequency of a free bubble. The numerical solutions of the R-P equation obtained here are in very good agreement with our experimental data [99, 100, 101]. This will be discussed later in Chapter 4.

Conclusion

In this chapter, the theory of bubble dynamics has been discussed starting from the very basics of the response of the bubble to a static pressure. The bubble

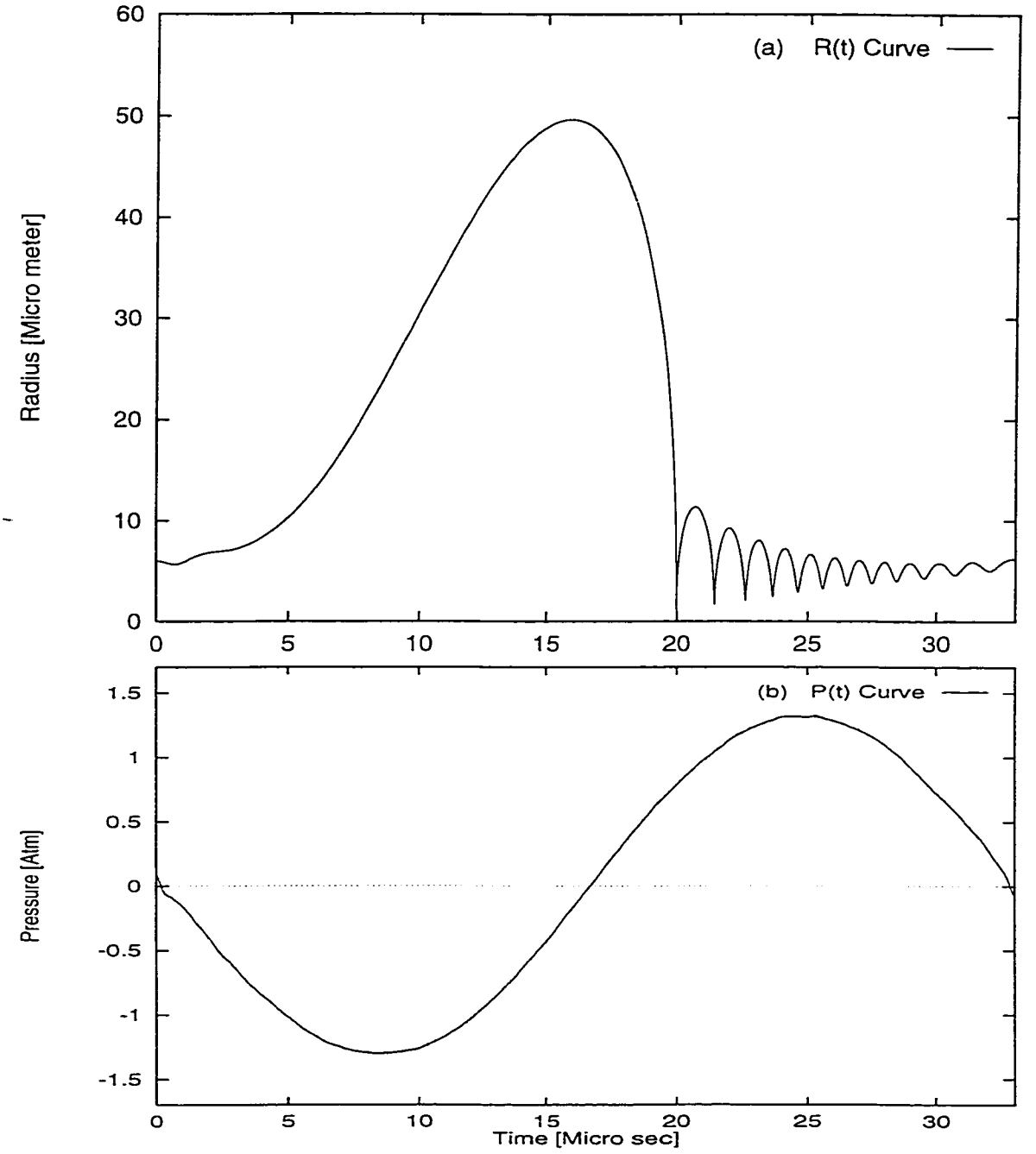

Figure 2.1: Radius and driving pressure as a function of time

Table 2.1: **Table of Parameters**

Values of the Parameters used in the R-P Equation			
Parameter	*Symbol*	*Value*	*Unit*
Ambient Pressure	P_0	$1.01325 * 10^5$	$Pascal$
Ambient Temperature	T_0	294	K
Driving Pressure Amplitude	P_a	$1.49 * 10^5$	$Pascal.$
Ambient Radius	R_0	$6.0 * 10^{-6}$	m
Driving Frequency	f	$30.6500 * 10^3$	Hz
Core Radius	h	$\frac{R_0}{8.86}$	m
Ratio of Sp. Heat	κ	1.4	-
Speed of Sound in the Liquid	c	$1.550 * 10^3$	ms^{-1}
Density of the Liquid	ρ	$1.033 * 10^3$	kgm^{-3}
Viscosity of the Liquid	μ	$2.1 * 10^{-6}$	m^2s^{-1}
Surface Tension of the Liquid	σ	0.0694	kgs^{-2}

equation of the particular case of interest for SBSL has also been described in detail. The pressure and temperature generated by the dramatic collapse can be calculated by the Eqs. (2.16) and (2.17). The adiabatic equation of state for the gas has been considered. From the $R(t)$ curve it is also clear that the bubble wall attains at least the speed of sound in the liquid, thus violating the basic assumption of incompressibility of the liquid. Still as will be seen, the R-P equation reproduces the experimental $R(t)$ quite nicely. Different coupling mechanisms have also been discussed proving the validity of several assumptions made during the derivation of the R-P equation. Finally, a typical $R(t)$ along with a typical driving pressure $P(t)$ curve have been shown in figure 2.1. For a complete description of the SL phenomenon, the thermodynamic properties of the gas, the concept of the allowance of the generation of shock waves and the plasma properties of the gas should be taken into account.

Chapter 3

Experimental Setup

Introduction

In this chapter, a detailed description of the experimental setup along with the experimental methodology to investigate SBSL will be presented. At first, the experimental setup will be described and a schematic diagram of the setup will be shown as well. The experimental setup consists of two systems: (i) SBSL production system and (ii) SBSL detection system. Secondly, a complete description of how to produce SBSL will be documented. The methodology of producing SBSL can divided into two parts such as (i) preparing the liquid and (ii) step by step experimental procedure. Furthermore, detection of SBSL phenomenon such as the SL pulse, AE pulse and the light scattering to measure the $R(t)$ will be discussed in

a separate section. In this context, a detailed description of the experimental setup to study the effect of ambient pressure on SBSL will also be presented. Finally, a conclusion will be drawn at the end of the chapter.

3.1 Experimental Setup

SBSL Production System

Before the experiment can be set up, because of the low level of SL intensity, it is necessary to isolate it from the ambient light of the laboratory. A light tight wooden box of dimensions 4ftx2.5ftx2.5ft was built. It was painted black to reduce the reflections of light. To provide the necessary electrical supplies bulkhead wall mount BNC connectors were used. During the experiment, the box can be completely sealed off from stray light by just closing the front panel tightly with the help of a latch. A rubber gasket was used to provide a light-tight fit around the edges. The levitation cell as well as all the detection systems are placed in side the box.

The schematic diagram of the experimental setup is shown in figure 3.1. The levitation cell used in the experiments was a 500 ml spherical flask made of glass (Pyrex). The radius of the flask is approximately 5 cm. A neck (B 24/29) of diameter 2.4 cm and length 5 cm was attached to the flask. The flask was filled

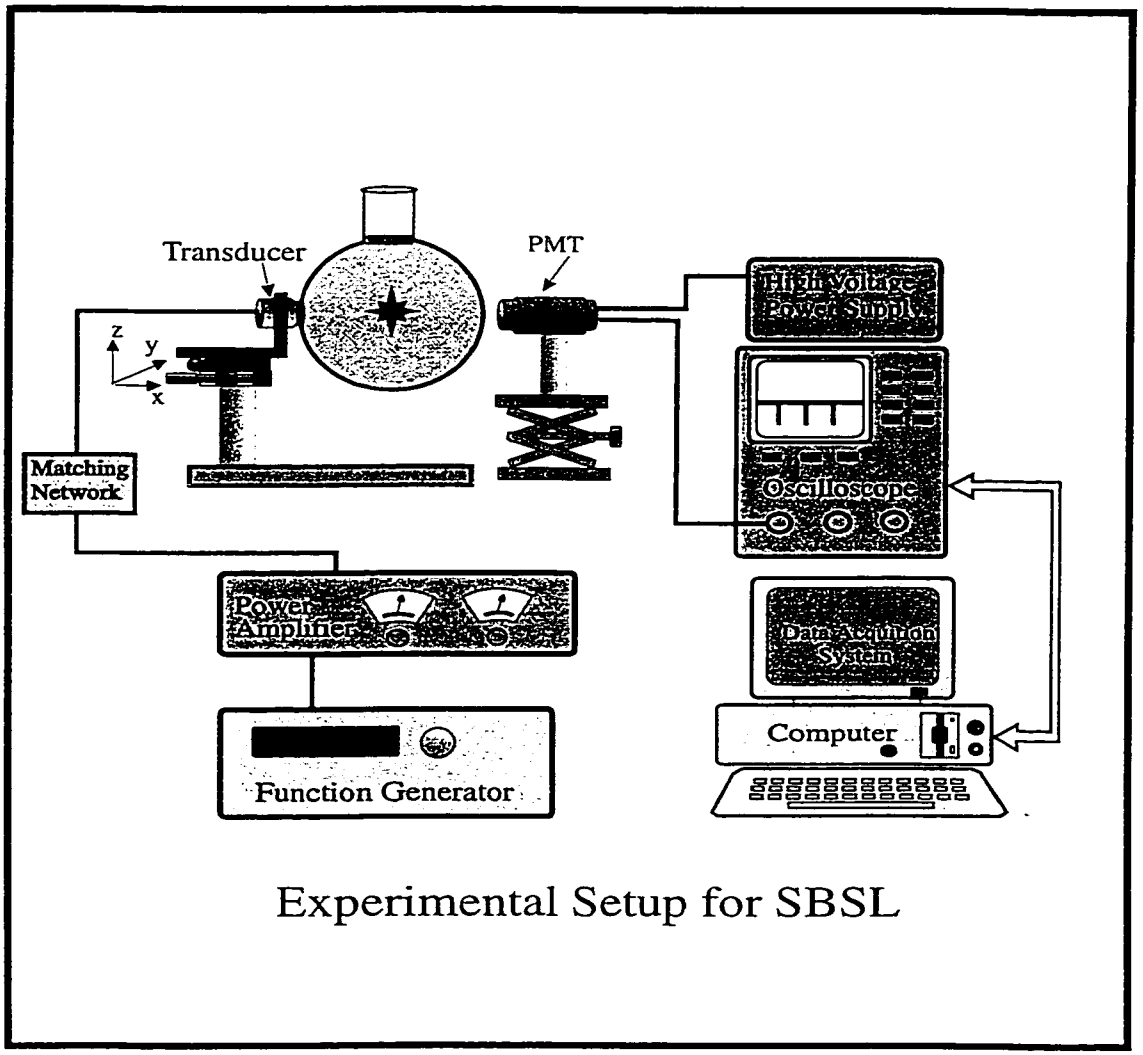

Figure 3.1: Schematic diagram of the experimental setup

up to the bottom of the neck with a water/glycerine mixture. The preparation of the liquid will be described in the next section. The liquid mixture was filled to the bottom of the neck so that the fluid level makes the mass of the liquid approximately spherical, thus minimizing the free surface area. The shape of the surface of water in the neck would be deformed by any vibration and consequently affect the phenomenon. Therefore, flasks with smaller necks are preferable for the experiments.

The stationary acoustic field for levitating the bubble was provided by a piezo-electric transducer which was glued to the flask with silicone II (GE brand). The lead zirconate titanate (PZT) transducer (Sensor - from Sensor Technology Limited) is cylindrical in shape. It is housed in a steel jacket and provided with a BNC connector for electrical signal input. The diameter and thickness of it are about 4 cm each. The natural resonance frequency of the transducer is 50 kHz. It was however, driven at the fundamental resonance frequency of the flask system about 17.5 kHz in our experiments. Due to its piezo-electric property the ceramic produces mechanical vibration at the frequency of the impressed driving signal. This mechanical vibration was then coupled to the flask with the help of a coupler such as silicone. To increase the amount of coupling, a small glass lens was fused to the spherical flask. The lens is plano-concave in shape with the same curvature as that of the spherical flask. The diameter of the lens is about 2.5 cm. The flat end face

of the transducer was glued to the flat surface of the lens with silicone adhesive. For a good and rigid bonding between the two surfaces it was kept undisturbed for more than 48 hours. The whole levitation cell was mounted by the transducer on a two dimensional positioning system (see figure 3.1). The resolution of movement in both directions was accurate to 50 microns.

The flask system was driven at its fundamental resonance frequency of about 17.5 kHz. The precise frequency control was provided by a Wavetek function generator (Model 29). The resolution of the synthesizer is accurate to 0.1 Hz at the typical operating frequency. The stability is typically 1 ppm per degree outside the room temperature. The sinusoidal output of the function generator was first amplified by an stereo power amplifier (model Realistic MPA-100 from Inter TAN Canada Ltd.). It delivers 100 watts per channel (8 ohms) from 20 Hz to 20 kHz. There is an extremely bad impedance match between the output of the amplifier and the input of the transducer. The output impedance of the amplifier is less than an ohm whereas the input impedance of the transducer is of the order of kilo-ohms. Generally, the transducer is a capacitive element with high input impedance. So to achieve the maximum amount of power transmission through the transducer a matching network is necessary. This impedance matching was done by inserting an audio output transformer (Model 1650 R from Hammond Manufacturing Co. Limited) between the power amplifier and the transducer. The

primary impedance is 5.0 kohms and the secondary is 4-8-16 ohms. The power output of the transformer is 100 Watts. A small PZT (lead zirconate titanate) pill transducer is glued to the bottom of the flask to monitor the acoustic driving pressure in a non-invasive manner. Piezo-electricity is a reversible process, so that when a mechanical wave passes through a piezo-electric crystal or ceramic, the charges in the crystal plane oscillate producing an electrical signal at the same frequency as that of the incident mechanical wave. The preparation of the liquid and the step by step experimental procedure how to get SL will be described next.

3.2 Producing SBSL

3.2.1 Preparing the Liquid

One of the most important parts of the SBSL experiment is to degas the water. The physical picture considered here is the following: A single bubble is in clean water saturated with dissolved air. The bubble is at rest and it is isolated meaning that it is not trapped on a wall or on a minute dust particle. Such a gas bubble would generally dissolve as gas diffuses out of the bubble to the surrounding liquid. However, if a sound field is applied, the pulsations of the bubble may allow the diffusion of gas into the bubble. This process known as rectified diffusion has

already been discussed in section 2.2.1. For a sound pressure amplitude of a few atmospheres, gas inflow due to rectified diffusion becomes so large that a gas bubble in air saturated water would grow rapidly and eventually it will become so large that it would be impossible to trap the bubble by the acoustic field. See section 3.2.3 for more details. In order to keep the bubble stable and make it pulsate in the acoustic field such that sonoluminescence can be obtained, a part of the air must be removed. By reducing the gas concentration in the liquid, the net gas inflow could be balanced with the gas outflow due to standard diffusion process and hence an equilibrium condition can be achieved. This process of reducing the air concentration is known as degassing of the liquid.

Two different de-gassing techniques have been used in the present work. The first was by simple boiling. A 1000 ml flat bottomed spherical shaped flask (Pyrex) fitted with an air tight stopper was used. One end of the glass stopper was drawn to a very narrow hollow rod of diameter of about 5 mm by heating in the glass blowing center. A rubber tubing of length about 5 cm was then attached to the rod. This whole stopper system prevents or slows down the re-entry of air into the flask and only allows the steam to pass out from the system.

Since the volume of the levitation cell used in the experiments was 500 ml, approximately 750 ml (three fourths of the flask) of water was poured into the flask. The water used in the experiment was nano-pure water with typical resistivity of

16-17 MOhm-cm. The flask was then placed on a hot plate and kept at rolling boiling for about three quarters to an hour. The rubber tubing was then clamped tightly and placed in the sink and allowed to cool down in flowing water for almost half an hour. There would be a vacuum created on top of the water in the flask which would help keep the water well degassed.

Approximately 120 gm of 99.99% pure glycerine was carefully poured into the levitation cell. The degassed water was then slowly poured into the cell so that the water runs down the cell's wall. This was done just to avoid quick regassification [142]. Then the whole liquid was slowly and carefully stirred by a glass rod to obtain a homogeneous mixture of water and glycerine. The mixture was approximately 25 weight percent of glycerine. The levitation cell was then sealed air tight with a sub-a-seal septum. A stainless steel wire was inserted through the top of the septum to poke the liquid surface to create air bubbles.

Secondly, degassing can be done cavitating the liquid vigorously by ultrasound while keeping a vacuum pump running. A Drierite ($CaSO_4$) column packed in a glass cylinder acts as water trap preventing water vapor to contaminate the pump oil. This process was performed whenever the liquid in the cell became gassy after a few days.

3.2.2 Measuring the Gas Concentration

Once the liquid has been prepared, the next step was to measure the dissolved gas concentration in it. This has been done by two different methods. Firstly, by using a Dissolved Oxygen Meter (DO Meter - from Orion model 810). This meter measures dissolved oxygen concentration using "Clark type" polarographic electrodes. Electrodes measure the partial pressure of oxygen, which is the fraction due to oxygen multiplied by the total pressure. These electrodes have a thin organic membrane covering a layer of potassium chloride (KCl) based electrolyte and two metallic electrodes. Oxygen diffuses through the membrane and is electro chemically reduced at the cathode. A carefully fixed polarizing voltage is imposed across the electrodes so that only oxygen is reduced causing a measurable amount current to flow. The greater the oxygen partial pressure, the more oxygen diffuses through the membrane in a given time and hence the more current. A thermistor is built into the probe measurement system, which compensates for the membrane temperature. The atmospheric pressure has been manually entered into it prior to calibration. The meter uses the cathode current, sample temperature, barometric pressure and salinity information to calculate the dissolved oxygen in the liquid. The instrument needs a calibration point to correctly measure the oxygen concentration. This can be done quickly in water saturated air, and is done in special

calibration chamber with a water reservoir. Once the calibration is done, the concentration of oxygen has been first measured in the non-degassed water/glycerine mixture having the same glycrine concentration as used in the experimental work. Then the oxygen concentration has been measured in the degassed water/glycerine mixture. The degree of degassing has been calculated by the ratio of the oxygen concentration of the degassed to the non-degassed liquid. Generally the gas concentration in the experimental liquid varied from 20% to 40% of the saturation concentration.

- Secondly, the concentration of oxygen and air in the liquid have also been measured by a fiber optic sensor system (FOXY - from Ocean Optics , Inc.). The probe is an optical fiber one end of which is coated with a thin layer of hydrophobic sol-gel material. A ruthenium complex is trapped in the sol-gel matrix which protects it from water. A LED (light emitting diode) excites the ruthenium complex at $\sim$ 475 nm and it emits energy at $\sim$ 600 nm. which will be transferred to the oxygen molecule in a non-radiative manner when it encounters an oxygen molecule. Hence the fluorescence signal will be decreased. The degree to which process occurs depends on the concentration of oxygen molecules. The fluorescence is related quantitatively to the partial pressure of oxygen through the Stern-Volmer equation: $\frac{I_0}{I} = 1 + k_{P_{O_2}}$, where I_0 is the intensity of fluorescence at zero pressure of oxygen and I is the intensity of fluorescence at a pressure P of oxygen. k is the

Stern-Volmer constant.

The FOXY kit consists of a bifurcated fiber, a LED source, and a fiber optic spectrometer (S2000 Miniature Fiber Optic Spectrometer from Ocean Optics, Inc.). Basically, the spectrometer measures the intensity (in terms of counts) of the two wavelengths. A two point calibration has been done (one at zero oxygen and another one at normal air) to obtain the value of k. Since the medium of measurement is water/glycerine, the calibration for zero oxygen has been done in water/glycerine (glycrine concentration was the same that had been used in our experiments) with zero oxygen. The oxygen in water/glycerine was stripped off by adding a pinch of sodium hydrosulphite. Once the calibration was done, the oxygen concentration was found out by putting the probe in the liquid. In this case, as expected the oxygen concentration varied from (20% - 40%) of saturation concentration. The concentration of gas in the liquid has been measured several times during the experiment.

3.2.3 Step by Step Experimental Procedure

Once the liquid has been prepared and its gas concentration has been measured, the next step is to find out the proper resonance frequency of the flask system. This has been done by inserting a PZT hydrophone (SPRH-S-1000 from Specialty

Engineering Associates) into the liquid through the neck of the flask from the top. The hydrophone is 1.0 mm in diameter and held magnetically with the help of a Z-directional positional system (see figure 3.1). The hydrophone was positioned in such a way that the tip of it rests roughly at the center of the flask. The output of the hydrophone was fed into the input of a A101, 100 MHz preamplifier (from Specialty Engineering Associates) the output of which was connected to a Lecroy 9310M, 300 MHz dual channel scope. The coupling of the scope was kept at 50 ohm. The hydrophone is a high output impedance instrument, so a preamplifier with a high input impedance and a 50 ohm output impedance has been used to properly match the impedances. Once the hydrophone was properly set, the audio amplifier was tuned to a frequency of about 17 kHz (see Table 3.1 for a rough estimate) . The volume control knob of the amplifier was then turned slowly so that the output of the hydrophone could be observed properly on the scope. The voltage division of the scope was set to about 20 mV/div. The signal usually reads (100 mV peak to peak). The frequency was then varied and the output of the hydrophone was observed closely. When the output became maximum a bubble was inserted by poking the liquid surface by a needle or a wire. If the bubble goes straight to the center of the flask then most probably the resonance has been found. But to become 100% certain the drive amplitude could be slowly increased without changing the frequency to observe if there is any light coming out from the

bubble in a darkened room. If the bubble does not emit light or moves away and ultimately vanishes then another resonance has to be found out by the same way as described above. If the bubble is trapped and emits light, the acoustic drive amplitude could be set in this setting.

After the resonance frequency was found, the drive amplitude was increased gradually. The bubble movement as a function of acoustic drive has been discussed in greater detail by Gaitan *et al.* [45] and Barber *et al.* [51]. The various regimes of bubble motion as a function drive amplitude, P_a has been shown in figure 3.2.

In a recent paper Matula *et al.* [147] discussed the bubble levitation in SBSL regime in the light of the Bjerknes force. Equating the average Bjerknes force with the average force due to buoyancy the equilibrium position of the bubble has been calculated. It has been shown that at low driving pressure, during the negative part of the acoustic cycle (when the bubble is relatively large) the bubble is pushed towards the pressure anti-node. While during the compressive part of the cycle (when the bubble is small), the bubble has been forced away from the anti-node. However, as the volume is smaller in the latter case, the force is also smaller. As a result, over a full acoustic cycle the bubble is directed towards the pressure anti-node. For more complete reference please see [148, 149, 150].

At low drive amplitude, the bubble would rise to the surface as the buoyant forces will be dominant. So the bubble could not be trapped. Above the **trapping**

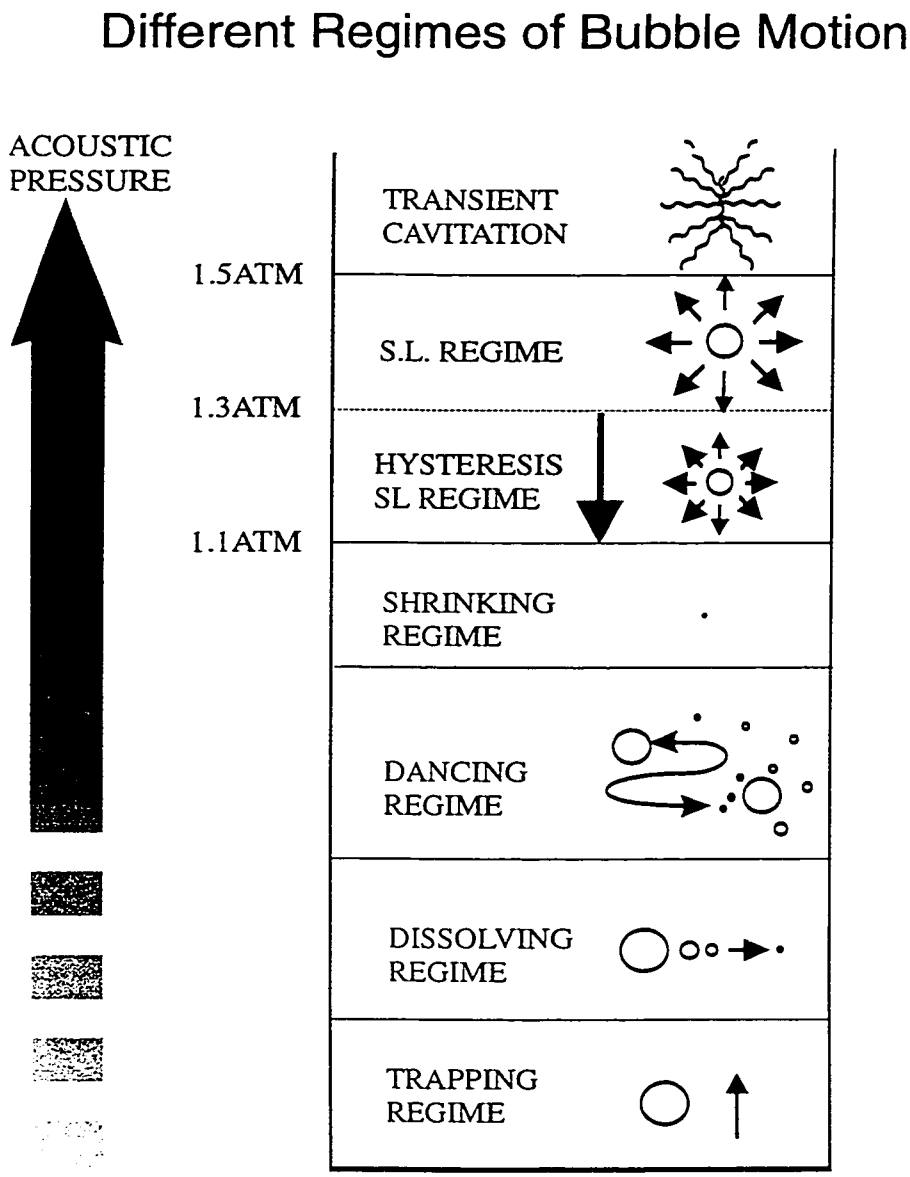

Figure 3.2: Bubble regime as a function of drive amplitude.

threshold the bubble would stay around the pressure anti-node (near the flask center) and the bubble would automatically adjust its position so that the buoyant force is balanced by the Bjerknes force. The bubble would gradually dissolve if the drive is not kept above the **dissolving threshold.** As seen from the figure 3.2, the bubble loses its stability and starts dancing beyond the **dancing threshold.** In this regime the bubble moves violently around the center of the flask. The bubble pinches off microbubbles and this pinch off leads to a recoil of the bubble making it appear that the bubble is dancing. As the drive level is gradually increased, the dancing becomes vigorous and then all on a sudden the dancing ceases. The bubble then becomes stabilized however, the bubble shrinks in size so that it becomes almost invisible to the naked eye. With the gradual increase of drive level the bubble starts glowing very dimly at the **lower SL threshold.** But it gets brighter and brighter as the drive is increased. At or near the **upper SL threshold**, the bubble starts again pinching off microbubbles and due to recoil of the microbubbles the parent bubble appears to be dancing or jiggling. The bubble becomes dim and regains its brightness in the time scale of seconds. Unfortunately, the brightness cannot be increased indefinitely. Above the upper SL threshold, the bubble suddenly disappears, probably due to shape instabilities.

3.2.4 Acoustical Resonance Modes Inside the Spherical Cell

In this context, it is important to discuss the acoustic modes present inside the liquid filled spherical cell. The observation of SBSL depends on the possibility of trapping a single bubble in a stationary sound field. Such a field can be obtained by considering a volume of liquid enclosed in a spherical resonator of radius a oscillating in the radial direction [51]. Since the liquid is compressible but invisid, the oscillations will propagate as sound waves i. e. longitudinal displacement of the fluid. The normal modes of vibration can be found from the solution of the wave equation in spherical co-ordinate system with appropriate boundary conditions. The induced pressure $p(r,t)$ field obeys the three dimensional wave equation:

$$\frac{1}{r}\frac{\partial^2}{\partial r^2}(rp) + \frac{1}{r^2\sin\theta}\frac{\partial}{\partial\theta}(\sin\theta\frac{\partial p}{\partial\theta}) + \frac{1}{r^2\sin\theta}\frac{\partial^2 p}{\partial\phi^2} = \frac{1}{v^2}\frac{\partial^2 p}{\partial t^2} \tag{3.1}$$

where v is the speed of sound in the liquid.

Since the system is linear, a solution will be sought as a superposition of normal modes. It is expected that the pressure is finite at the origin and the velocity of the fluid particles would finite at the boundaries at any time and zero everywhere at $t = 0$.

Hence the standing wave modes inside the spherical cell will be given as:

$$p(r,\theta,\phi,t) = p_0 j_l(kr) P_m^l(\cos\theta)\sin(m\phi)e^{i\omega t} \tag{3.2}$$

where $k = \omega/v$ is the wave number and $P_m^l(\cos\theta)$ represents the associated Legendre polynomial.

Since the acoustic impedance of water is much larger than that of air [146], it is expected that the pressure at the boundaries ($p(a) = 0$) should be zero at any time. a is the radius of the sphere.The resonance frequencies at any time are given by:

$$\nu_{l,n} = \frac{v\alpha_{l,n}}{2\pi a} \tag{3.3}$$

where $\alpha_{l,n}$ are the zeros of the lth order spherical Bessel function.

$$j_l(\alpha_{l,n}) = 0 \tag{3.4}$$

It is to be noticed that equation 3.3 does not rely on m. For a given value of l, there are $l + 1$ possible values of $0 \leq m \leq l$. Hence $l + 1$ degenerate modes are expected with resonance frequencies $\mu_{l,n}$.

The physical situation of the experiment demands that, there should be pressure anti-node at $r = 0$, and there is no degeneracy. For spherically symmetric situations, $l = 0$ and hence m is also equal to zero. Hence the zeroth order spherical Bessel function is

$$j_0(kr) = \frac{\sin(kr)}{kr} \tag{3.5}$$

where zeros would exist if $\alpha_{0,n} = n\pi$. Hence from 3.3

$$\nu_{0,n} = \frac{vn}{2a} \tag{3.6}$$

are the frequencies of the spherically symmetric acoustic modes. The Table 3.1 below [51] lists all the resonance frequencies of water filled flasks used commonly in experiments. The speed of sound in the mixture has been taken to be $1.5 * 10^5$ cm/s. Figure 3.3 shows the lowest three modes with $l = 0$, and $n = 1, 2, 3$. Our experimental conditions are slightly different. We used water/glycerine mixture instead of pure water. Also the thickness of the glass and the open neck of the spherical cell have not been taken into account in the derivation of resonance frequency. That is why our experimental fundamental resonance frequency (17.5 kHz) is slightly higer than the calculated resonance frequency (15.2 kHz) for a 500 ml spherical cell filled with only pure water.

3.3 SBSL Emissions Detection Systems

Now that the phenomenon can be produced, it is time to measure a few phenomena associated with SBSL. Here a brief account of the detection system will be presented.

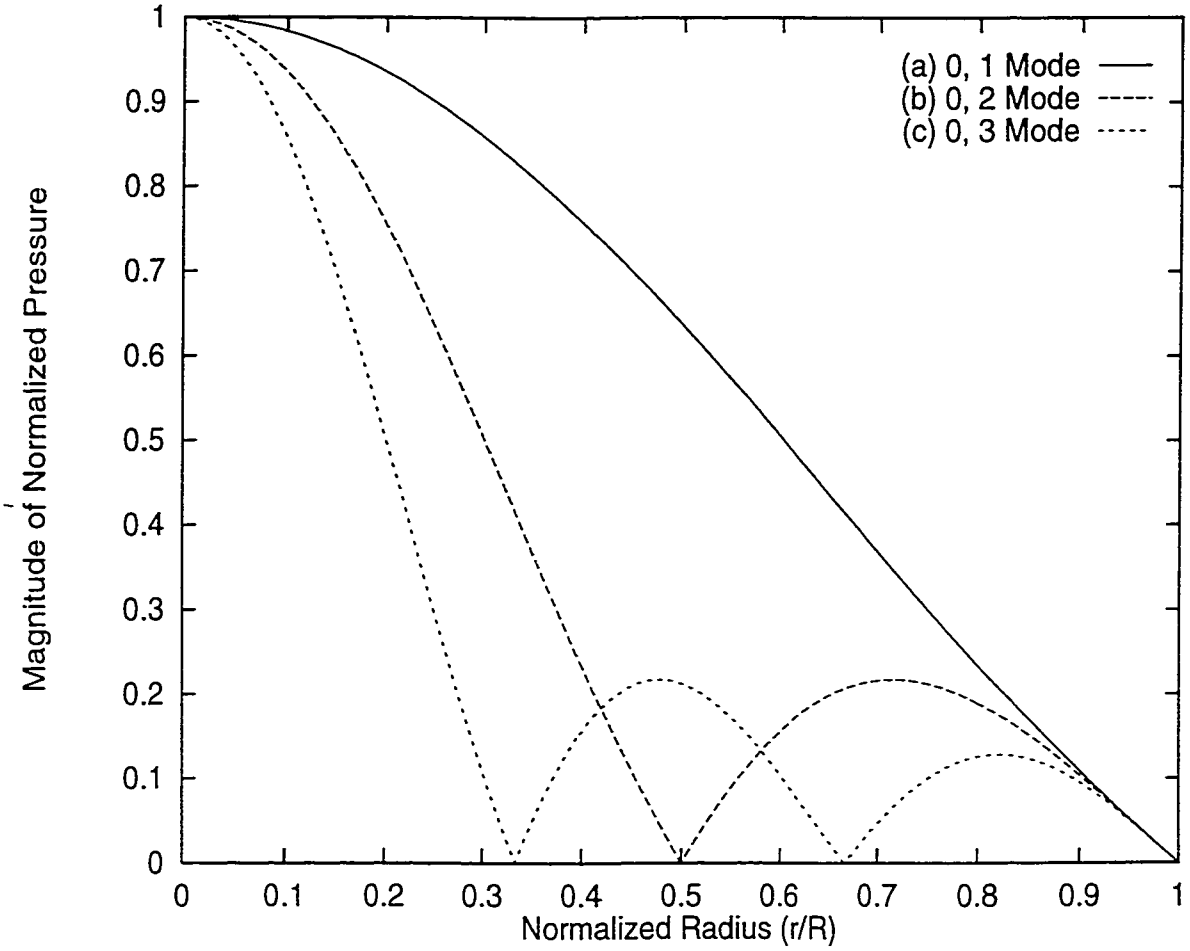

Figure 3.3: The first three spherically symmetric modes in a water-filled levitation cell. Both the radius and the pressure have been normalized. A three dimensional projection of the field yields spherically symmetric shape modes.

Table 3.1: **Theoretical Resonance Frequencies of Water Filled Spherical Flasks**

Volume	*Radius*	$f_{0,1}$	$f_{0,2}$	$f_{0,3}$
(ml)	(cm)	(kHz)	(kHz)	(kHz)
10	1.34	56.0	112.0	168.0
100	2.88	26.0	52.1	78.1
250	3.91	19.2	38.4	57.3
500	4.92	15.2	30.5	45.7
1000	6.20	12.1	24.2	36.3

3.3.1 SL Pulse Detection System

Gaitan *et al.* [27] observed the SL pulse and their original work clearly showed the synchronicity of light pulses with the driving acoustic signal. Later Barber *et al.* [46, 47] estimated a lower bound to the pulse width and number of photons emitted from SL. More recently, Gompf *et al.* [48] and others resolved the SL pulse width by time-correlated single photon counting technique. Here the goal is not to measure the pulse width but it is rather just to capture SL pulses and to

observe the their synchronicity with the acoustic drive signal. Naturally, a high gain photo-multiplier tube (PMT model Philips XP2230H) has been used. The PMT is a 44 mm aperture bi-alkaline type D photocathode. It is a 12 stage tube. This type of tubes are intended for the use in experiments where the number of photons to be detected is very low. The tube features a high cathode sensitivity and a good linearity with respect to photon flux at a fixed wavelength combined with very low background noise. The quantum efficiency of the tube at 401 nm. is about 28%. The gain of the tube at 2300 V is $3 * 10^7$. The typical anode pulse rise time is 1.6 ns. at 2500 V. The tube has been driven by a high voltage source (model 230-03R from BERTAN High Voltage) at a voltage of about 2300 V. This high voltage source can supply upto 3000 V. The output current varies from 0-5 mA.

With the PMT, emission of a SL pulse in each acoustic cycle has been observed. It has also been noticed that the pulses are highly synchronous. A closer look at figure 3.7 clearly shows that the SL pulse comes once in each acoustic cycle when the bubble is at or near its minimum radius. The figure 3.7 shows the synchronicity of the SL pulse with the acoustic drive while an individual SL pulse could not be resolved with the help of this experimental setup, it could be used to determine the number of photons emitted by the sonoluminescing bubble. This will be discussed in the next chapter. Figure 3.4 shows the SL pulse emitted by a collapsing bubble.

The PMT was driven at a voltage of 2300 Volts by a high voltage source.

3.3.2 AE Pulse Measurement System

It is expected that when the bubble undergoes a dramatic collapse, it would emit a SL pulse as well as an acoustic pulse in the liquid surrounding the bubble. Hallaj *et al.* [143] reported the emission of acoustic pulses from the collapsing bubble. Later Weninger *et al.* [64] observed the acoustic emission and measured the amplitude of the principal AE pulse. Matula et al. [66] and Dan *et al.* [65] presented a detailed investigation of the acoustic emission associated with SBSL.

In our laboratory, two very sensitive and sophisticated hydrophones have been used to measure the acoustic emissions from the bubble. One of them (model SPRH-S-1000 from Specialty Engineering Associates) is 1 mm in diameter stainless steel jacketed PZT hydrophone. According to the manufacturer, this hydrophone has an almost linear response in the 1 to 30 MHz range. This hydrophone has been calibrated 1-20 MHz from the manufacturer. As mentioned earlier when a mechanical wave passes through a piezo-electric crystal, the charges in the lattice structure oscillates at the same frequency as that of the mechanical wave and as a result an electrical signal will be generated. By noting this signal and with a proper calibration in terms of voltage/Pa, it is possible to find out the pressure amplitude

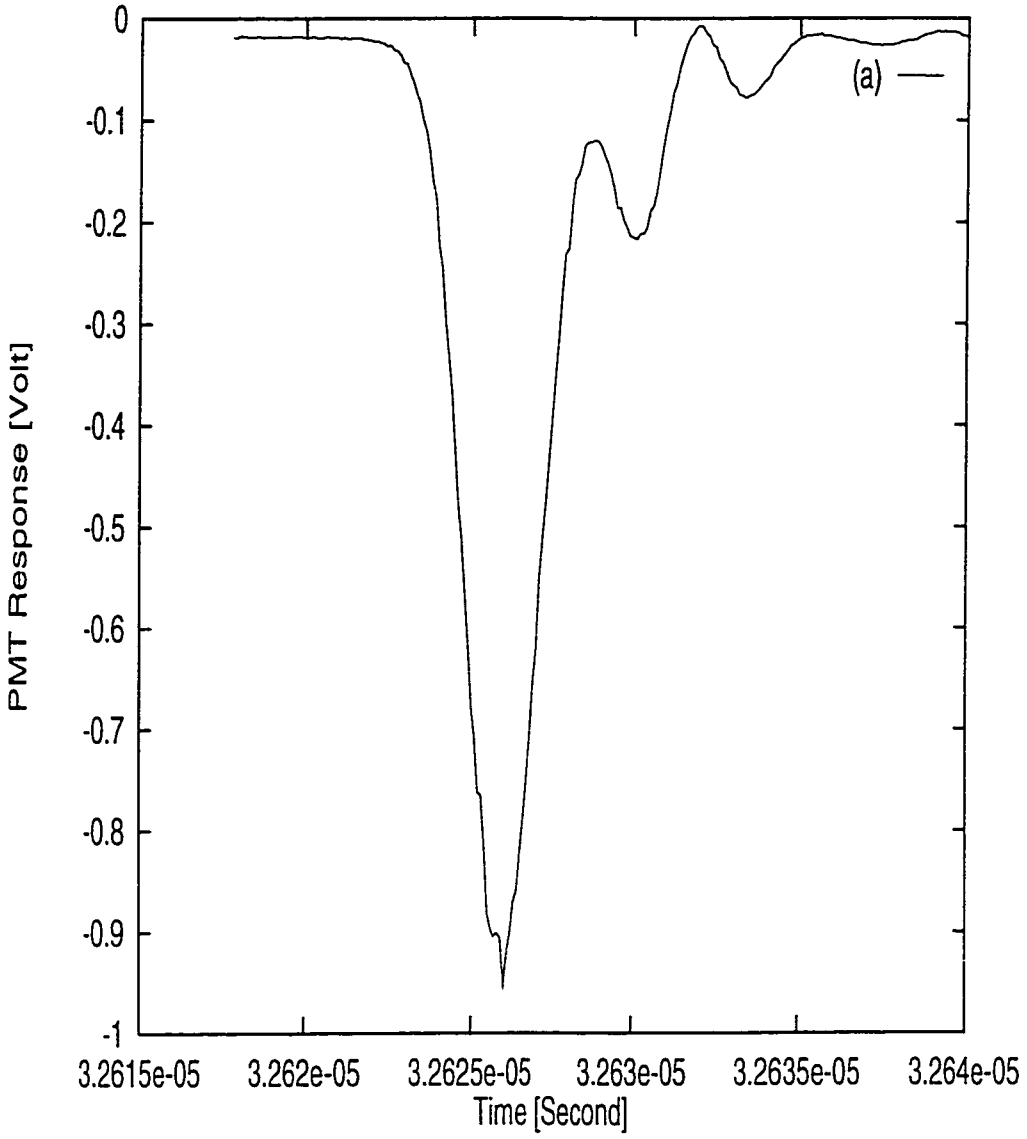

Figure 3.4: SL pulse as picked up the Philips XP2230H PMT driven at 2300 Volts. The gain of the PMT is $3 * 10^7$ at 2300 Volts.

at the point of measurement. The hydrophone has been used in conjunction with an A101 preamplifier as discussed earlier.

The other hydrophone that has been used was a 75 micron diameter PVDF hydrophone (model HP 0.075 mm from Precision Acoustic Limited, England). The sensitive element is made of a piezo-electric membrane which is polyvinylidene fluoride. The sensor material is 9.0 micron thick. The typical probe sensitivity is 12 nV/Pa (equivalent to -278.4 dB re 1V/μ Pa). The probe can be directly attached to a submersible preamplifier (model HP1 from Precision Acoustics Ltd.). A DC coupler (model DC1 from the same vendor) provides a DC signal (28 Volt) needed to power the preamplifier. Again the preamplifier is attached to minimize the multiple reflections of the signal due to impedance mismatch. Since the signal level sensed by this hydrophone is very small because of the minute size of the sensitive element, a booster amplifier (model HA1 from the same vendor) has also been used to boost up the voltage gain a minimum of 25 dB. The bandwidth of the booster amplifier is 50 kHz to 125 MHz. In summary the 1 mm diameter hydrophone has been used to detect the acoustic emissions associated after bounces after the main bubble collpase. These signals are extremely small in amplitudes and requires lager diameter hydrophones. On the other hand, the 75 micron diameter hydrphone has been used for its faster rise time response. This hydrophone can be placed as close as approximately 0.75 mm away from the bubble without disturbing it appreciably.

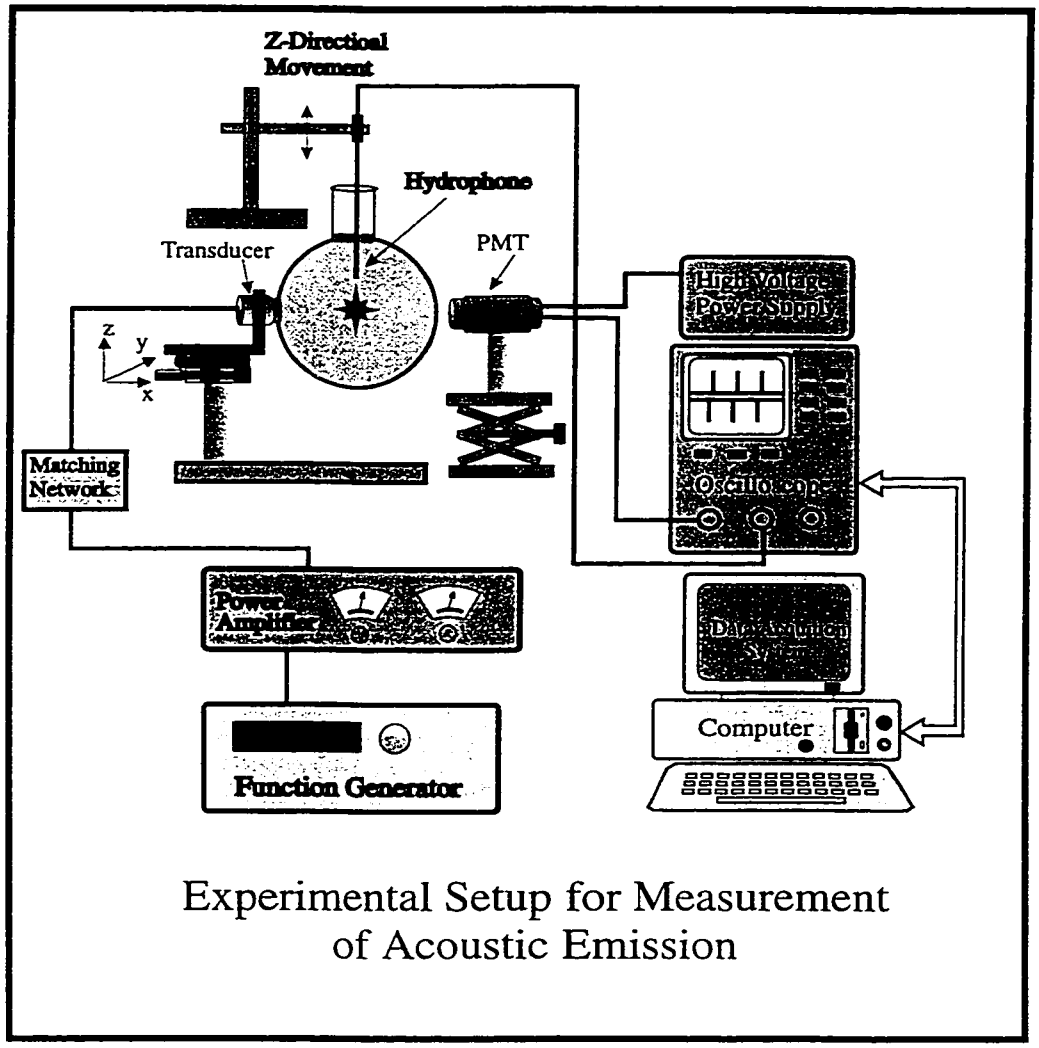

Figure 3.5: Schematic diagram of the experimental setup to measure acoustic emissions from SBSL.

A schematic diagram to measure the acoustic emission is shown in figure 3.5. The hydrophones have been introduced into the levitation cell from the top through the neck. They are attached with rods made of magnetic materials and held vertically with the help of a groove made of magnets as well. The movement of the hydrophones could be controlled to about ± 25 micron in both up and down directions.

The acoustic emission spikes shown in figure 3.6 have been measured with the SPRH-S-1000 hydrophone. The acoustic signature usually consists of a large spike corresponding to the principal collapse of the bubble along with 2-3 smaller amplitude spikes which could be associated with the after bounces. The 75 micron PVDF hydrophone was not sensitive enough to capture the signals of the after bounces. The acoustic emissions will be discussed in detail later in Chapter V.

3.4 Light Scattering Experiment

Gaitan [45] did some preliminary experiments on light scattering from sonoluminescing bubbles. Barber *et al.* [52] reported experimental radius versus time curves of a sonoluminescing as well as non sonoluminescing bubble. The radius of the bubble as a function of time has been measured by the usual Mie scattering [144] technique. In the ray optics limit [145], the intensity of scattered light is

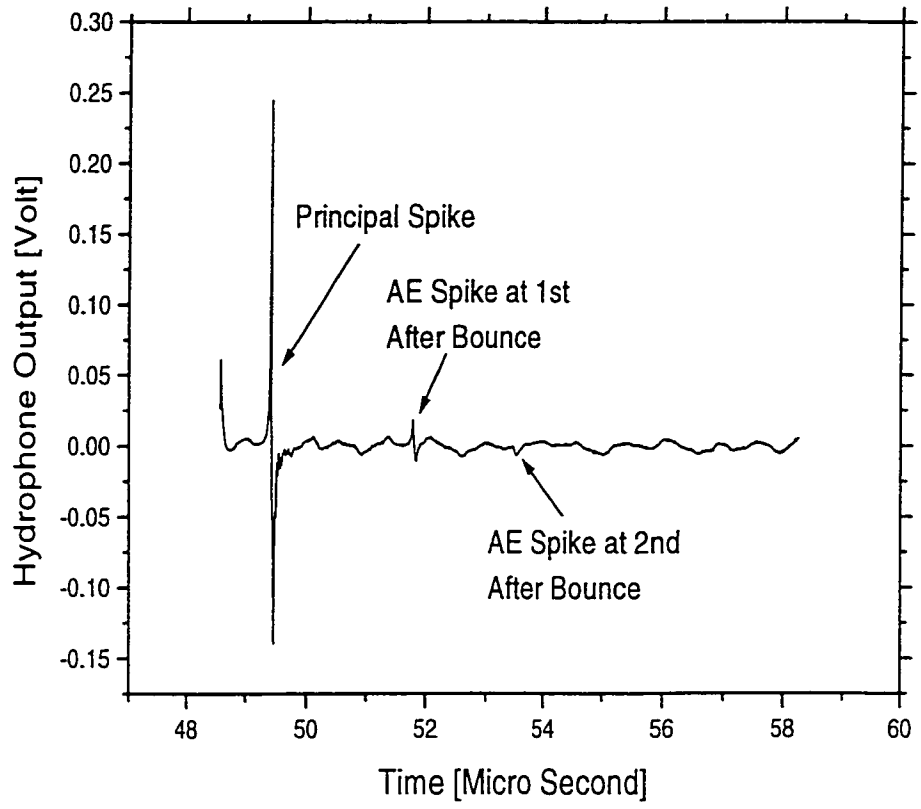

Figure 3.6: Acoustic Emission (AE) from the collapsing bubble picked up by a 1 mm diameter SPRH-S-1000 hydrophone placed approximately 1-2 mm from the bubble. The 17.5 kHz driving signal has been filtered out by a high pass filter using the Labview software. Liquid temperature was 21 C.

directly proportional to the square of the bubble radius. The bubble has been illuminated by a narrow beam from a He-Ne laser (model Melles Griot 05-LPH-991) at 632.8 nm. The average power of the beam is about 30 mW. A PMT (model Philips XP2230H) placed at about 80 degrees from the forward direction of the incident beam collected the scattered light. A short focal length (about 6cm) biconvex lens of aperture of 5 cm was placed in front of the PMT to focus the scattered light on it. The output of the PMT, $V(t)$ has been fed into a Lecroy (model 9310 M) scope with a sampling rate of $100 * 10^6$ samples/sec. The signal was averaged over 100 traces to increase the signal to noise ratio (SNR), and stored into a computer for further processing. The background signal, $V(R = 0)$ which is present keeping the laser and PMT on but with no bubble present has also been averaged over 100 traces and stored. The bubble radius is directly proportional to the square root of the signal $V(t)$ subtracted from the background $V(R = 0)$. A calibration is required to convert these data into bubble radius. This will be discussed later in chapter IV. The scope was triggered by the sync output of the function generator. Once the light scattering experiment has been done, the position of the bubble was marked immediately by the laser. The hydrophone was then slowly brought down so that the tip of it just reaches the bubble position. The drive amplitude has been kept at the same level. The scope has again been triggered with the same sync output of the function generator. The phase and amplitude of the output pill

transducer was also measured with respect to those of the hydrophone for further calibration of the driving pressure amplitudes. Figure 3.7(a) shows the square root of the voltage generated by the scattered light from the PMT. Figure 3.7(b) shows the the output of the hydrophone in volts. The phase of the bubble collapse can be determined from this figure. This helps in fitting the R-P equation with the experimental data.

3.5 Description of Experimental Setup to Study the Effect of Ambient Pressure on SBSL

The experimental setup to investigate the dependence of SBSL on ambient pressure is shown in the figure 3.8. The basic components of the experimental system remain the same as those used to get SBSL. However some modifications of the system have been carried out to facilitate the variation of ambient pressure. A system has been built so that the ambient pressure could be either decreased or increased. Furthermore, it is to be noted that in a set of runs either the ambient pressure has been decreased or increased monotonically. The basic idea of modification of ambient pressure means modifying the pressure above the liquid in the levitation cell. To achieve this, the liquid head must be isolated from the atmo-

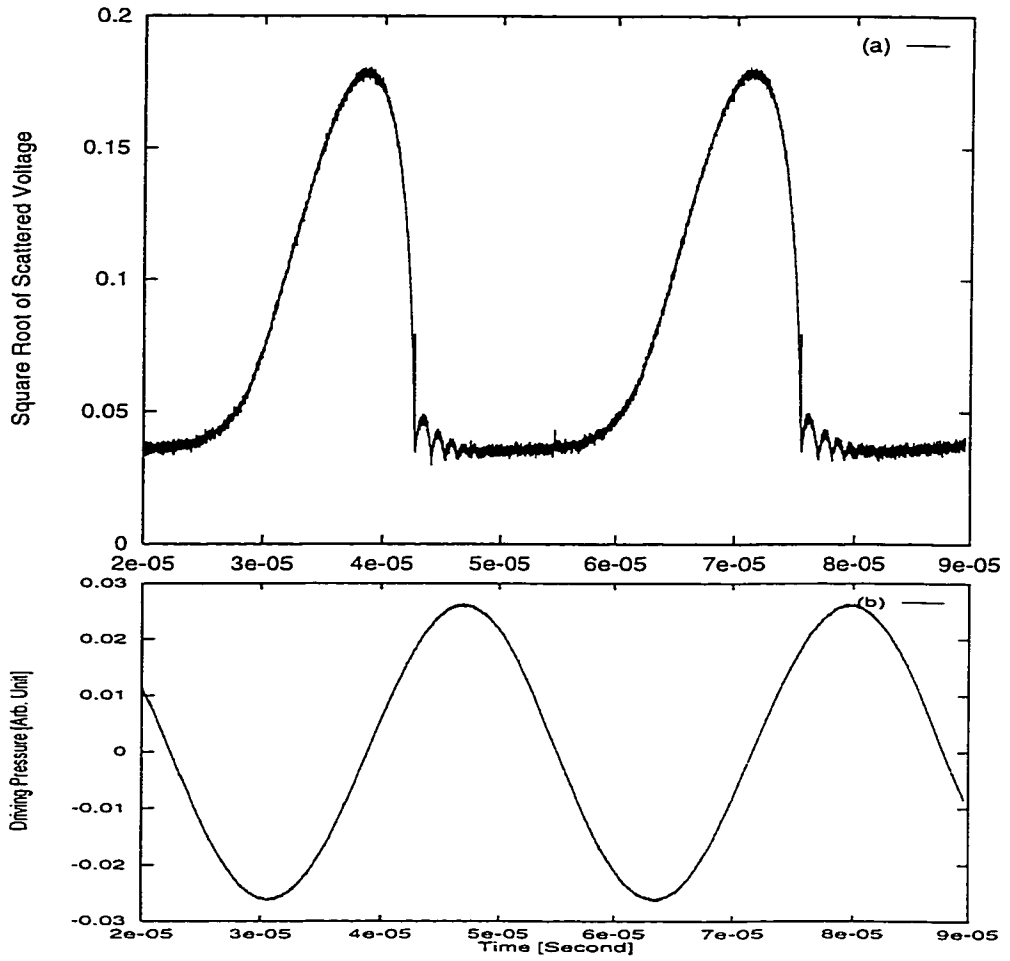

Figure 3.7: (a) Square root of the scattered light subtracted from the background light when the laser and the PMT were on but no bubble was present. (b) The output of the hydrophone at the bubble position with no bubble. From these two curves the R(t) of the bubble can be obtained by fitting the curve (a) with the R-P equation, as described in detail in Chapter IV

spheric pressure surrounding the levitation cells and at the same time provisions should be made so that the cell could be pressurized or depressurized. Moreover, to create bubbles in the cell under acoustic cavitation, the top of the liquid surface needs to be poked with a thin wire or a needle. The open neck of the spherical flask has been sealed tightly with a septum (model suba-seal - from Aldrich Chemical Company, Inc.). A thin but rigid stainless steel wire has been introduced from the top of the septum to poke and create bubbles whenever necessary. A thin film of vacuum grease has been added on the septum to prevent air from going in or leaving out of the cell. The grease did not contaminate the liquid in the cell.

To change the ambient pressure on top of the liquid, a gas handling feature has been built and fused to the neck of the cell. The gas handling manifold consists of a narrow cylindrical glass tube with two valves which are screwed securely to the glass tubing and two openings made of glass as well. A hand operated vacuum pump (Model-Mityvac - from Neward Enterprises, USA) fitted with a vacuum gauge has been attached to one of the openings with the help of a 1/4 inch internal diameter clear plastic tubing. To get a very precise measurement of the vacuum inside the cell a very precise vacuum gauge (model Ashcroft type - 1082) with an accuracy of 2.54 mm of Hg has also been attached to the pump with the help of a Y-shaped coupler. The other opening is used to introduce air into the cell once one set of experiment has been finished to establish the normal conditions again and repeat

the experiment all over.

The same experimental setup has been used to increase the pressure inside the cell. However, in this case the hand-operated pump has been replaced and instead pure air from a cylinder has been allowed to flow into the cell. The flow of air has been controlled very carefully and the increment of ambient pressure has been measured with a pressure gauge (Moore Product Co.). The range of the gauge is 30psi. The resolution of the gauge is 1psi. It is to be noted that the time scales involved in the experiments were much shorter than the diffusion time of air in the liquid so that the concentration of the gas in the liquid remained unchanged.

Summary

In this chapter, the general description of the experimental setup and the step by step procedures to obtain SBSL have been described. The different elements used to produce the phenomenon as well as the instruments needed to detect the different SBSL phenomena have been described in detail. A simple description of the acoustical resonance modes inside the liquid filled spherical flask has been provided. This chapter will serve as the basis of the next two chapters where the ambient pressure effects and the experimental measurements on AE will be discussed. Furthermore, the general characteristics of the SBSL experiments have

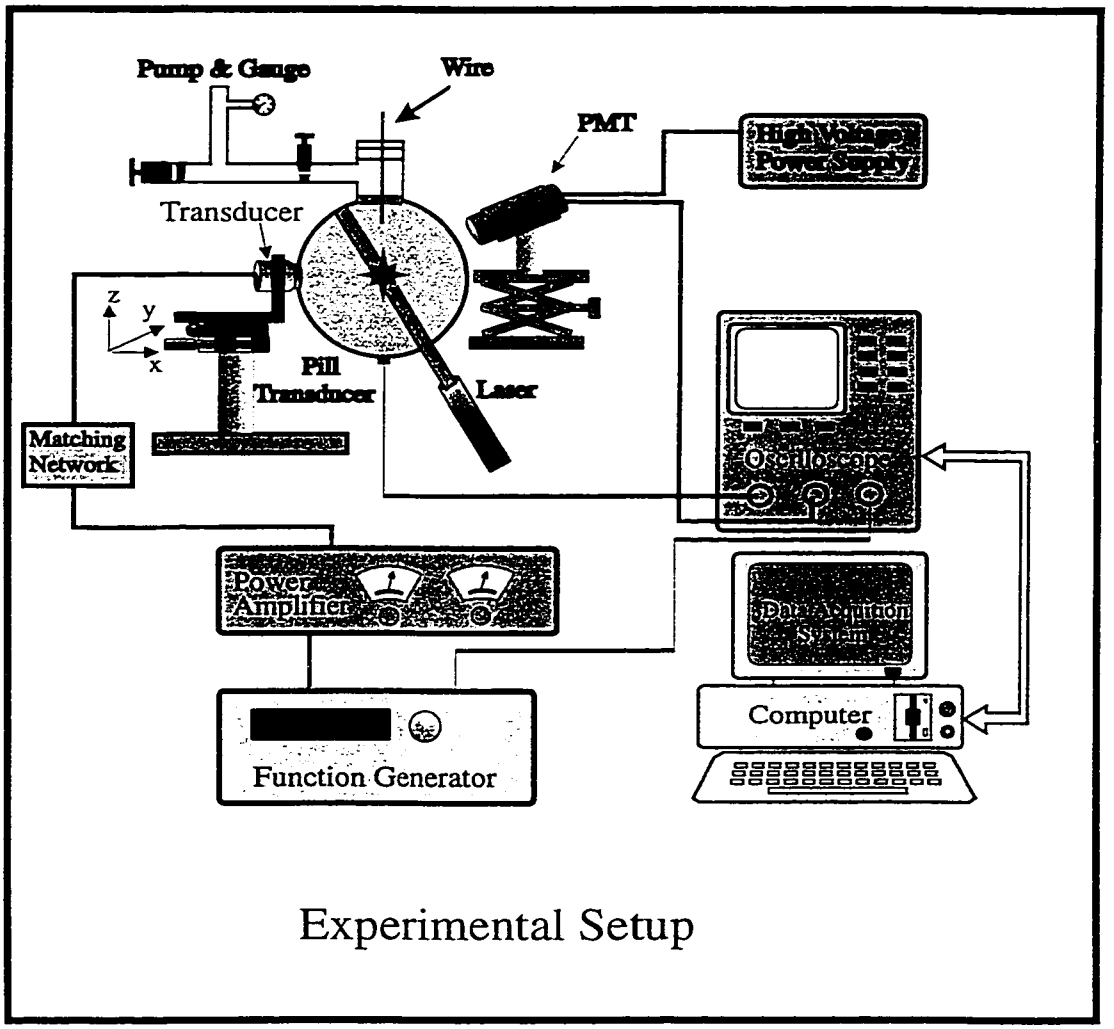

Figure 3.8: Schematic diagram of the experimental setup to study the effect of ambient pressure on SBSL.

also been described in this chapter.

Chapter 4

Effect of Ambient Pressure on SBSL

Introduction

The first complete and well controlled experimental study of the influence of variation of ambient pressure, P_0, on bubble dynamics and the resulting SBSL will be presented here. At first, the purpose of the research of the dependence of SBSL on ambient pressure will be discussed. Secondly, following Kondic *et al.* [151] a theoretical analysis of the effect of ambient pressure on SBSL will be introduced. A significant increase in SL radiation as well as the modification of the bubble dynamics with the decrease of ambient pressure have been predicted by Kondic *et*

al. Thirdly, the experimental results of the variation of ambient pressure on SBSL will be presented. An excellent agreement between the experimental results and the theoretical predictions has been found. Next, a detailed discussion of these results will be given. Finally, a conclusion will be drawn at the end of the chapter.

4.1 Goal of the Research on Ambient Pressure Effect on SBSL

From the RP equation (Eq. 2.13) of the bubble dynamics, it is clear that the ambient pressure plays a very important role in the dynamics of the bubble. So it is expected that modifications of P_0 will have a significant impact on the bubble dynamics and hence in the light emission as well. By combining experimental results with theoretical analysis, a further insight into the basic mechanism of the SL radiation will be achieved. The importance of this research is emphasized by the need to better understand other experiments where a variation of P_0 might occur, such as microgravity experiment [152, 153, 154] or closely related experiments performed in a strong magnetic field [155]. Moreover. these results are also relevant to the recently proposed *Dissociation Hypothesis* [93, 95]. Considering these aspects, an experimental investigation of the effect of ambient pressure on

SBSL has been carried out.

4.2 Theory

Recent experimental and theoretical work explained many aspects of sonoluminescence. The details of the SBSL emission have been explored in different liquids, with varied liquid temperature, gas contents etc. (see [53, 156] for extensive reviews). Yet there has been no detailed experimental study of the modification of bubble dynamics as well as the change of SL emission with the variation of ambient pressure. In a recent article Kondic *et al.* [151] advanced a rather elaborate theoretical investigation of the effect of ambient pressure on SBSL.

Epstein and Plesset [157] have shown that a static (unforced) gas bubble of radius, R_0 in an infinite, incompressible liquid that is either saturated or undersaturated with gas, dissolves over a diffusive time scale $\sim \rho_0 R_0^2 / D(c_0 - c_i)$, where ρ_0 is the ambient gas density inside the bubble, c_0 is the saturated concentration of the gas in the liquid and c_i is the concentration of gas in the liquid far from the bubble. D denotes the diffusion constant of the gas in the liquid. However, bubbles located in an acoustic field of sufficient amplitude may grow. This growth process is known as rectified diffusion as discussed in detail in section 2.2.1. Rectified diffusion process competes with the static (standard) diffusion process and

if the acoustic pressure amplitude is greater than a threshold value it may balance the static diffusion. Now, in the case of SBSL, it has been observed experimentally that a sonoluminescing bubble has constant SL phase over billions and billions of cycles. The picosecond time scale jitter between the successive flashes shows that the mass (equilibrium size) of the bubble remains accurately constant [27, 47, 78] over a long period of time.

Following Kondic [151], it is assumed that a single bubble in a liquid is subject to an ambient pressure, P_0 and an acoustic pressure amplitude, P_a with frequency, ω. The bubble radius, $R(t)$ will oscillate about the equilibrium radius, R_0 due to the acoustic field.

The average rate of change of the number of moles of gas inside the bubble is given b

$$\frac{dn}{dt} = 4\pi D R_0 c_0 \left[\langle R/R_0 \rangle + R_0 \left(\frac{\langle (R/R_0)^4 \rangle}{\pi D t} \right)^{1/2} \right] H, \tag{4.1}$$

where

$$H = \frac{c_i}{c_0} - \frac{\langle p(R(t)) \rangle_4}{P_0}. \tag{4.2}$$

where

$$\frac{\langle p(R(t)) \rangle_4}{P_0} = \frac{\langle p \rangle_4}{P_0} \tag{4.3}$$

and

$$\langle p \rangle_4 = \frac{\int_0^T p(R(t)) R^4 dt}{\int_0^T R^4 dt} \tag{4.4}$$

is the weighted mean of the gas pressure inside the bubble. Hence, the ignoring vapor pressure, equilibrium points ($\frac{dn}{dt} = 0$) satisfy the condition [158]

$$\frac{c_i}{c_0} = \frac{\langle p \rangle_4}{P_0} \tag{4.5}$$

The equilibrium points will be stable if the derivative of the weighted average of the gas pressure inside the bubble with respect to equilibrium bubble radius, $\beta \equiv \frac{d\langle p \rangle_4}{dR_0} > 0$

The R. H. S. of Eq. 4.4 can be calculated from the RP dynamics which involves P_a, P_0, and R_0 along with other parameters. The RP equation which is used for calculation can be written as:

$$\begin{aligned} R\ddot{R}(1 - \frac{\dot{R}}{c_l}) + \frac{3}{2}\dot{R}^2(1 - \frac{\dot{R}}{3c_l}) &= \frac{1}{\rho_l}(1 + \frac{\dot{R}}{c_l})\left[P_l(R,t) - P_0 - P_a(t + \frac{R}{c_l})\right] \\ &\quad + \frac{R}{\rho_l c_l}\frac{dP_l(R,t)}{dt} \end{aligned} \tag{4.6}$$

Here $P_l(R,t)$ is the pressure in the liquid just next to the bubble wall. $P_a(t + \frac{R}{c_l})$ denotes the time delayed driving pressure, P_0 and ρ_l are the ambient pressure and the liquid density respectively. The gas pressure P_g can be related to the liquid pressure by

$$P_l = P_g - \frac{2\sigma}{R} - 4\nu_l\rho_l\dot{R}/R \tag{4.7}$$

where ν_l is the kinematic viscosity of the liquid. The mass flow between the liquid and the bubble and the stability of the bubble with respect to surface instabilities

have been calculated taking $P_g(V - V^{exc})^{\kappa} = const$, where V is the volume of the bubble and V^{exc} is the excluded volume and κ is the polytropic exponent. All the calculations were performed with standard values of parameters related to air and water. The frequency of the acoustic field was taken to be 26.4 kHz.

Figure 4.1 shows a plot of $\langle p \rangle_4$ as a function of R_0 for several values of P_0, while P_a is kept constant at 1.40 atm. Equilibrium corresponds to $\langle p \rangle_4 / P_0 = c_i/c_0$. At large values of P_a, $\langle p \rangle_4$ develops oscillations as a function of R_0. Hence it is expected that there will be several equilibrium points corresponding to a range of c_i/c_0. In the figure 4.1 the straight line corresponds to $c_i/c_0 = 0.0026$. Corresponding to this line the solid bullets represent equilibrium points where $\beta > 0$, meaning that at these equilibrium radii, the bubble is diffusively stable.

However, the plot in figure 4.2 shows $\langle p \rangle_4$ as a function of R_0 for different values of P_0 at $P_a = 1.10$ atm. Here the straight line corresponds to $c_i/c_0 = 0.1$ and the corresponding solid bullets denote that the equilibrium points are unstable since they lie in the negative slop region which means $\beta < 0$.

In figure 4.3 each line represents equilibrium values of R_0, for which total mass flow during one acoustic cycle is zero. As shown in figure 4.3(a), the equilibrium points are mostly unstable as the slopes of the curves are negative. Here $c_i/c_0 = 0.2$ for $P_0 = 1.0$ atm. This value is chosen as it is the most common value used in most of the experiments. The value of the ratio c_i/c_0 has been modified as P_0

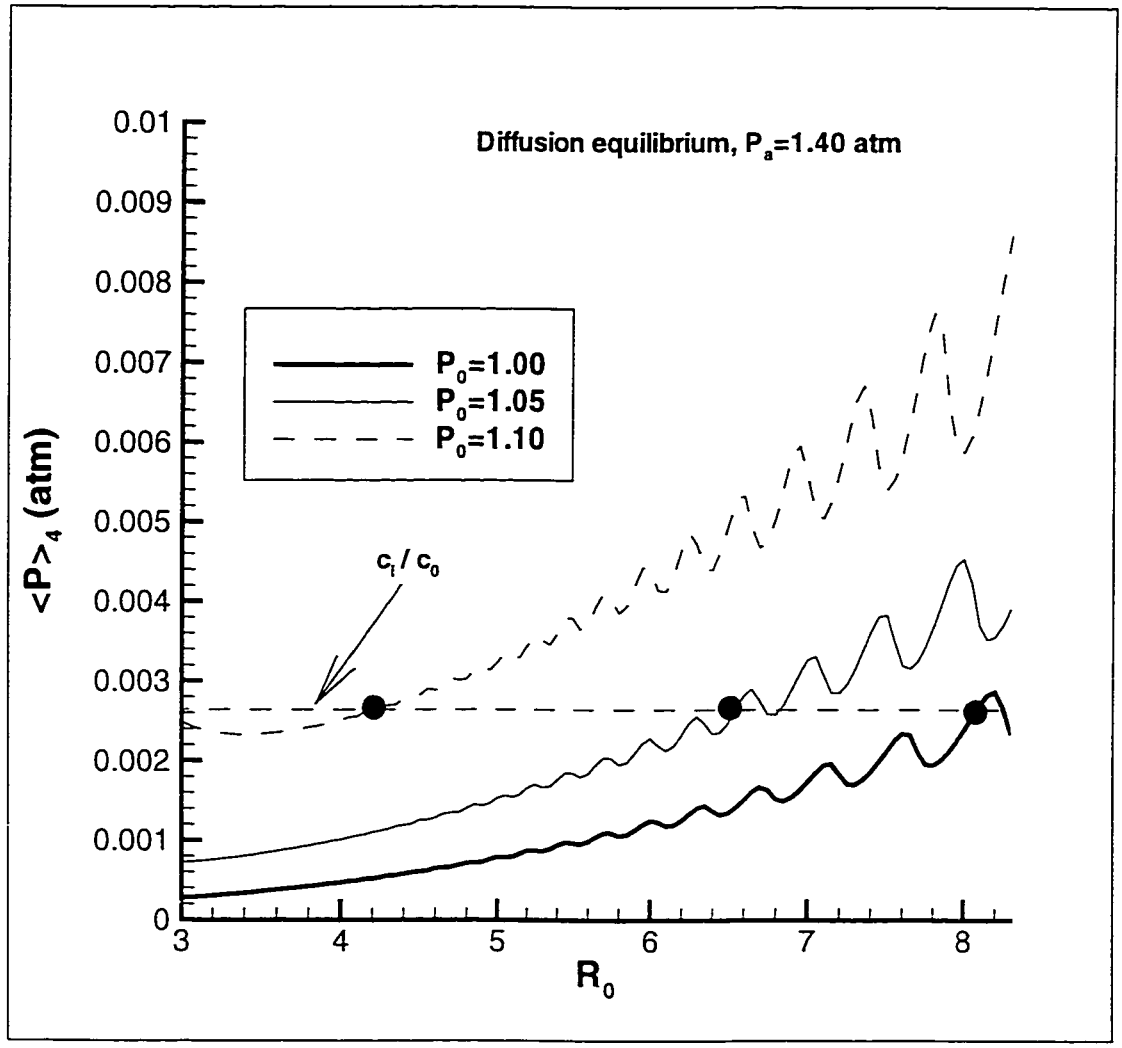

Figure 4.1: The quantity $\langle p \rangle_4$ plotted as a function of R_0 for different values of P_0 at $P_a = 1.40$ atm. [Courtesy of L. Kondic.]

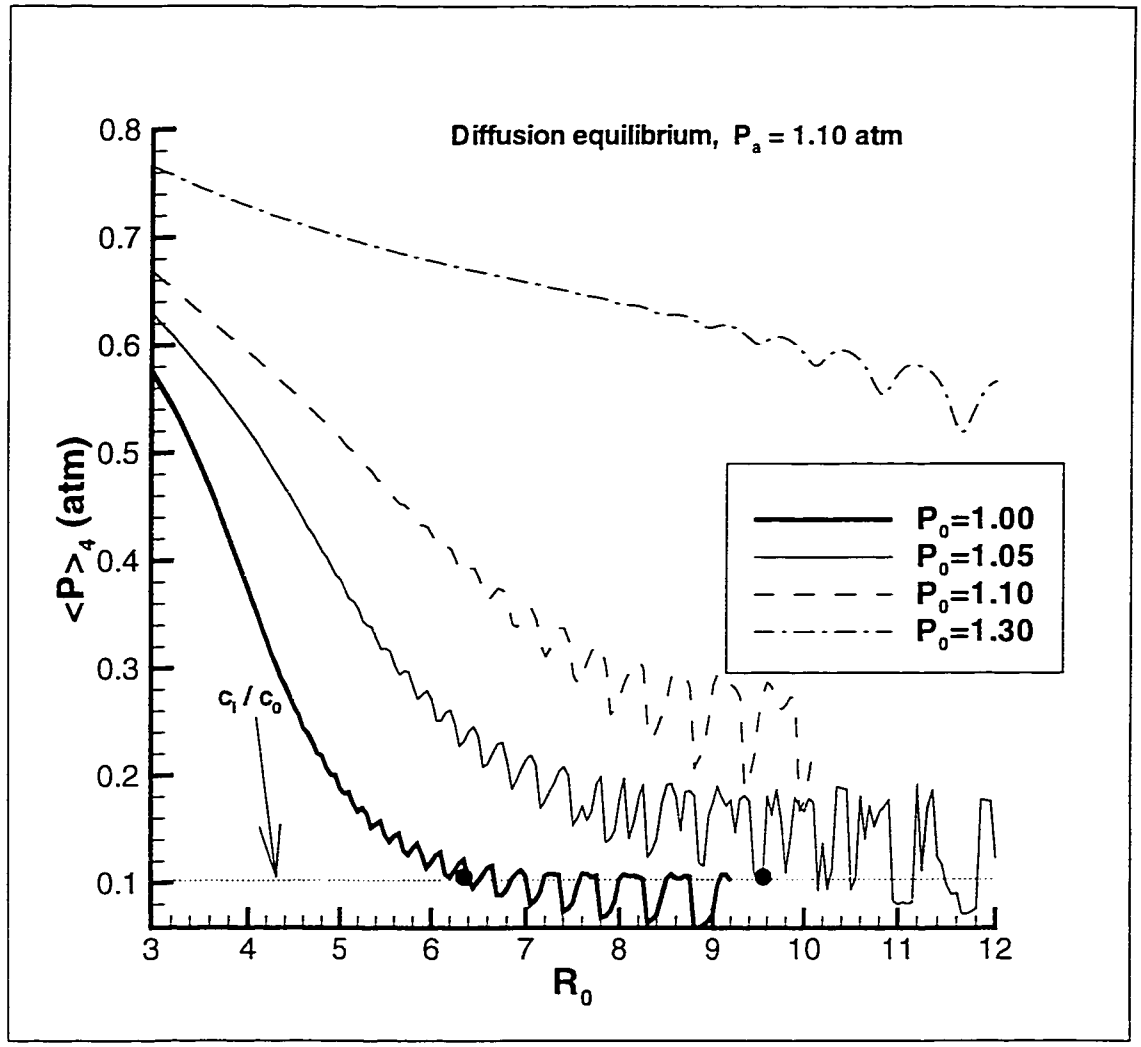

Figure 4.2: The quantity $\langle p \rangle_4$ plotted as a function of R_0 for different values of P_0 at $P_a = 1.10$ atm. [Courtesy of L. Kondic.]

is changed following Henry's law. $c_i/c_0 = 0.2$ represents the case when the bubble contains air inside it.

From figure 4.3(a) it is observed that if P_0 is decreased while keeping P_a constant, R_0 has to jump from one curve to another resulting in an decrease of R_0 [a possible path is shown in figure 4.3(a)].

It is now known that there is a severe discrepancy [78] between the hydrodynamically calculated phase space parameters and experimental measurements. An air bubble fails to achieve diffusion stability whereas an argon bubble does. To account for this, Lohse *et al.* [93, 95] suggested a theory that chemical reaction inside an air bubble leads to the production of water solvable products which leave the bubble, and the bubble rectifies itself to an argon bubble. If it is assumed to be the case, then a plot of P_a versus R_0 with $c_i/c_0 = 0.002$ is relevant. This plot is shown in figure 4.3(b).

In figure 4.3(b) if the curve $P_a = 1.0$ atm is considered, it is now observed that the equilibrium is mostly stable, since the slope of the equilibrium curve is positive for typical values of R_0. Moreover, if the ambient pressure is decreased, the equilibrium radius is also now increased [a possible path is shown if figure 4.3(b)].

Hence the theory of ambient pressure predicts that a change of ambient pressure P_0 and a subsequent measurement of R_0 will provide information regarding the

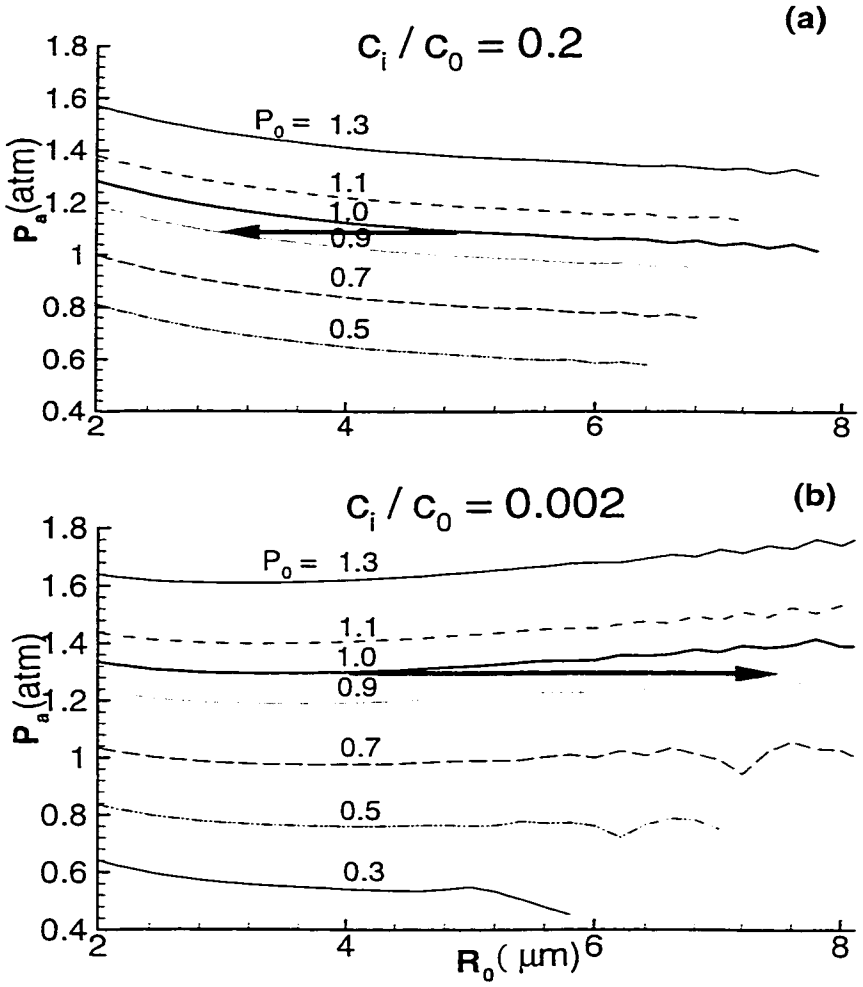

Figure 4.3: Equilibrium bubble radius for a 20% air saturated water: (a) $c_i/c_0 = 0.2$ (air is in the bubble); (b) relevant $c_i/c_0 = 0.002$ (e.g., only argon is left in the bubble). In (a) equilibrium is mostly unstable since the slope of the curves is negative whereas in (b) equilibrium could be stable. [Courtesy of L. Kondic.]

dissociation hypothesis. Additionally, the stability of the bubble as P_0 is varied, is an very important factor.

The modifications of the bubble dynamics with the variation of P_0 are shown in figure 4.4. Here the bubble radius has been plotted as function of time for one complete cycle of acoustic drive. Kondic et al. [151] obtained dynamics by solving the R-P equation 4.6, modified in order to incorporate the first order corrections proportional to $\dot{R}/c_l$ (where $\dot{R}$ is the bubble wall velocity and c_l is the speed of sound in liquid). It is observed from the figure 4.4 that the expansion ratio as well as the collapsing velocity of the bubble decrease (see inset of 4.4).

It is expected that the modification of the bubble dynamics will modify the character of SL radiation. A plot of SL radiation as a function of P_0 has been shown in figure 4.5. As mentioned earlier, as P_0 is increased, the bubble undergoes weaker oscillations resulting in a weaker emission of light. The results of SL radiation are calculated from gas dynamics [139]. The plot shows a sharp decrease of SL intensity as P_0 is increased. However, there is a weak increase in SL radiation with the increase of P_0 while P_a/P_0 is kept constant.

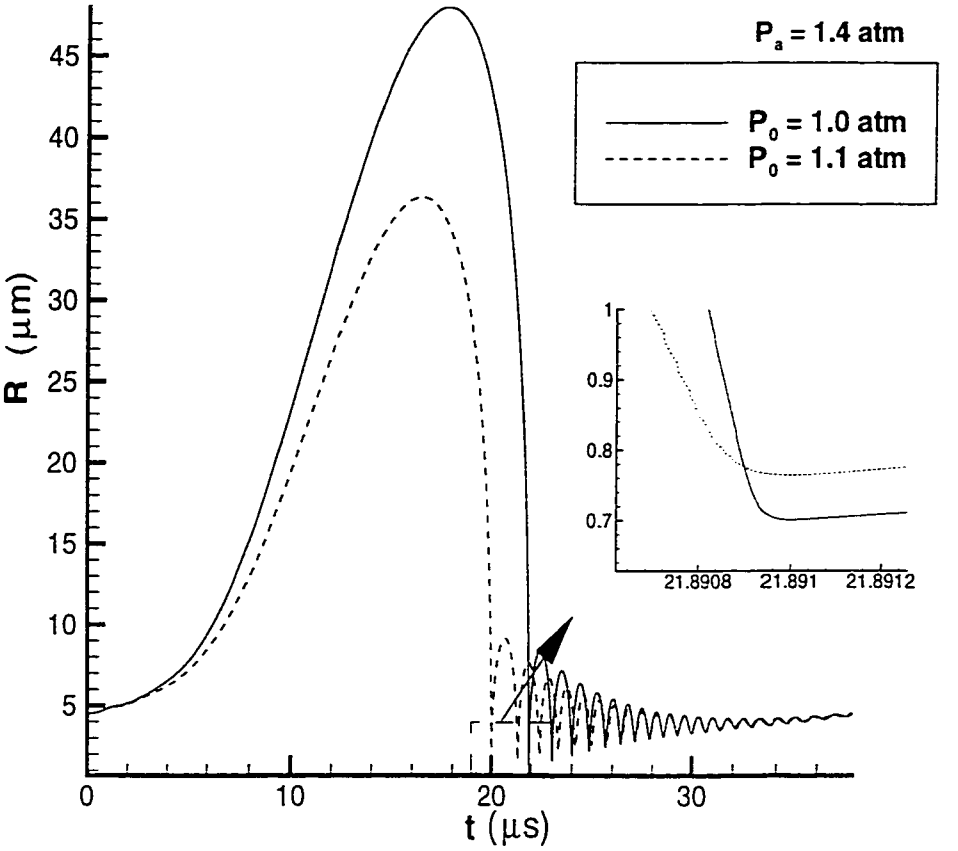

Figure 4.4: Bubble radius versus time during one complete acoustic driving cycle for different values of P_0. In the inset the first minima of the bubble radius are shown. [Courtesy of L. Kondic.]

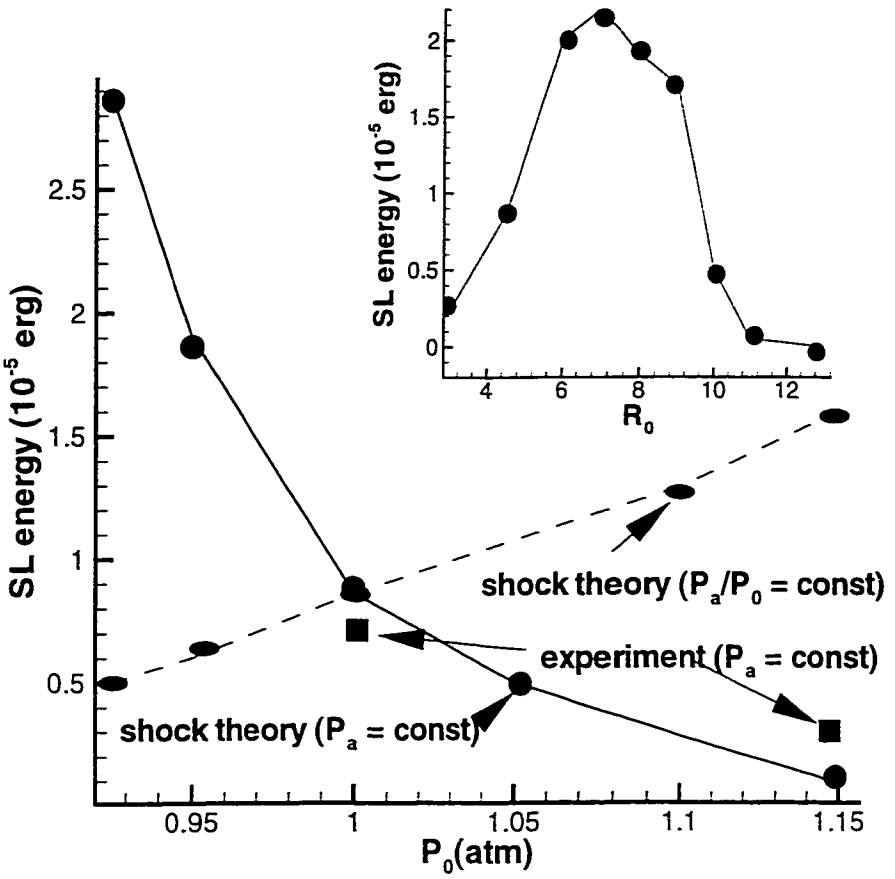

Figure 4.5: SL radiation in the visible range of the spectrum as a function P_0. [Courtesy of L. Kondic]. The circles (solid line) refer to fixed $P_a = 1.4$ atm; the ellipses (broken line) to fixed ratio $P_a/P_0 = 1.4$. Experimental data are preliminary [159, 160] and were obtained with 50 % degassed water. The inset shows the dependence of SL intensity on R_0; here $P_0 = 1.0$ atm., $P_a = 1.4$ atm. [Courtesy of L. Kondic.]

4.3 Results and Discussions

4.3.1 Decreasing the Ambient Pressure

Figure 4.6 shows the square root of $V(t)$, subtracted from the background signal, for different values of P_0. The acoustic pressure amplitude, P_a, as well as all other experimental parameters are kept constant, and only P_0 is modified. The physical size of the bubble and the driving pressure amplitude was determined by fitting the data to the Rayleigh-Plesset (R-P) equation in the part of the cycle where this equation is known to accurately reproduce the bubble dynamics [52]. While it is possible to measure P_a at the bubble position directly, this procedure is not very accurate. It is advantageous to obtain both P_a and R_0 as fitting parameters directly from $R(t)$ curve for $P_0 = 1$ atm. For fitting the R-P equation to the experimental results, 1) the expansion ratio, R_{max}/R_0; 2) the full width at half maximum, and; 3) the phase of the first minimum of the $R(t)$ curves have been used. Figure 4.7(a) shows both experimental data and the fit for $P_0 = 1.0$ atm. This procedure, which is an extension of recently proposed suggestion to use $R_0 = R(t)$ at $P_a = 0$ [161], allows one to very precisely determine both P_a and R_0, avoiding the problems related to the scatter of data due to the analog to digital conversion (ADC) of the scope in the $R(t)$ curves.

Once P_a is obtained from the data for $P_0 = 1$ atm, it is kept fixed, so that R_0

is a single fitting parameter for the $R(t)$ curves obtained with different P_0. As can be seen from figure 4.7(b), it is possible to obtain an almost perfect agreement in the slow expansion part of the cycle where the R-P equation is expected to hold. All three quantities (full width, R_{max}/R_0, and the phase of the first minimum) are reproduced very well with a single parameter, R_0. It is to be noted here that according to Henry's law, the modification of ambient pressure P_0 also modifies the ratio of gas concentration c_i/c_0. In our experiments, the gas concentration was kept constant. However, during calculation the gas concentrations were corrected accordingly following the Henry's law. However, the after bounces are not modeled accurately, implying that there is another damping mechanism that becomes important during the collapse phase, that is not included in the R-P equation. The quality of the fitting procedure is not influenced by this discrepancy. More relevant is the heat transfer between the bubble and the liquid, which we model by a polytropic exponent approach. Recent works [162, 163, 164] suggest that one should assume perfect heat exchange between the bubble and the liquid; we use this approach and note that the results for our fitting parameters depend only weakly on this assumption. Further, the results are independent of which "bubble" equation is used; as long as one is concentrated on the slow expansion part of the cycle, the R-P equation does as good a job as more elaborate (e.g. Keller) equations.

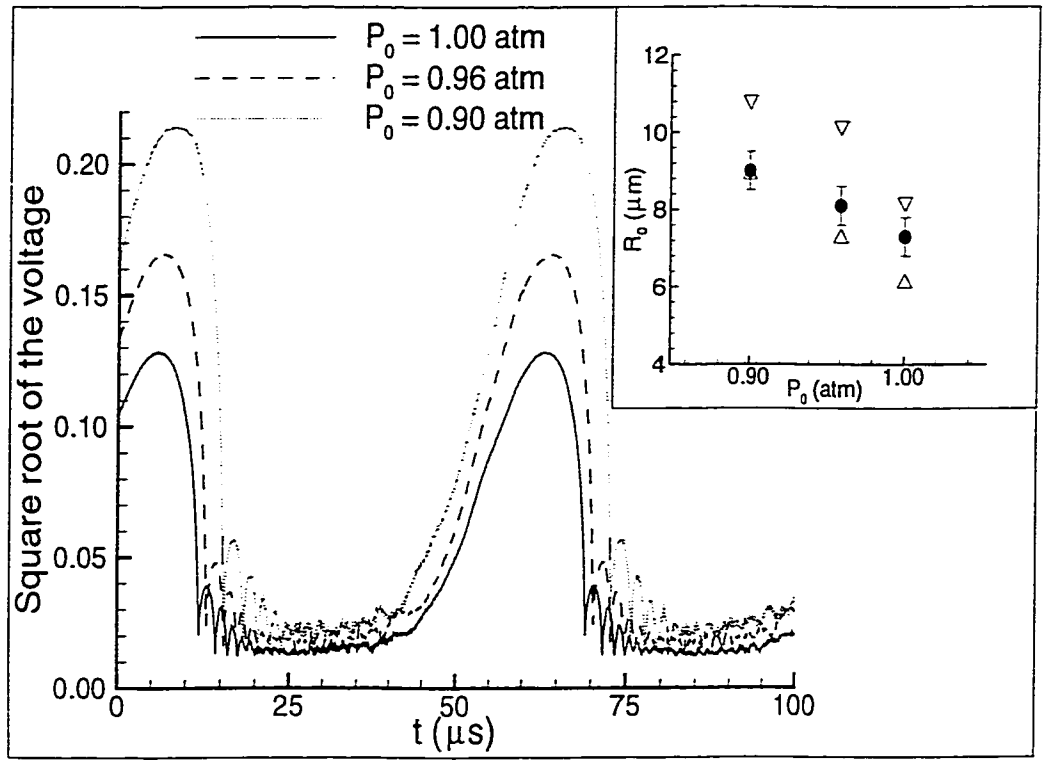

Figure 4.6: Experimental $R(t)$ curves as ambient pressure P_0, is varied. The inset shows the results for R_0: experiment ($\bullet$) and diffusion theory (Δ and ∇) obtained assuming polytropic exponent $\gamma = 1.0$ and 1.67, respectively. The estimated combined experimental and fitting uncertainty is also shown. Here acoustic pressure P_a is kept constant at 1.29 atm, $\frac{c_L}{c_0}$ is kept constant at 0.23 (correction factor included during the theoretical fitting process as P_0 is changed). The driving frequency was 17.465 kHz and temperature of the liquid was 21 C.

From figure 4.6 we calculated that R_{max}/R_0 changes from 8.35 to 9.29. The dependence of R_0 on P_0 is also shown. While the change of R_{max}/R_0 can be understood based on the R-P equation [151], the change of R_0 follows from the details of the mass transfer between the bubble and liquid.

It is the interplay between two competing mass flow mechanisms that leads to a stable (constant mass) bubble on a time scale which is long compared to the acoustic period. One mass flow process is standard diffusion that leads to the flow of the gas out of the bubble, and does not depend on P_a. The other one is rectified diffusion, that leads to the flow in the opposite direction, and is due to the asymmetry of gas diffusion process. The bubble spends more time in the expansion part, so that more gas flows into the bubble during this time, than escapes during the compression part [80, 129, 91]. This effect does depend on P_a, so that there is a value (or values) of P_a when equilibrium is obtained, leading to a time independent equilibrium bubble radius, R_0. R_0 also depends on P_0, and the degree of degassing, c_i/c_0. Here c_i is the concentration of gas in the liquid, and c_0 is the saturation concentration (which depends on P_0 through Henry's law).

The degree of degassing plays a significant role in determining how R_0 depends on P_a and P_0 [151]. If one assumes that the concentration of air in the liquid is relevant ($c_i/c_0 = 0.23$ in figures. (4.6 and 4.7), then the theoretical results shown in figure 4.3(a) predict a *decrease* of R_0 when P_0 is decreased, and P_a kept constant,

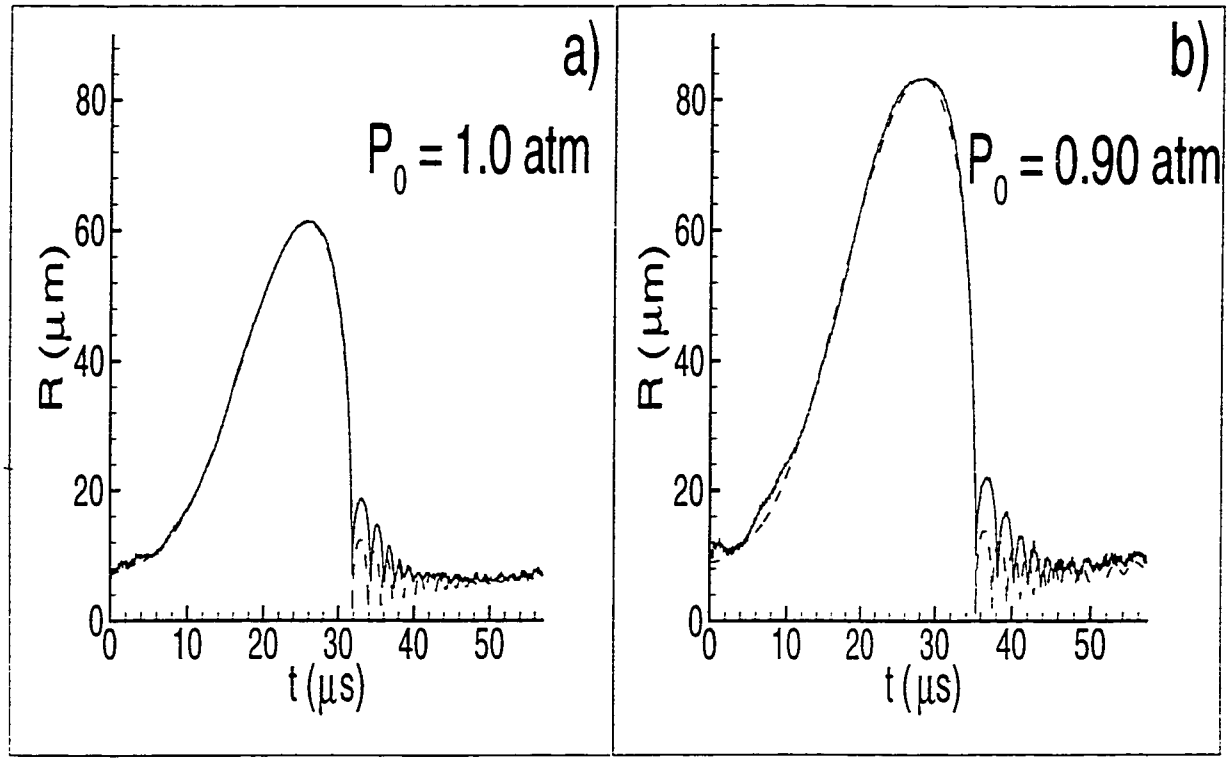

Figure 4.7: The experimental results and the fits for two values of P_0. In a) P_a and R_0 were used as fitting parameters (R_0 = 7.3 μm, P_a = 1.29 atm); in b) we used P_a = 1.29 atm, and the best fit was obtained at R_0 = 9.0 μm. The measured liquid viscosity was 0.021 cm^2/s, and surface tension was 69.4 dyn/cm at liquid temperature 21 C. The driving frequency was 17.465 kHz and c_i/c_0=0.23.

in obvious contradiction with Figure 4.6. Further, the theoretically obtained equilibrium is unstable [151], whereas in our experiment we observe stability on a long time scale, measured in hours. On the other hand, assuming that only argon is left in the bubble, the relevant concentration ration is $c_i/c_0 = 0.0023$ and now figure 4.3(b) applies. In this case, the theory predicts an *increase* of R_0, as we observe in the experiment. This clear-cut result confirms the dissociation hypothesis [93, 95].

Figure 4.6 (insert) shows experimental and two families of theoretical values for R_0 as a function of P_0. The theoretical values were obtained using $c_i/c_0 = 0.0023$ and the standard Eller-Flynn theory [80], where either isothermal (Δ) or adiabatic (∇) conditions in the bubble were assumed. Neither of the theoretical results fits the experimental ones very well; still, it can be concluded that the isothermal and adiabatic assumptions are the limiting cases and that the heat exchange between the bubble and the liquid puts the bubble somewhere between these two extremes. However, in both the experimental and theoretical results, there is an obvious trend indicating an increase in R_0 as P_0 is decreased.

It is now time to concentrate on the SL emission. Figure 4.8(a) shows the number of photons emitted in a single SL pulse, as P_0 is varied, while P_a is kept constant. The procedure of photon counts has been described later (see [51] for details). Roughly linear growth is observed as P_0 is decreased. This result could be qualitatively understood by inspection of figure 4.6. First, R_{max}/R_0 increases

as P_0 is decreased, leading to a stronger collapse. Second, there is a shift in the phase relative to the acoustic field as P_0 is reduced; the first minimum of the bubble radius, at which the SL pulse is emitted, happens later in the bubble cycle. Consequently, more time is left for energy storage.

The calculation of the intensity of SL radiation is still a subject of debate. The only consistent calculations of SL radiation gave shock wave solutions in the gas during its compression phase and calculated SL intensity based on either bremsstrahlung [140, 105] or radiative transport theory [139]. These studies have been criticized by other workers [163, 164, 165], since heat conduction between bubble and liquid was not included. The references [163, 164, 165] propose that simple adiabatic heating might be responsible for SL emission, although this hypothesis is in contradiction with experimental results [48, 49]. Recent experiments [109] suggest that the situation is more complex. In this work, we used the approach presented in [139] has been used to calculate the number of photon emitted for our experimental conditions. These results are also given in Fig. 4.8(a); the experimental values for R_0 are used, and the parameters applicable to pure argon bubbles are assumed. The estimates of photon flux do not account for the bandwidth of the PMT window, which we assume to have a constant quantum efficiency for all photon wavelengths. In fact, the quantum efficiency peaks at about 28% in the vicinity of 401 nm, and drops off at both ultraviolet (UV) and

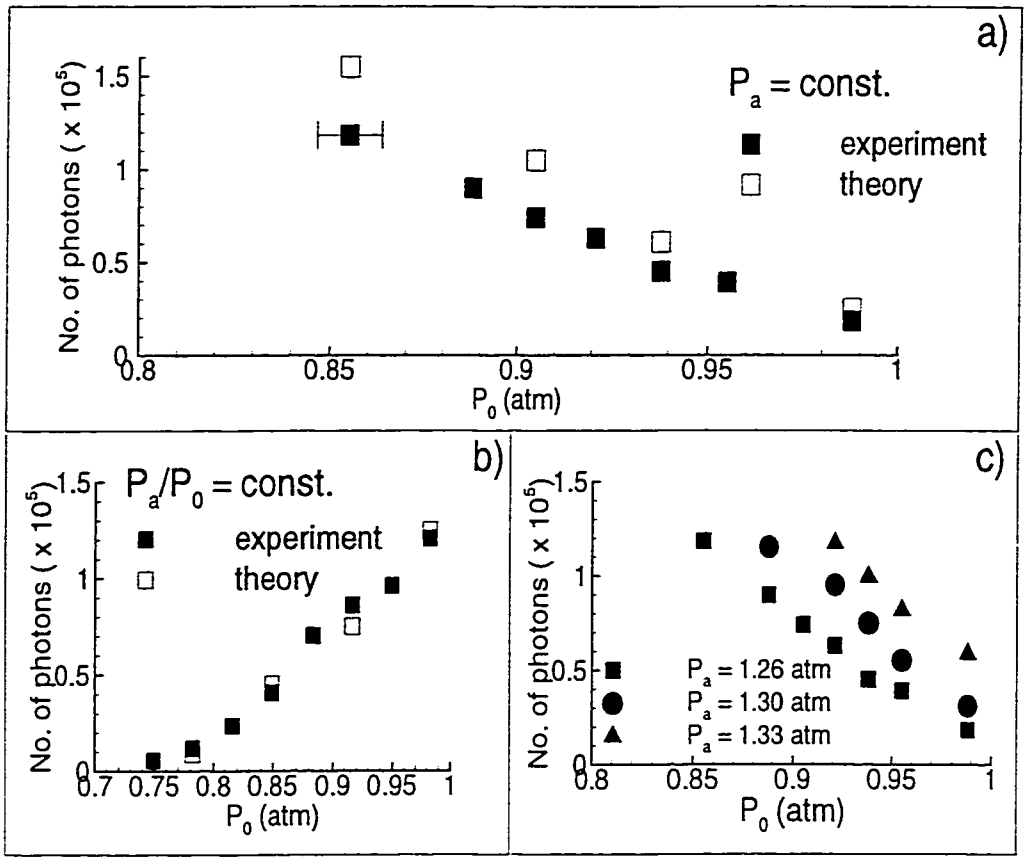

Figure 4.8: Number of photons in a single SL pulse versus P_0 (here $c_i/c_0 = 0.255$): a) for constant $P_a = 1.26$ atm; b) for constant ratio $P_a/P_0 = 1.41$; c) with P_a as a parameter. Typical experimental uncertainty is also shown in a) (the uncertainty of the number of photons is represented by a symbol size). Experimental results were not corrected for absorption in the liquid and flask walls; theoretical results were scaled down to experimental ones. The driving frequency was 17.465 kHz. The liquid temperature was 21 C. Spectral response of the PMT at a fixed wavelength was taken to calculate the number of photon.

infrared (IR) wavelengths. This means that we may in fact be underestimating the number of photon presents at the shorter and longer wavelengths. Changes in bubble emission brightness could be due in part to shifts in photon wavelength as well as changes in photon flux.

This ambiguity is a common problem associated with interpreting flux changes based on a broad-band PMT measurement. The better way to execute the experiment is to use a calibrated spectrometer to determine the wavelength-resolved photon flux. Such an instrument was not available, and even the more refined approach is severely limited because we still have to deal with the presence of the UV cutoff of the water itself. The use of a single, bandwidth-limited PMT was deemed adequate, given the absorptive properties of the water.

Another interesting question is the change of the SL emission as P_0 is varied, but the ratio P_a/P_0 is kept fixed. Figure 4.8(b) shows that both the experimental and theoretical results increase approximately linearly as P_0 is increased. This observation is consistent with the theoretically proposed increase of the expansion ratio as P_0 is increased, but P_a/P_0 kept constant [136].

Finally, the question of possible increase of maximum SL emission as P_0 is varied will be addressed. Since the SL intensity increases as P_0 is decreased and P_a kept constant (figure 4.8(a), it appears that by decreasing P_0 one could obtain a stronger pulse. However, in the experiment we find that, if P_a is kept constant,

and P_0 is decreased, for some critical value of $P_0 = P_0^{crit}$, the bubble becomes unstable and disappears. It has been found that $P_0^{crit} = P_0^{crit}(P_a)$; for lower P_a it is possible to go to lower values of P_0, without inducing instability. Figure 4.8(c) shows the results for the number of photons emitted, for three different values of P_a, as P_0 is varied. For all values of P_a, it has been observed that the maximum no. of photons is approximately the same. It appears that, at least in the probed parameter range, possible increase of the maximum SL output by changing P_0 is prevented by the limitations imposed by the stability requirements.

The intensity of steady-state SL emission is limited by three requirements: 1) a bubble be stable with respect to the gas diffusion; 2) it be stable with respect to shape instabilities [91, 166, 167], and 3) its position in the liquid does not change with time [147]. The instability due to mass flow is characterized by a rather slow process of bubble growth, possible break up and/or production of micro-bubbles [96]. Breaking up of the bubble has not been observed; as P_0 is decreased below a critical value, the bubble typically drifts away from the pressure antinode. If P_0 is further decreased, the bubble disappears. It is conjectured that it is the combination of the requirements 2) and 3) above which limits the SL intensity. More detailed experimental results and theoretical analysis of this effect will be given elsewhere [168].

4.3.2 Increasing the Ambient Pressure

Experiments have also been performed where the ambient pressure over the liquid head has been increased slowly. The increment of pressure has been performed by allowing controlled amount of air from a gas cylinder into the levitation cell by a gas handling system. The results of increasing ambient pressure are shown in figure 4.9. Again the physical size and the driving pressure amplitude were determined by fitting the experimental data to the R-P equation. For figure 4.9(a) the frequency of the driving pressure is 30.65 kHz. The best fit of the experimental data to the R-P equation was obtained when equilibrium radius, R_0 is equal to 6.0 μm and driving pressure amplitude is 1.49 atm (see figure 4.9(a)). The ambient pressure P_0 was 1.0 atm when the experiment was performed. When the ambient pressure on top of the liquid was increased to 1.1 atm keeping all the other experimental parameters same the fitted equlibrium radius was determined to be 4.8 mum. This is shown in figure 4.9(b). Furthermore, the intensity of the light decreases with increasing ambient pressure as shown in figure 4.10.

4.4 Summary

In conclusion, the first systematic measurements of the modifications of bubble dynamics and SL emission as the ambient pressure is varied has been reported

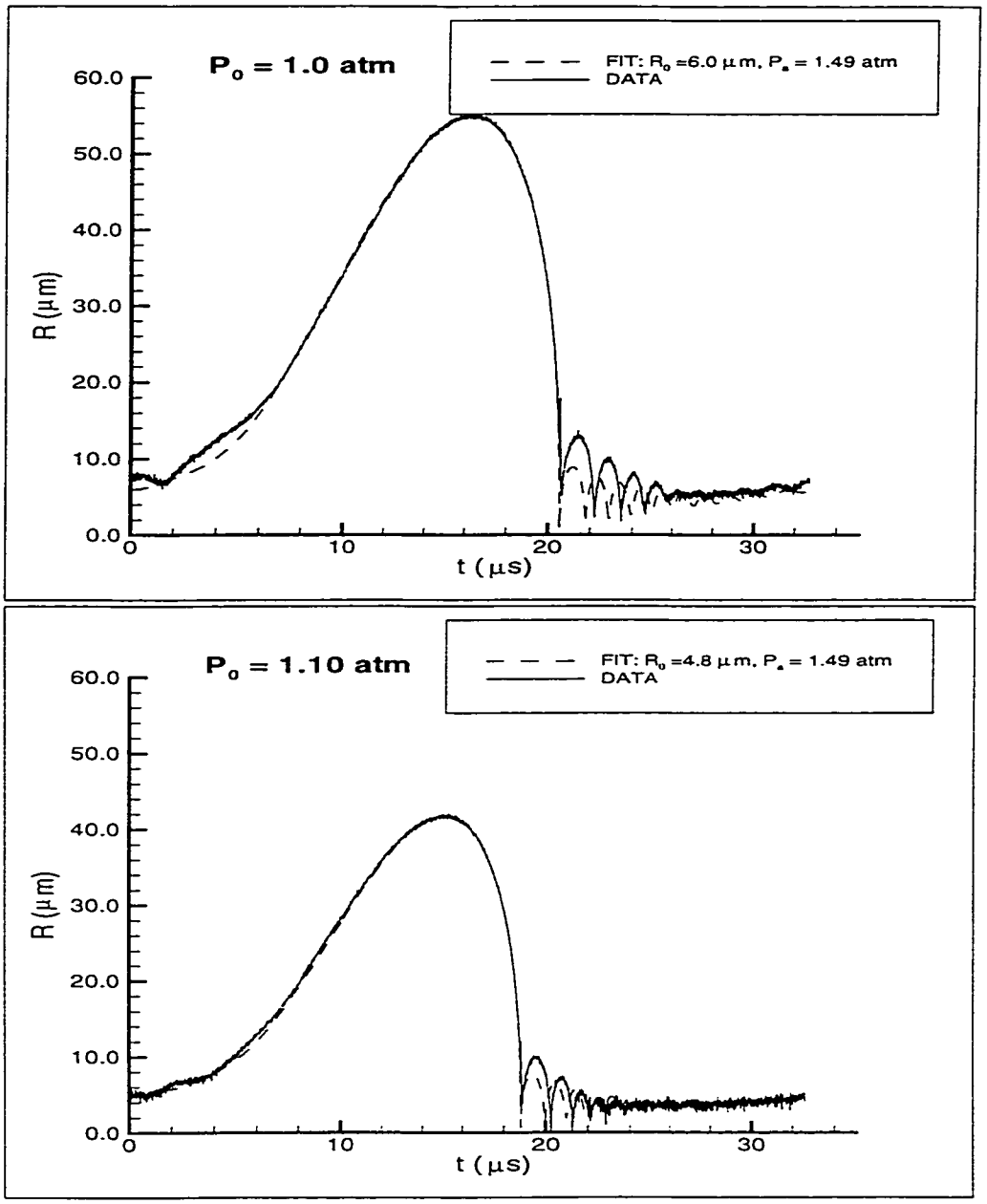

Figure 4.9: Experimental $R(t)$ curves as ambient pressure P_0 is increased at constant P_a. The driving frequency was 30.650 kHz and the liquid teperature was 21 C and c_i/c_0=0.4.

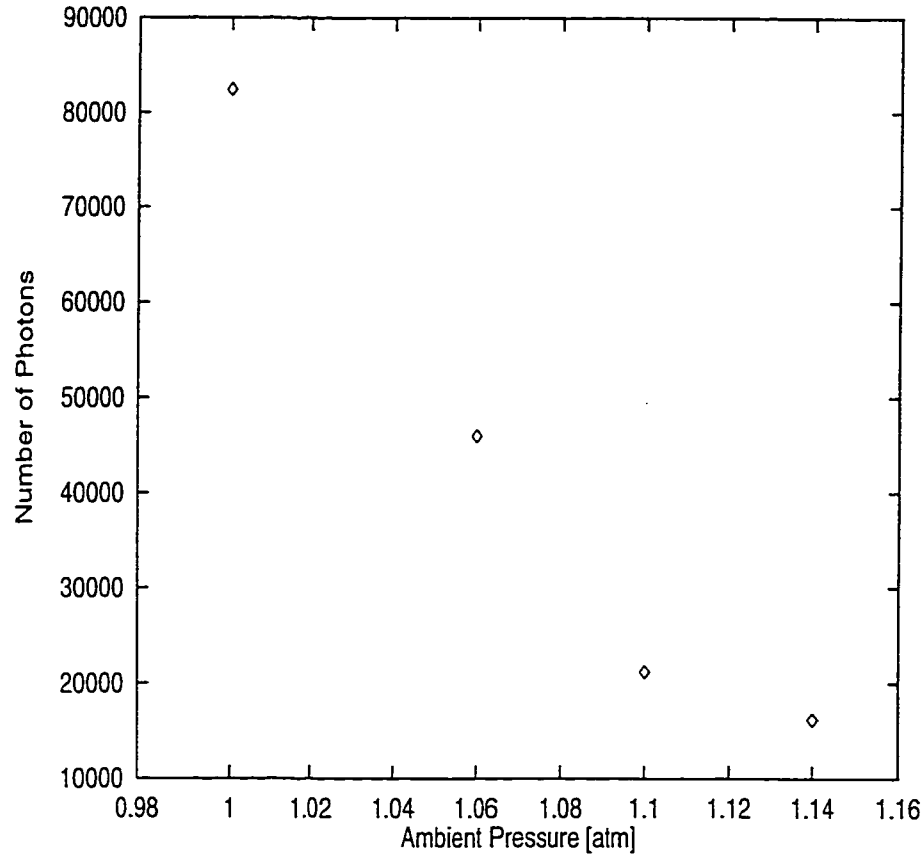

Figure 4.10: Number of photons in a single SL pulse as a function of increasing ambient pressure, P_0 for constant P_a. The driving frequency was 30.650 kHz. The liquid temperature was 21 C. The gas concentration was kept constant at 0.4 times of saturation concent ration.

here. A complete theoretical analysis and experimental results on the effect of ambient pressure on SBSL have been discussed. A strong increase of the number of photons emitted in a SL pulse is observed as the ambient pressure is reduced. Next, in agreement with the dissociation hypothesis, it has been observed that the equilibrium bubble radius increases as the ambient pressure is decreased. Further work in this direction will allow for even more precise comparison of our experimental results with theoretical predictions. In particular, these experiments will serve as an important test for a variety of SL theories.

Chapter 5

Acoustic Emission from SBSL

Introduction

It has been observed so far that the studies of SBSL mainly centered on measuring the properties of the emitted light. However, it is expected quite normally that the collapsing bubble will also launch acoustic waves in the liquid surrounding the bubble. Hallaj et. al. [143] were the first to observe AE spikes from a single bubble at different acoustic drive amplitudes in the SL and non SL regime. The study showed a large amplitude pulse corresponding to the initial collapse followed by smaller amplitude pulses corresponding to the rebounds. Weninger et. al. [64] reported the instrument limited rise time of 10 ns for the outgoing acoustic pulse with a pressure amplitude of 3 atm. at 1 mm away from the bubble. Similar results

have been observed by Ceccio *et al.* [171] from individual cavitation bubbles in a flow and by single bubble created in explosive conditions. Dan *et al.* [65] investigated acoustic emission from different regimes of bubble motion and compared these time domain results with the results of light scattering experiments. The results show that the principal acoustic pulse corresponds to the main collapse while the other pulses are emitted at the minimum of the respective after bounces. The authors reported an instrument limited rise time to 10 ns for the principal spike. Recently Matula et. al. [66] reported a detailed study on acoustic emissions from a single bubble using a 200 μm aperture PVDF needle hydrophone and a focused 10 MHz transducer. For the needle hydrophone, the instrument limited rise time of the principal spike is 5.2 ns and the amplitude is 1.7 atm at 1 mm away from the bubble. Observations of several signals with the 10 MHz focussed receiver corresponding to the after bounces were also reported. Wang et al. [172] have measured the emitted pressure wave which is produced at the collapse phase with a fiber optic probe hydrophone (FOPH). The spatial resolution of the hydrophone is 100 μm and its bandwidth ¿ 1GHz. The authors observed that the amplitude of the emitted acoustic wave increases from 1 to 3 atm. at a distance 2.5 mm above the bubble with increasing driving pressure in the sonoluminescing regime. The full width at half maximum (FWHM) of the acoustic wave also increases from 7 ns to 30 ns depending on the driving pressure amplitude and the dissolved gas

concentration in the liquid.

This chapter deals with the experimental results of acoustic emission, AE in the dancing, shrinking and sonoluminescing regimes of a single bubble trapped in a 17.5 kHz driving acoustic field. At first the goal of this research will be presented. The principal results of the theoretical analysis of the emitted pressure wave in the host liquid will be described next. The experimental setup to measure acoustic emissions has already been described in section 3.3.2. The results of the light scattering technique are used to find a correlation between the two types of emissions from the bubble. The setup for the the light scattering technique has also been explained in section 3.4. Next, the experimental results and discussions of the results will be presented. A qualitative comparison of the results with the available theories will be advanced along with a conclusion at the end.

5.1 Goal of the Research on Acoustic Emission

The RP equation (Eq. 2.13) which describes the motion of a bubble trapped in an acoustic field quite accurately is highly nonlinear in character. An analysis of the radius versus time, $R(t)$ curve shows that the acceleration of the collapsing bubble during the final moments of its collapse reaches extremely large values. Consequently it is expected that this violent collapse will also launch acoustic

waves in the liquid. It is possible to measure the properties such as amplitude and rise time of the emitted wave with a hydrophone placed in the vicinity of the bubble. By comparing the amplitude of the emitted wave with the results of theoretical models, it would be possible to estimate the pressure generated at the center of the collapsing bubble. Previous studies of acoustic emissions have been carried out in cavitation fields where several individual bubbles cavitate in an uncorrelated and transient fashion. As a result it has never been possible to detect the emitted signal from a single bubble and the experimental studies principally based on the spectral characteristics of "noise" signal measurements. The discovery of SBSL opened the avenue for measuring the SBSL emissions in a very controlled and accurate way. The objective of the present work is to compare the AE with light scattering and with recent theories. An additional goal is to perform a detailed study of the after bounces in different regimes of the bubble motion and again compare the results with light scattering in the same regimes.

5.2 Theoretical Overview

Despite the fact that the microscopic origin of SBSL eludes us, the dynamics of the bubble wall motion can be described fairly well by the hydrodynamic theory of the Rayleigh-Plesset (RP) equation [17]. Numerical simulations of this equation show

that the bubble grows during the rarefaction part of the acoustic drive pressure and undergoes a catastrophic collapse at the beginning of the compression phase. This leads to extremely high calculated temperature, pressure and density in the center of the bubble at the minimum of the collapse. The simulations of the RP equation also show that the collapse is followed by a series of after bounces at approximately the free bubble resonance frequency. The high pressure attained during the bubble collapse launches outgoing acoustic spikes in the liquid at or near the moment as SL is emitted. This effect can be studied by placing a needle hydrophone in the vicinity of the bubble.

On the theoretical side, Lee et. al. [169] calculated the shock pulse emanating from a sonoluminescing gas bubble by using analytical solutions of the conservation equations for the gas inside the bubble and the Kirkwood-Bethe hypothesis for the outgoing wave. According to their calculation the theoretical gas pressure at the bubble wall is about 10^4 atm. and the rise time of the shock pulse is about $5 - 7$ ns. The calculated pressure amplitude at a distance 1 mm from the bubble center is about 7.5 atm. Elze et. al. [170] carried out a detailed theoretical investigation of the acoustic emission by the sonoluminescing bubble. The effect of sound emission by the sonoluminescing bubble has been incorporated into the equation of motion and the non-perturbative method has been employed which used higher order perturbation expansion in $\frac{\dot{R}}{c}$ (where $\dot{R}$ is the bubble wall velocity and c is

the velocity of sound in the liquid) to account for the appropriate damping factor. The authors considered the bubble dynamics by taking into account the homologous rather than homogeneous bubble interior. According to their calculation the amplitude of the pulse at a distance 1 mm from the bubble is approximately 4.5 atm. The rise time (from one-half to maximum amplitude) is 40 ps and pulse decay time is 260 ps.

Matula et. al. [66] calculated the pulse amplitude and the pulse width for the principal spike by two different methods. The hydrodynamic model took into account the fact that the acoustic emission occurs due to the shock generated within the bubble due to the collapse. The calculated pressure amplitude is 2 bar at 1 mm from the bubble. The pulse width is 40 ps. In bubble dynamics model, the acoustic emission is believed to be generated due to the large deceleration that arrests the bubble wall's inward collapse. In this model the calculated pressure pulse at 1 mm away from the bubble is 15 atm. and the pulse width is 20 ns.

5.3 Experimental Results

The basic experimental observation of SBSL emissions is shown in figure 5.1. During the rarefaction part of the acoustic driving signal (a), the net pressure in the liquid goes to negative and the bubble expands by rectified diffusion process. By

the time the bubble grows to its maximum volume, the pressure inside the bubble drops and the compression phase of the driving signal sets in. The bubble at this moment undergoes a dramatic collapse followed by a few after bounces whose period of oscillation is determined approximately by the pulsating resonance of a free bubble in the liquid. (b) shows the square root of scattered laser light subtracted from the background along with SL pulses picked up by a photo detector. Trace (c) is the signature of AE, the large amplitude spike can be associated with the principal spike whereas the smaller amplitude spikes correspond to the after bounces. The delay between the SL spike and the main collapse is due to the finite speed of sound in water/glycerine mixture.

The intensity of the scattered light by the bubble in three different regimes of bubble motion is shown in figure 5.2. The intensity of the scattered light by a spherical bubble is directly proportional to the surface area of the bubble or the square of the radius of the bubble, so that the radius $R(t)$ of the bubble can be deduced from the scattered intensity. From the figure it is clear that the bubble is larger in the dancing regime than it is in the shrinking regime. The after bounces are the largest in the dancing regime. The acoustic emission in the above mentioned three regimes is shown in figure 5.3. It is to be noted that the acoustic signature follows the same behavior as the light scattering one. AE for the main spike and the first and second after bounces for the three regimes of bubble motion are shown in

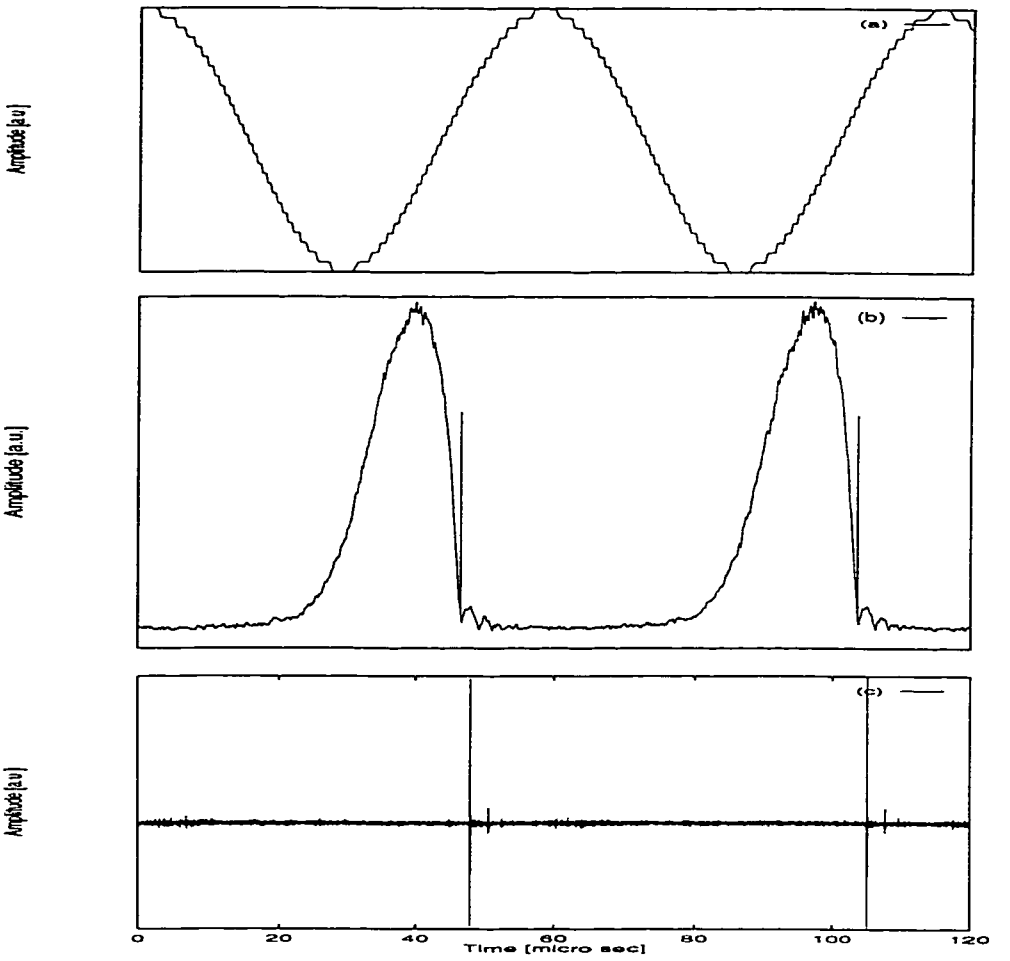

Figure 5.1: Experimental observation of SBSL emissions showing (a) driving acoustical signal measured by a 1 mm diameter PZT hydrophone (SPRH-S-1000 from Specialty Engineering Associates), (b) square root of PMT output subtracted from the background noise which can be used to determine $R(t)$ and (c) the AE spikes. The 17.5 kHz driving acoustic signal has been filtered out. The time delay between the SL spike and the principal AE spike is due to the finite speed of sound in the water/glycerine mixture. The liquid temperature was 21 C.The liquid was partially degassed.

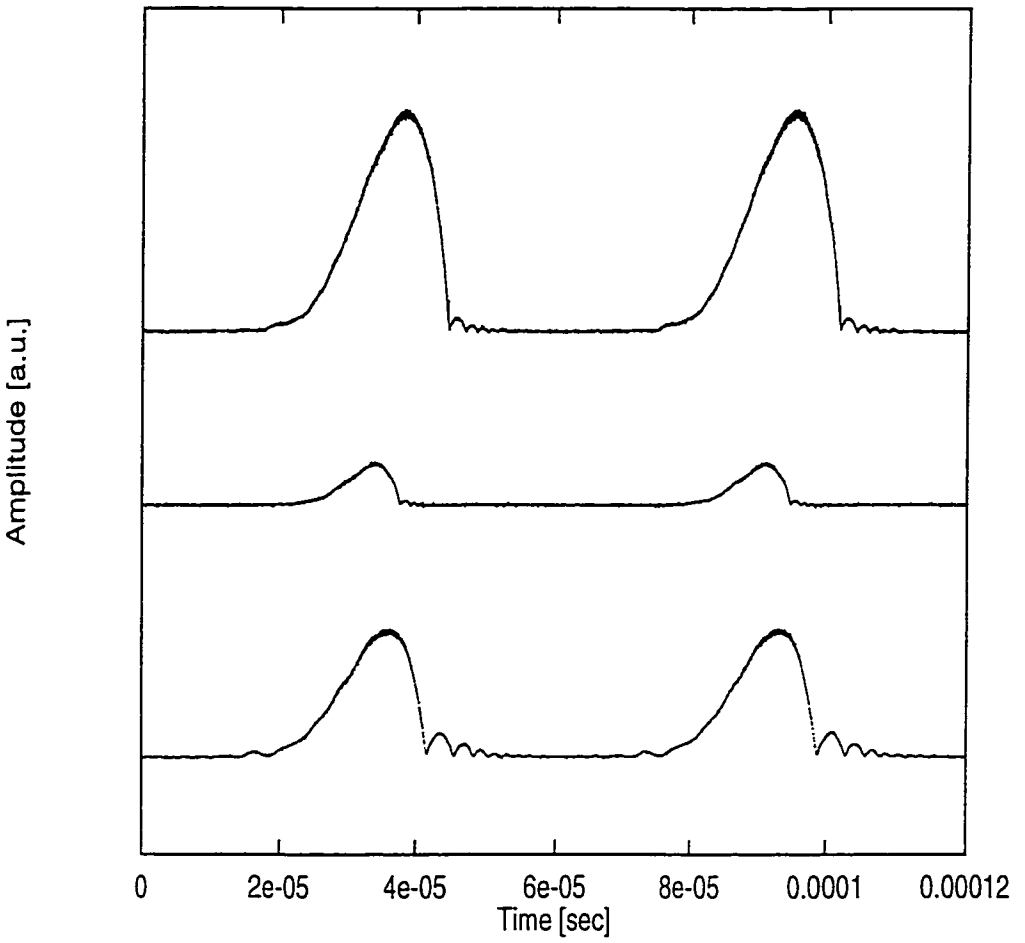

Figure 5.2: The intensity of the light scattered by the bubble in three different regimes of bubble motion. The scattered light is picked up by a PMT placed at an angle about 80 degrees with respect to the forward direction of the laser beam. The curves are vertically shifted but the scale remains the same. The top, middle and the bottom curves represent the uncalibrated $R(t)$s of the bubble in SBSL, shrinking, and dancing regimes respectively. The experimental conditions were the same as mentioned in Fig. 5.1.

figure 5.4. Going down each of the three columns it is to be noticed that the relative amplitudes are the same as shown in figure 5.3. For the first column we observe structure after the main pulse in all three regimes, similar to that observed by Matula et. al. in SBSL regime. Like these authors, we associate this with multiple reflections and ringing in the element of the hydrophone. As expected from the $R(t)$ results the widths of the after bounces for AE are considerably larger than for the main spike in each regime. Since the instrument limited rise time of the hydrophone is about 10 nanoseconds, the FWHM and the rise time for the main spike in the three regimes are essentially instrument limited except perhaps for the FWHM in the dancing regime. The width of the principal spike in the SBSL regime ($\sim$ 20 ns) is in rough agreement with that reported by Matula et. al. ($\sim$ 25ns). The rise times and the FWHM for the first and second after bounces are considerably larger and hence their measurement is less affected by the instrument limited risetimes. All of these results have been summarized in Table 5.1.

Figure 5.5 shows the principal spike emitted by a sonoluminescing bubble. The spike is measured by a 0.75 μm PVDF hydrophone placed at 1 mm above the bubble. As seen from the figure the amplitude of the spike is about 24 atm with a pulse rise time of about 5 ns. The hydrophone is used in conjunction with a booster amplifier with a voltage gain of about 28 dB. According to the calibration, 1nV represents 1 Pa at 40 MHz. Calibration has been performed at

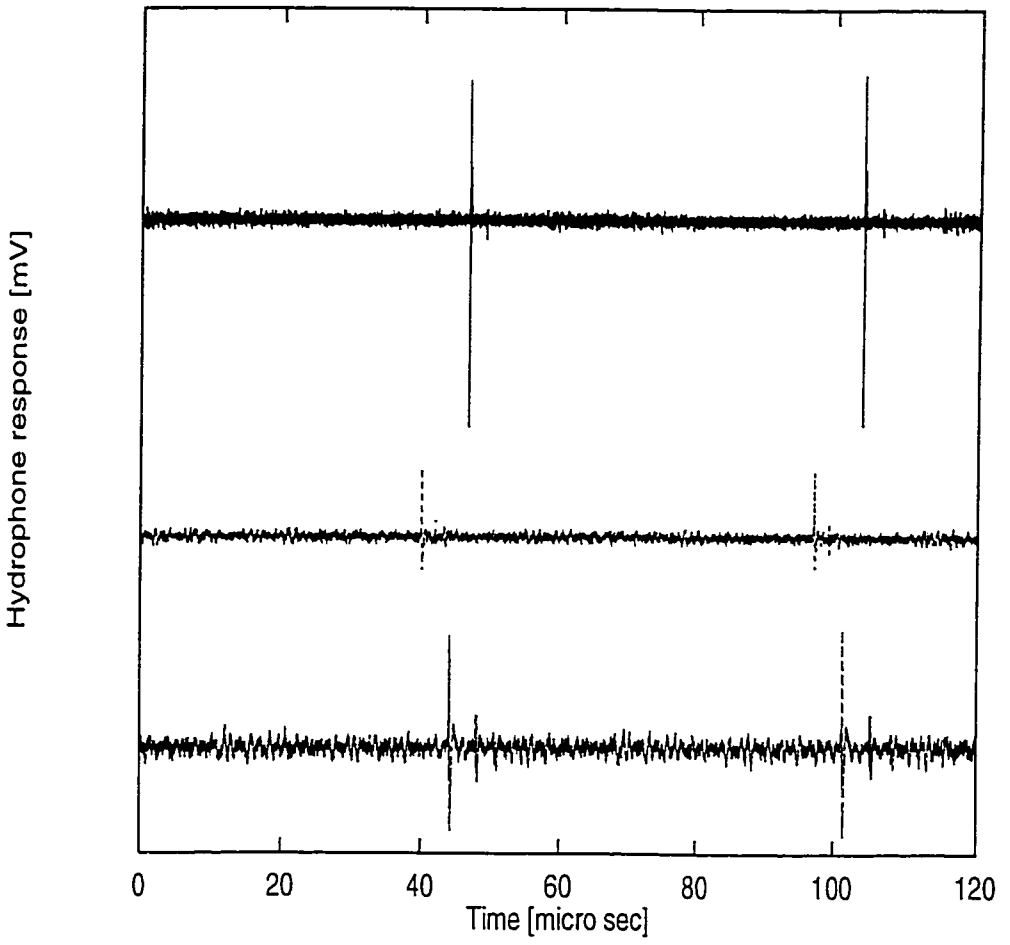

Figure 5.3: Acoustic emissions from the same three regimes as mentioned in figure 5.2. It is to be noticed that the acoustic signature follows that same behavior as the light scattering one. In all cases the 17.5 kHz driving signal has been filtered out by data processing by Labview software package. The experimental conditions were the same as mentioned in Fig. 5.1.

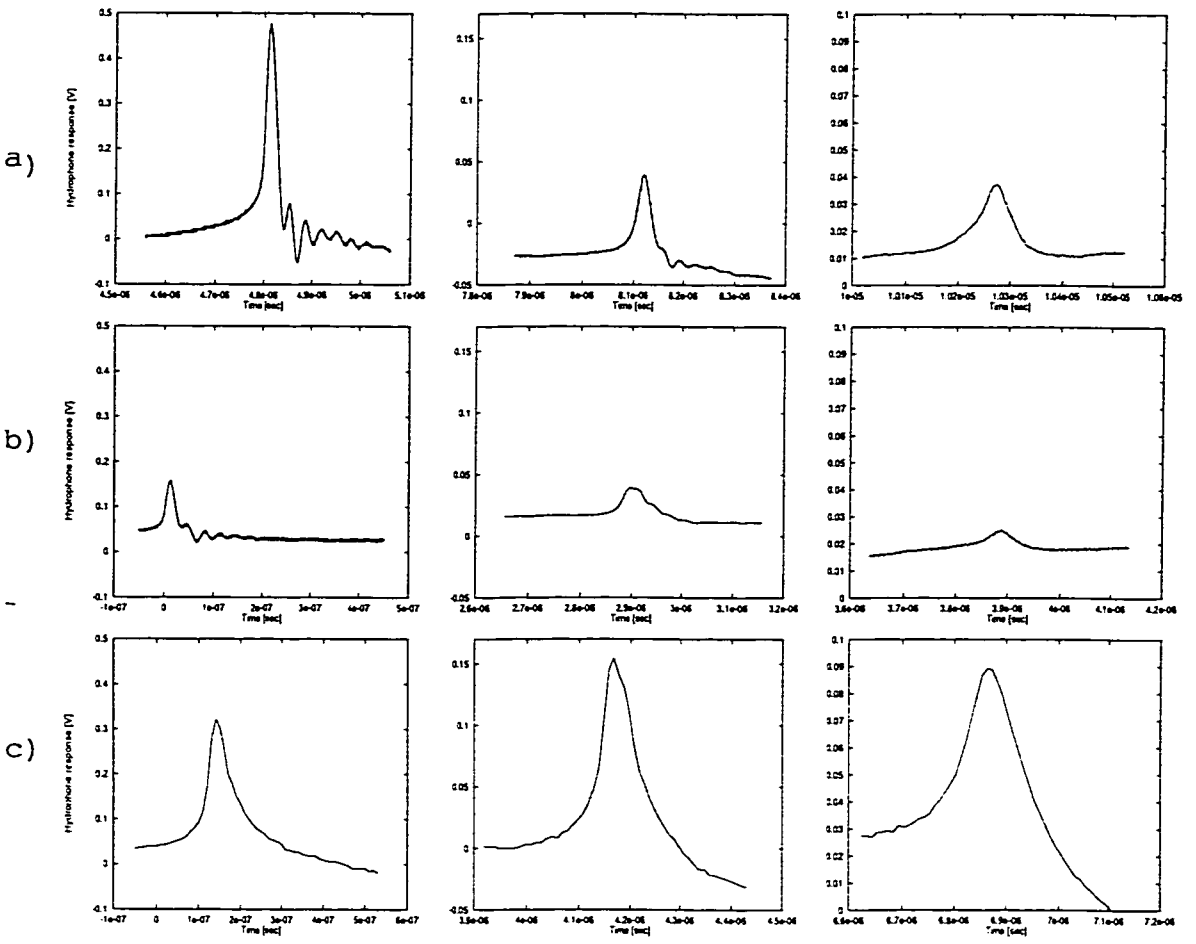

Figure 5.4: The principal AE spike (i) and the acoustic emissions associated with the after bounces (ii) and (iii) in the same three regimes; (a) SBSL, (b) Shrinking and (c) Dancing. Scales are all the same on the horizontal (Time) axis and same for each column on the vertical (Hydrophone Response) axis. The driving 20 kHz signal has not been filtered out. According to the calibration of the hydrophone ($4.104 * 10^{-}6$ V/Pa at 20 MHz) the pressure amplitude of the principal spike is 1.16 bar at 7.28 mm from the bubble.

Table 5.1: **The rise time and full width at half maximum (FWHM) of the principal spikes and the first and second after bounces in three different regimes with PZT hydrophone.**

Bubble Regime		**Principal Spike (ns)**	**1st After Bounce (ns)**	**2nd After Bounce (ns)**
SBSL	Rise Time	11	24	60
	FWHM	21	28	60
Shrinking	Rise Time	11	27	46
	FWHM	18	47	50
Dancing	Rise Time	15	61	92
	FWHM	47	70	106

NPL, England. However, it should be mentioned here the hydrophone response to a delta function pressure wave is not known. Hence unfortunately the deconvolution of the measured signal from the response of the instrument have not been carried out.

Table 5.2: **Principal AE Spike: Theoretical Versus Experimental Values**

	Y. P. Lee *et al.*	**H. T. Elze** *et al.*	**Matula (Hydro--dynamics)**	**Matula (Bubble-. -dynamics)**	**Our Measured values**
Amplitude 1 mm from the bubble (atm)	7.5	4.5	2	15	24
Rise Time (ns)	5-7	0.040	0.040	5.2	~ 5

5.4 Discussions of Results

The nature of the dancing and SBSL regimes have been well established in previous studies of SBSL. The existence of the shrinking regime can be explained as follows

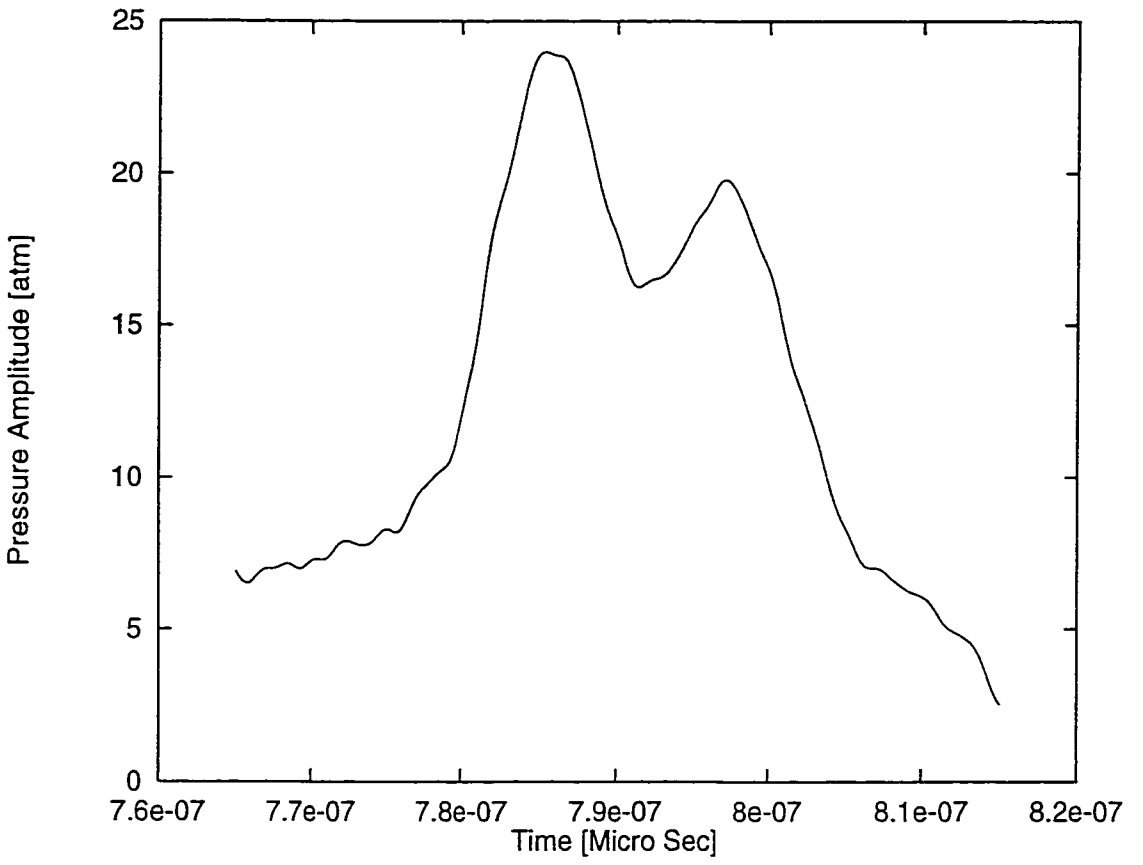

Figure 5.5: The principal spike in SBSL regime measured by a 0.75 μm PVDF hydrophone placed at about 1 mm above the bubble. The response of the hydrophone has not been deconvoluted. The experimental conditions were the same as mentioned in Fig.5.1.

[93]. As the driving pressure amplitude is increased the temperature inside the bubble increases. When the temperatures generated by the bubble collapse are beyond the dissociation temperature of oxygen (O) and nitrogen (N) ($\gg$ 9000 K), O and N radicals are produced which react with H and O radicals formed from the dissociation of water vapor. Rearrangement of the radicals leads to the formation of NO, OH, and NH which ultimately dissolve into water leading to the formation of H_2O_2 ,HNO_2 and HNO_3 among other products. These products are passed into the surrounding water. As the solubility of these compounds is enormous they will not be recollected during the next bubble cycle. By this chemical process the bubble gets rid of the reactive gases such as O_2 and N_2 and eventually the bubble shrinks in size compared to its size in the dancing regime.

As seen from figure 5.4, the present work gives qualitative information on the amplitude and structure of the after bounce signals, as to first order the measurements are not instrument limited. A detailed knowledge of the after bounces could be important for a full, unified description of the SBSL phenomenon. For example, Hilgenfeldt et. al. [136] pointed out that the after bounces give important information on the structure of the expansion ratio and the diffusive equilibrium stability conditions. As a first step towards a more general description, in what follows the AE signals have been correlated with the $R(t)$ determined by light scattering.

To compare AE with light scattering, three separate but related aspects; resonance frequency, amplitude and energy emission are considered. Figure 5.2 shows the natural resonance period of a bubble after its first collapse. The period of pulsating resonance of a free bubble is given by Minnaert's [127] formula:

$$T_{R_0} \approx \frac{2\pi R_0}{(3\gamma)^{0.5}} \left(\frac{\rho}{P_0 + \frac{2\sigma}{R_0}} \right)^{\frac{1}{2}} \tag{5.1}$$

where R_0 is the equilibrium radius of the free bubble, i.e. when the pressure in the liquid is equal to the ambient pressure P_0. γ is the ratio of specific heats and σ and ρ are the surface tension and density of the liquid respectively. From Figure 5.2 the measured value of T_{R_0} from both AE and light scattering experiment is approximately 2 μs. According to Minnaert's formula thus implies that the equilibrium radius of the bubble is about 5.0 μm. Thus both $R(t)$ and AE data lead to the same value of the equilibrium radius of the bubble.

Finally, it is of interest to compare the experimental results for the main AE spike with predictions of the theoretical models. Since each model uses different assumptions and approaches and the details are unknown in some cases our results are compared with each one in turn. The theories give pressure at 1mm from the bubble. A larger diameter, higher sensitivity hydrophone has been used in order to observe the after bounces; it was placed about 7 mm from the bubble to avoid perturbing the latter. For comparison with theory, the amplitude has been

extrapolated using a *fraclr* varaition for non shock and shock pulses. Clearly the two models predicting FWHM of 40 and 300 ps have frequencies in the GHz range. These high frequency components will have propagation distances much shorter than 7 mm, even much shorter than 1 mm for the highest frequencies. Further, due to the restricted bandwidth of the hydrophone of about 30 MHz it has not been possible to detect these high frequency components, even if the hydrophone were placed closer to the bubble. Therefore in the present study it has not been possible to compare our experimental results with the high frequency theories.

Following the solution for the field radiated by a pulsating sphere in a liquid [67] Matula et. al. presented the second model which corresponds to acoustic emission at the moving bubble interface due to the deceleration of the wall. The prediction of the model are $p = 15$ bar and a FWHM of 20 ns at 1 mm from the bubble using the same bubble parameters. This would give $p = 2$ bars and FWHM $\sim$ 20 ns at 7.28 mm. Given the uncertainties these results are in reasonable agreement with our measurements.

The other model, that of Lee et. al., considers shock emission from the violently collapsing bubble, where the gas pressure at the bubble wall at the moment of emission is about 10^4 bars. The shock wave pressure predicted at 7.28 mm is 1.03 atm and the calculated rise time of the shock is about 5 ns. The predicted

amplitude (not taking into account acoustic absorption) is in very good agreement with our measurements while the rise time is not inconsistent with our instrument limited measurements. The calculated values of the pressure amplitude and the rise time of the principal spike in SBSL regime at 1 mm from the bubble along with our experimental results are shown in Table 5.2. It must be mentioned here that the response of the hydrophone (PVDF 0.75 μm) has not been deconvoluted from its intrinsic response.

The predictions of both of these models are compatible with our experimental results, given the uncertainties and unknowns in the various parameters. In this sense our conclusions are similar to those of Matula *et al.* who were unable to determine whether the principal mechanism of AE was due to a deceleration or to a shock model. For reasons already mentioned, however, no model, including those predicting a very sharp AE spike, can be ruled out at this stage.

Very recently Pecha and Gompf reported a streak image with high spatial and temporal resolution of the final phase of the bubble collapse [173]. The authors concluded that the high pressure generated in the last moment of the dramatic bubble collapse results in the generation of a shock wave. This shock wave propagates in the surrounding liquid with a velocity of about 4000 m/s. It is also reported that the amplitude of the shock wave gets attenuated much faster than $\sim 1/r$ and the calculated pressure very close to the bubble wall could be as

high as 40-60 kbar.

5.5 Summary

The present work shows that there is a good correlation between AE and $R(t)$ determined by light scattering in the various bubble regimes. Due to instrumental limitations the intrinsic width of the main AE spike cannot be determined; those for the after bounces are considerably larger and it is believed that those reported here are close to the intrinsic values. Likewise a determination of the true pressure amplitude can only be made by a deconvolution of the measured data with the hydrophone response functions. Based on the observed AE amplitude of the main spike, of the four theoretical calculations available, those of Lee et. al. are in best agreement with experiment. However, further work is needed before a firm conclusion can be reached on this point.

Chapter 6

Conclusion

6.1 Summary of the Dissertation

The phenomenon of single bubble sonoluminescence was observed for the first time only about a decade ago. In this short time the exotic nature of the phenomenon has attracted researchers from almost all areas of science and engineering to take a very active part in an attempt to unfold the mysteries behind it. As a result of vigorous research in this subject, it has been studied thoroughly and carefully. The properties of the SBSL emissions and the bubble dynamics have been studied in a part of parameter space. Towards this end, one of the parameters namely the ambient pressure, P_0 above the liquid has been varied. Secondly, one of the SBSL emissions, acoustic emission (AE) has also been studied. The following

achievements have been accomplished:

- The first complete and controlled study of the effect of ambient pressure on SBSL has been carried out. Results have been obtained for both increasing and decreasing ambient pressure.
- The resulting modifications of the bubble dynamics (radius versus time $R(t)$) were recorded by the usual Mie scattering technique.
- The results of the modification of the equilibrium bubble radius prove the recently proposed *dissociation hypothesis.*

Furthermore, the study of the acoustic emission provides information regarding the following:

- Pulse widths (FWHM), rise times, and amplitudes of emitted waves from the collapsing bubble at a specific distance from the bubble have been measured, as explained many of these observations were instrument limited.
- A correlation between the results of the light scattering experiment with those of acoustic emission has also been established.
- The principal spike as well as emissions associated with the after bounces have been studied in three different regimes; (1) SBSL, (2) Shrinking, and (3) Dancing.

6.2 Summary and Conclusions

The following conclusions can be drawn from the experimental work of the dissertation:

6.2.1 Ambient Pressure Effect

- The first systematic measurements of the modifications of the bubble dynamics and SL emission with the variation of ambient pressure have been performed. The equilibrium radius, R_0 increases from 7.3 μm to 9.0 μm as the ambient pressure, P_0 is decreased from 1.0 atm to 0.9 atm keeping P_a constant at 1.29 atm. Similarly, R_0 decreases from 6.0 μm to 4.8 μm when P_0 is increased from 1 atm to 1.10 atm at constant P_a (1.49 atm). It is noticed that the expansion ratio (R_{max}/R_{min}) increases as the ambient pressure is decreased.

- From the modification of the bubble dynamics, it has been observed that, in agreement with the dissociation hypothesis, the equilibrium bubble radius increases as the ambient pressure is decreased.

- The number of emitted photons per pulse increased about seven times when P_0 is decreased by only 15 %. On the other hand, increasing P_0 by the same

amount decreases the number of emitted photons by about the same order of magnitude.

- There is a approximately linear weak increment in the number of photons per pulse as P_0 is increased while keeping P_a/P_0 constant.

- It has been observed that it is not possible to push the limits of SL emission with decreasing P_0 continuously. Beyond a critical value of P_0 depending on P_a, different types of instabilities set in and the bubble ultimately disappears.

6.2.2 Acoustic Emission from SBSL

- A good correlation between the time domain results of AE and radius versus time $R(t)$ curves obtained by light scattering, in three different regimes of bubble motion has been found.

- The FWHM and rise times of the principal spikes associated with the main collapse are documented in Table 5.1. Similarly, the FWHM and rise times of the first and second after bounces in the SBSL, shrinking, and dancing regimes are mentioned as well. Due to instrumental limitations the intrinsic width of the main AE spike cannot be determined, those for the after bounces are considerably larger and it is believed that those reported here are close to the intrinsic values.

- The estimated pressure amplitude of the principal spike in SBSL regime associated with the first collapse at a distance 7.28 mm is about 1.2 atm (instrument limited and this is a lower bound).

6.3 Future Works

- It would be interesting to vary the dissolved gas concentration (i.e. changing c_i/c_0) without changing the other parameters of the host liquid significantly and observe the $R(t)$ curves. This will help to better understand the bubble dynamics and the role of ambient pressure as well.

- The determination of the light emitting region inside the bubble remains a challenge to the experimentalists.

- Measurements of acoustic emissions from SBSL performed with PZT hydrophones have been reported. However, in these reports the response function of hydrophones used have not been measured with extremely sharp pulses. As a result, the response function of hydrophones have not been deconvoluted from the measured signal. It would be interesting to do this and obtain the amplitude, rise time and pulse width of the acoustic emission only.

Bibliography

[1] D. Bernoulli, "Hydrodynamica, sive de viribus et motibus fluidorum comentarii", Stasbourg (1738)

[2] J. Thornycroft and S. W. Barnaby, Inst. Civ. Eng. **122**, 51 (1895)

[3] Lord Rayleigh, Phil. Mag. **34**, 94 (1917)

[4] W. T. Richards and A. L. Loomis J. Am. Chem. Soc. **49**, 3086 (1927)

[5] F. O. schmitt, C. H. Jhonson, and A. R. Olson, J. AM. Chem. Soc. **51**, 370 (1929)

[6] H. Beuthe, Z. Phys. Chem. A. **163**, 161 (1932)

[7] H. Frenzel and H. Schultes, Z. Phys. Chem. B. **27**, 421 (1934)

[8] N. Marinesco and J. J. Trillat, C. R. Acad. Sci. Paris, **196**, 858 (1933)

[9] P. Zimakov, C. R. Acad. Sci. USSR, **3**, 452 (1934)

[10] L. A. Chambers, Phys. Rev. **49**, 881 (1937); J. Chem. Phys. **5**, 290 (1937)

[11] R. O. Prudhomme and Th. Guilmart, J. Chem Phys. **54**, 336 (1957)

[12] P. D. Jarman, Proc. Phys. Soc. B **72**, 628 (1959)

[13] H. Kuttruff, Acoustica, **12**, 230 (1962)

[14] L. D. Rosenberg, Acoutica, **12**, 40 (1962)

[15] D. Srinivasan and L. V. Holroyd, J. Appl. Phys. **32**, 446 (1961)

[16] P. D. Jarman, Aust J. Phys. **23**, 319 (1970)

[17] A. J. Walton and G. T. Reynolds, Adv. Phys. **33**. 595 (1984)

[18] R. G. Verral and C. M. Sehgal, Ultrasonics **25**. 29 (1987)

[19] R. Esche, Acustica, **2**, AB208 (1952)

[20] K. Negishi, Acustica, **10**, 124 (1961); J. Phys. Soc. Jpn. **16**, 1450 (1961)

[21] K. S. Suslick, Sci. Am. **February**, 80 (1989)

[22] K. S. Suslick, Science **247**, 1439 (1990)

[23] E. B. Flint and K. S. Suslick, Science, **253**, 1397 (1991)

[24] W. B. McNamara III, Y. T. Didenko, and K. S. Suslick, Nature, **401**, 772 (1999)

[25] T. K. Saksena and W. L. Nyborg, J. Chem. Phys. **53**, 1722 (1970)

[26] L. A. Crum and G. T. Reynolds, J. Acoust. Soc. Am. **78**, 137 (1985)

[27] D. F. Gaitan, L. A. Crum, C. C. Church, R. A. Roy, J. Acoust. Soc. Am. **91**, 3166 (1992)

[28] S. Putterman, Physcis World, **August**, 18 (1999)

[29] P. R. Temple, R. W. Detenbeck, and W. L. Nyborg, J. Acoust. Soc. Am. **50**, 112 (1971)

[30] E. N. Harvey, J. Am. Chem. Soc. **61**, 2392 (1939)

[31] J. Frenkel, Acta Phys.-Chim. U.R.S.S. **12** 317 (1940)

[32] W. A. Weyl and E. C. Marboe, Research, **2**, 19 (1949)

[33] B. E. Noltingk and E. A. Neppiras, Proc. Phys. Soc. B, **63**, 674 (1950)

[34] P. D. Jarman, J. Acoust. Soc. Am. **32**, 1459 (1960)

[35] R. Hickling, J. Acoust. Soc. Am. **35**, 967 (1963)

[36] V. Griffing, J. Chem. Phys. **18**, 997 (1950); V. Griffing, J. Chem. Phys. **20**, 939 (1952)

[37] C. Seghal, R. G. Sutherland and R. E. Verall, J. Phys. Chem. **84**, 227 (1980)

[38] C. Seghal, R. G. Sutherland and R. E. Verall, J. Phys. Chem. **84**, 388 (1980);

[39] C. Seghal, R. G. Sutherland and R. E. Verall, J. Phys. Chem. **84**, 525 (1980)

[40] C. Seghal, R. G. Sutherland and R. E. Verall, J. Phys. Chem. **84**, 529 (1980)

[41] C. Seghal, R. G. Sutherland and R. E. Verall, J. Phys. Chem. **85**, 315 (1981)

[42] P. K. Chendke and H. S. Folger, J. Phys. Chem. **87**, 1362 (1983)

[43] M. Degrois and P. Baldo, Ultrasonics, **12**, 25 (1974)

[44] K. S. Suslick, E. B. Flint, M. W. Grinstaff, K. A. Kemper, J. Phys. Chem. **97**, 3098 (1993)

[45] D. F. Gaitan, Ph. D. Thesis, University of Mississippi (1990)

[46] B. P. Barber, R. Hiller, K. Arisaka, H. Fettermann, and S. J. Putterman, J. Acoust. Soc. Am. **91**, 3061 (1992)

[47] B. P. Barber and S. J. Putterman, Nature(London), **352**, 318 (1991)

[48] B. Gompf, R. Günther, G. Nick, R. Pecha, and W. Eisenmenger, Phys. Rev. Lett. **79**, 1405 (1997)

[49] R. A. Hiller, S. J. Putterman, and K. R. Weninger, Phys. Rev. Lett. **80**, 1090 (1998)

[50] R. A. Hiller, S. J. Putterman, and B. P. Barber, Phys. Rev. Lett. **69**, 1182 (1992)

[51] B. P. Barber, Ph. D. Thesis, University of California, Los Angeles (1992)

[52] B. P. Barber and S. J. Putterman, Phys. Rev. Lett. **69**, 3839 (1992)

[53] B. P. Barber, R. A. Hiller, R. Löfstedt, S. J. Putterman, and K. R. Weninger, Physics Reports, **281**, 65 (1997)

[54] J. D. N. Cheeke, Can. J. Phys. **75**, 77 (1997)

[55] R. A. Hiller, Ph. D. Thesis, University of California, Los Angeles (1995)

[56] C. Eberlein, Phys. Rev. Lett. **76**, 3842 (1996)

[57] C. Eberlein, Phys. Rev. A. **53**, 2772 (1996)

[58] J. Schwinger, Proc. Natl. Acad. Sci. USA, **89**, 4091 (1992)

[59] J. Schwinger, Proc. Natl. Acad. Sci. USA, **89**, 11118 (1992)

[60] J. Schwinger, Proc. Natl. Acad. Sci. USA, **90**, 958 (1993)

[61] J. Schwinger, Proc. Natl. Acad. Sci. USA, **90**, 2105 (1993)

[62] J. Schwinger, Proc. Natl. Acad. Sci. USA, **90**, 4505 (1993)

[63] J. Schwinger, Proc. Natl. Acad. Sci. USA, **90**, 7285 (1993)

[64] K. R. Weninger, B. P. Barber, and S. J. Putterman, Phys. Rev. Lett. **78**, 1799 (1997)

[65] M. Dan and J. D. N. Cheeke, IEEE Ultrasonic Sysposium Proceedings, **1**, 515 (1997)

[66] T. J. Matula, I. M. Hallaj, R. O. Cleveland, L. A. Crum, W. C. Moss, and R. A. Roy, J. Acoust. Soc. Am. **103**, 1377 (1998)

[67] A. D. Pierce, *Acoustics: An Introduction to Its Physical Principles and Applications*, McGraw Hill Book Company, New York (1981)

[68] K. A. Milton and Y. J. Ng, Phys. Rev. E. **55**, 4207 (1997)

[69] K. A. Milton and Y. J. Ng, Phys. Rev. E. **57**, 5504 (1997)

[70] I. Brevik, V. N. Marachevsky, and K. A. Milton, Phys. Rev. Lett. **82**, 3948 (1999)

[71] M. Visser, S. Liberati, F. Belgiorno, and D. W. Sciama, Phys. Rev. Lett. **83**, 678 (1999)

[72] H. P. Greenspan, and A. Nadim, Phys. Fluids A **5**, 1065 (1993)

[73] C. C. Wu and P. H. Roberts, Phys. Rev. Lett. **70**, 3424 (1993)

[74] C. C. Wu and P. H. Roberts, Proc. R. Soc. Lond. A, **445**, 323 (1994)

[75] R. A. Hiller, K. R. Weninger, S. J. Putterman, and B. P. Barber, Science, **266**, 248 (1994)

[76] L. Frommhold and A. A. Atchley, Phys. Rev. Lett. **73**, 2883 (1994)

[77] R. Hickling, Phys. Rev. Lett. **73**, 2853 (1994)

[78] R. Löfstedt, K. R. Weninger, S. J. Putterman, and B. P. Barber, Phys. Rev. E. **51**, 4400 (1995)

[79] B. P. Barber, K. R. Weninger, R. Löfstedt, and S. J. Putterman, Phys. Rev. Lett. **74**, 5276 (1995)

[80] E. Eller and H. G. Flynn, J. Acoust. Soc. Am. **37**, 493 (1964)

[81] L. A. Bernstein and M. R. Zakin, J. Phys. Chem, **99**, 14619 (1995)

[82] K. R. Weninger, R. A. Hiller, B. P. Barber, D. Lacoste, and S. J. Putterman, J. Phys. Chem. **99**, 14195 (1995)

[83] T. J. Matula, R. A. Roy, P. D. Mourad, W. B. McNamara III, and K. S. Suslick, Phys. Rev. Lett. **75**, 2602 (1995)

[84] E. B. Flint, K. S. Suslick, J. Am. Chem. Soc. **111**, 6987 (1989)

[85] K. S. Suslick and E. B. Flint, Nature, **330**, 553 (1987)

[86] L. S. Bernstein, M. R. Zakin, E. B. Flint, and K. S. Suslick, J. Phys. Chem. **100**, 6612 (1996)

[87] W. G. Unruh, Phys. Rev. D. **14**, 870 (1976)

[88] C. S. Unnikrishnan and S. Mukhopadhyay, Phys. Rev. Lett, **77**, 4690 (1996)

[89] A. Lambrecht, M.-T. Jaekel, and S. Reynaud. Phys. Rev. Lett. **78**, 2267 (1997)

[90] N. Garcia and A. P. Levanyuk, Phys. Rev. Lett. **78**, 2268 (1997)

[91] M. P. Brenner, D. Lohse, and T. F. Dupont. Phys. Rev. Lett. **75**, 954 (1995)

[92] D. Lohse, M. P. Brenner, and S. Hilgenfeldt, J. Acoust. Soc. Am. **100**, 2678 (1996)

[93] D. Lohse, M. P. Brenner, T. F. Dupont, S. Hilgenfeldt, and B. Johnston, Phys. Rev. Lett. **78**, 1359 (1997)

[94] S. Hilgenfeldt, D. Lohse, and M. P. Brenner, Phys. Fluids, **8**, 2808 (1996)

[95] D. Lohse and S. Hilgenfeldt, J. Chem. Phys. **107**, 6986 (1997)

[96] R. G. Holt and D. F. Gaitan, Phys. Rev. Lett. **77**, 3791 (1996)

[97] T. J. Matula and L A. Crum, Phys. Rev. Lett. **80**, 865 (1998)

[98] J. A. Ketterling and R. E. Apfel, Phys. Rev. Lett. **77**, 3791 (1996)

[99] M. Dan, J. D. N. Cheeke, and L. Kondic, Phys. Rev. Lett. **83**, 1870 (1999)

[100] M. Dan, J. D. N. Cheeke, and L. Kondic, Ultrasonics (in print) (2000)

[101] M. Dan, J. D. N. Cheeke, and L. Kondic, CD Rom Proceeding of the Joint Conference of ASA, EAA, and DAGA, 1PPAD-8 (1999)

[102] A. Prosperetti, J. Acoust. Soc. Am. **101**, 2003 (1997)

[103] M. S. Longuet-Higgins and H. Oguz, J. Fluid Mech. **290**, 183 (1995)

[104] T. Lepoint, D. D. Pauw, F. Lepoint-Mullie, M. Goldman, and A. Glodman, J. Acoust. Soc. Am. **101**, 2012 (1997)

[105] W. C. Moss, D. B. Clarke, D. A. Young, Science, **276**, 1398 (1997)

[106] L. A. Crum and T. J. Matula, Science, **276**, 1348 (1997)

[107] P. Mohanty and S. V. Khare, Phys. Rev. Lett. **80**, 189 (1998)

[108] L. Frommhold, Phys. Rev. E. **58**, 1899 (1998)

[109] M. J. Moran and D. Sweider, Phys. Rev. Lett. **80**, 4987 (1998)

[110] R. Pecha, B. Gompf, G. Nick, Z. Q. Wang, and W. Eisenmenger, Phys. Rev. Lett. **81**, 717 (1998)

[111] W. C. Moss, J. L. Levatin, and A. Szeri, J. Acoust. Soc. Am. **4**, 2290 (1999)

[112] S. Hilgenfeldt, S. Grosmann, and D. Lohse, Nature, **398**, 402 (1999)

[113] S. Hilgenfeldt, S. Grosmann, and D. Lohse, Phys. Fluids, **11**, 1318 (1999)

[114] R. Apfel, Nature, **398**, 378 (1999)

[115] V. Q. Vong and A. J. Szeri, Phys. Fluids, **8**, 2354 (1996)

[116] L. Yuan, H. Y. Chen, M. C. Chu, and P. T. Leung, Phys. Rev. E. **77**, 4265 (1998)

[117] A. Prosperetti, J. Acoust. Soc. Am. **61**, 17 (1977)

[118] A. Prosperetti, J. Fluid Mech. **222**, 587 (1991)

[119] T. G. Leighton, *The Acoustic Bubble*, (Academic Press) (1994)

[120] S. Hilgenfeldt, D. Lohse, and W. C. Moss, Phys. Rev. Lett. **80**, 1332 (1998)

[121] H. Poritsky, Proceedings of the first U. S. national congress on applied mechanics, edited by E. Sternberg (New York), 813 (1952)

[122] W. Lauterborn, J. acoust. Soc. Am. **59**, 283 (1976)

[123] M. S. Plesset, J. Appl. Mech. **16**, 277 (1949)

[124] E. A. Neppiras and B. E. Noltingk, Proc. Phys. Soc. B, **64**, 1032 (1951)

[125] R. Löfstedt, B. P. Barber, and S. J. Putterman, Phys. Fluids A, **5**, 2911 (1993)

[126] D. R. Lide, *CRC Handbook of Chemistry and Physics*, edited by D. R. Lide (1991)

[127] M. Minnaert, Phil. Mag. **16**, 235 (1933)

[128] E. A. Neppiras, Phys. Rep. **61**, 159 (1984)

[129] L. A. Crum, Ultrasonics, **22**, 215, (1984)

[130] L. A. Crum, J. acoust. Soc. Am. **73**, 116 (1983)

[131] L. A. Crum, J. acoust. Soc. Am. **73**, 121 (1983)

[132] A. Prosperetti, Ultrasonics, 69 (March 1984)

[133] A. Prosperetti, Ultrasonics, 115 (May 1984)

[134] A. Prosperetti, A. Lezi, J. Fluid Mech. **168**, 457 (1986)

[135] A. Prosperetti, L. A. Crum, and K. W. Commander, J. Acoust. Soc. Am. **83**, 502 (1988)

[136] S. Hilgenfeldt, M. P. Brenner, S. Grosmann, and D. Lohse, J. Fluid Mech. **365**, 171 (1998)

[137] L. Kondic, Ph. D. Thesis, City University of New York (1995)

[138] B. P. Barber, K. Weninger, and S. J. Putterman, Phil. Trans. R. Soc. Lond. A, **355**, 641 (1997)

[139] L. Kondic, J. I. Gersten, and C. Yuan, Phys. Rev. E, **52**, 4976 (1995)

[140] W. Moss, D. Clarke, J. White, and D. Young, Phys. Fluid, **6**, 2979 (1994)

[141] W. Moss, D. Clarke, J. White, and D. Young, Phys. Lett. A. **211**, 69 (1995)

[142] R. Hiller and B. P. Barber, Sci. Am. **272**, 78 (1995)

[143] I. M. Hallaj, T. J. Matula, R. A. Roy, and L. A. Crum, J. Acoust. Soc. Am. **100**, 2717(A) (1996)

[144] H. C. Van de Hulst, *Light Scattering by Small Particles* (Wiley, New York) (1957)

[145] G. E. Davis, J. Opt. Soc. Am. **45**, 572 (1955)

[146] L. Kinsler, A. Frey, and J. Sanders,*Fundamental od Acoustics*, (Wiley & Sons.) (1982)

[147] T. J. Matula, S. M. Cordry, R. A. Roy, and L. A. Crum, J. Acoust. Soc. Am. **102** (1997)

[148] R. E. Apfel, Ph. D. Thesis, Harvard University, Boston (1970)

[149] R. E. Apfel, J. Acoust. Soc. Am. **49**, 145 (1971)

[150] M. A. Weiser and R. E. Apfel, J. Acoust. Soc. Am. **71**, 1261 (1982)

[151] L. Kondic, C. Yuan, and C. K. Chan, Phys. Rev. E, **57**, R32 (1998)

[152] T. J. Matula, J. E. Swalwell, V. Bezzerides, P. Hilmo, M. Chittick, L. A. Crum, J. Acoust. Soc. Am. **102**, 3185 (1997)

[153] R. G. Holt, R. A. Roy, and S. C. Wyatt, J. Acoust. Soc. Am. **105** No. 2, Pt 2, 960 (1999)

[154] S. C. Wyatt, M. S. Thesis, Boston University, Boston (2000)

[155] J. B. Young, T. Schmiedel, and W. Kang, Phys. Rev. Lett. bf 77, 4816 (1996)

[156] L. A. Crum, T. J. Mason, J. L. Reisse, and K. S. Suslick, *Sonochemistry and Sonoluminescence*, NATO ASI Series, Kluwer Academic Publishers, Vol. 524 (1998)

[157] P. S. Epstein and M. S. Plesset, J. Chem. Phys. **18**, 1505 (1950)

[158] M. P. Brenner, D. Lohse, D. Oxtoby, and T. F. Dupont, Phys. Rev. Lett. **76**, 1158 (1996)

[159] L. Kondic, C. K. Chan, and C. Yuan, J. Acoust. Soc. Am. **100**, 2678 (1996)

[160] C. K. Chan, C. Yaun, and L. Kondic (unpublished)

[161] J. A. Ketterling and R. E. Apfel, Phys. Rev. Lett. **81**, 4991 (1999)

[162] S. Hilgenfeldt, D. Lohse, and M. P. Brenner, Phys. Fluids. **8**, 2808 (1996)

[163] M. M. Fyrillas and A. J. Szeri, J. Fluid. Mech. **277**, 381 (1994)

[164] V. Q. Vount, A. J. Szeri, and D. A. Young, Phys. Fluids **11**, 10 (1999)

[165] K. Yasui, Phys. Rev. E **56**, 6750 (1997)

[166] A. I. Eller and L. A. Crum , J. Acoust. Soc. Am. **47**, 762 (1970)

[167] A. Prosperetti, Quart. Appl. Math. **34**, 339 (1977)

[168] in preparation

[169] Y-P. Lee, S. W. Karng, J-S. Jeon, and H-Y. Kwak, J. Phys. Soc. Japan, **66**, 2537 (1997)

[170] H-T. Elze, T. Kodama, J. Rafelski, Phys. Rev. E **57**, 4170 (1998)

[171] S. L. Ceccio, and C. E. Brennen, J. Fluid Mech. **233**, 633 (1991)

[172] Z. Q. Wang, R. Pecha, B. Gompf, and W. Eisenmenger, Phys. Rev. E **59**, 1777 (1999)

[173] R. Pecha and B. Gompf, Phys. Rev. Lett. **84**, 1328 (2000)